A Framework for Explicit Model Predictive Control using Adjustable Robust Optimization and Economic Optimization of an Industrial-Scale Sulfuric Acid Plant

by

Manuel Alejandro Tejeda Iglesias

A thesis
presented to the University of Waterloo
in fulfillment of the
thesis requirement for the degree of
Master of Applied Science
in
Chemical Engineering

Waterloo, Ontario, Canada, 2018

Author's Declaration

I hereby declare that I am the sole author of this thesis. This is a true copy of the thesis, including any required final revisions, as accepted by my examiners.

I understand that my thesis may be made electronically available to the public.

Abstract

Optimization plays an important role in the operation of chemical engineering systems. Due to their typical size, different optimization tools and techniques are required to improve the efficiency in process operations. In this thesis, a mathematical tool is developed to address the issue of optimal control for linear systems under uncertainty. Also, a comprehensive plant model describing the behaviour of an industrial-scale Sulphuric Acid plant is developed to assist in identification of the optimal operating conditions under uncertainty

Model predictive control (MPC) is considered an attractive strategy for the optimal control of complex chemical engineering systems. Conventional MPC involves solving an optimization problem online to determine the control actions that minimize a performance criterion function. The high computational expense associated with conventional MPC may make its application challenging for large-scale systems. Explicit MPC has been developed to solve the optimization problem offline. In this work, adjustable robust optimization (ARO) is used to obtain the explicit solution to the MPC optimization problem offline for discrete-time linear time invariant systems with constraints on inputs and states. In the robust model formulation an uncertain additive time-varying error is introduced to account for model uncertainty resulting from plant-model mismatch caused by un-measurable disturbances or process nonlinearities. The explicit solution is an optimal time-varying sequence of feedback control laws for the control inputs parameterized by the system's states. The control laws are evaluated in a time-varying manner when the process is online using state measurements. This study shows that the resulting control laws ensure the implemented control actions maintain the system states within their feasible region for any realizations of the

uncertain parameter within the uncertainty set. Three case studies are presented to demonstrate the proposed approach and to highlight the benefits and limitations of this method.

The optimal operating condition to which an optimal controller will drive a large industrial-scale plant is identified using a different set of tools. In this thesis, an industrial-scale sulfuric acid plant is considered. The production of sulfuric acid is an important process due to its many applications and its use as a mitigation strategy for Sulphur dioxide (SO_2). The reactor of the sulfuric acid plant has been the focus of many studies, and thus there has been very limited works in the literature that have analyzed the complete sulfuric acid plant. In this work, the flowsheet for an industrial-scale sulfuric acid plant with scrubbing tower is presented. The model is developed in Aspen Plus V8.8 and it is validated using historical data from an actual industrial plant. A sensitivity analysis was carried out, followed by optimization using two alternative objective functions: maximization of plant profitability or productivity. The optimization was extended to consider uncertainty in key operating and economic parameters. The results show that changes could be made in the current optimal operating condition of the plant to improve the annual profit of the process.

Acknowledgements

First and foremost, I would like to acknowledge my supervisor, Professor Luis Ricardez-Sandoval. This journey has not only been an opportunity for me to develop my technical skills and grow professionally but it has also been a period of great personal growth. There were many challenges, as well as triumphs, but without your support this likely would have been a different final product. You are passionate about your work and you do not back down from the challenge until the final result has been delivered to the highest caliber. Thank you for always pushing me to achieve the best even when I thought I could do no better.

Secondly, I would like to thank my family for their continuous support. My mother and father provided continuous emotional and professional guidance y mis abuelos siempre me animaron. To my sis, I am thankful that this time gave us the opportunity to re-kindle our relationship and make us best friends.

Thirdly, I would like to acknowledge the group of friends that has been crucial during this time. To Jude, Jason, and Mitch: we're getting spread out from our Millrise-Evergreen neighborhood we grew up in, but we don't let this keep us apart, and for that I'm thankful. To my roommate and good friend Hashim: you taught me to not always say 'yes' and somehow, I turned out to be the messy one. Thank you. To my future co-founder and good friend James: I wish we had started brainstorming our 'hustles' in the first year of our degrees and I look forward to continuing to work on them.

Finally, I would like to thank my girlfriend Tanya. I could not have asked for a kinder and more compassionate partner to have shared this journey with. You were always there for me when I needed your support and for that I am forever grateful.

For their technical and financial support to this work, I would like to thank CCC Sulphur Products, NSERC, and the OGS.

Table of Contents

List of Figures

List of Tables

List of Abbreviations

ARO	Adjustable robust optimization
aro-MPC	Adjustable robust optimization model predictive control
ARC	Adjustable robust counterpart
AF	Air Flow
CPU	Central processing unit
CO_2	Carbon dioxide
CS1	Case study 1
CS2	Case study 2
DNA	Data not applicable
GA	Genetic algorithm
GPS	Generalized pattern search
GS	Gas Strength
H_2S	Hydrogen sulfide
H_2SO_4	Sulfuric acid
HX34T	E-103 and E-104 Temperature
HX5T	E-105 Temperature
HX6T	E-106 Temperature
HX7T	E-107 Temperature
HX8T	E-108 Temperature
MPC	Model predictive control
mp-MPC	Multi-parametric model predictive control
NaOH	Sodium hydroxide
NRTL	Non-random two-liquid model
O_2	Oxygen
OBJ1	Objective 1
OBJ2	Objective 2
OP1	Operating Condition 1
OP2	Operating Condition 2
OPD	Operating Condition Design

PEM	Proton-exchange membrane
pH	E-24 Recirculation pH
PK101	C-101 Height
PK102	C-102 Height
PK103	C-103 Height
PK24	E-24 Height
PK25	E-25 Height
PM	Performance metric
SBS	Sodium bisulfite
Sc1	Scenario 1
Sc2	Scenario 2
Sc3	Scenario 3
Sc4	Scenario 4
SO_2	Sulfur dioxide
SO_3	Sulfur Trioxide
SRO	Static robust optimization

List of Symbols

$\boldsymbol{\theta}$	Other model parameters captured in the explicit MPC solution
$\Delta \mathrm{z}_i$	Change in parameter z between sampling intervals i and $i-1$
$\boldsymbol{\Phi_0}$	Bounded factor matrix relating primitive factors to $\mathbf{x}$
$\boldsymbol{\Phi}_1$	Bounded factor matrix relating primitive factors to $\mathbf{e}$
$\boldsymbol{\xi}$	Uncertain primitive factors
ξ	Set of parameters considered uncertain in the sulfuric acid optimization problem
$\boldsymbol{\varsigma}$	Definition of the uncertainty set
Ξ	Set to which the primitive factors belong
β	Bounded factor parameter
$\propto$	Parameter used to adjust the size of the uncertainty set in aro-MPC
$\mathbf{A}$	State-space matrix that multiplies the states
$\mathbf{B}$	State-space matrix that multiplies the inputs
$\mathbf{C}$	State-space matrix that multiplies the outputs
$\mathbf{D}$	State-space matrix that multiplies the disturbances or errors
$\mathbf{d}$	Input disturbance
$\mathrm{dV}/\mathrm{d}t$	Derivative of variable V with respect to variable t
$\mathbf{e}$	Uncertain additive time-varying error
$\mathbf{e}^L$	Lower bound on the uncertain additive time-varying error
$\mathbf{e}^U$	Upper bound on the uncertain additive time-varying error
$\mathbf{ez}$	Vector of ones
$\boldsymbol{f}$	A general function
F	Number of factors in the bounded factor uncertainty set
$\mathrm{F_h}$	Flowrate of the hot inlet stream
$\mathrm{F_c}$	Flowrate of the cold inlet stream
H	Enthalpy
i	Number of sampling intervals into the future
$\dot{M}_z$	Mass flowrate of component z
$\mathrm{N_z}$	Dimension of size z

P	Prediction horizon
$\mathbf{p}^L, \mathbf{p}^U$	Dual variables
p_z	Price of component z
$\mathbf{q}$	Objective cost associated with difference between process output and setpoint
Q_{E-110}	Heat duty of the cooling tower E-110
$\mathbb{R}$	Real number system
$\mathbf{r}$	Process setpoint
$\mathbf{r}^L, \mathbf{r}^U$	Dual variables
t	Sampling interval
t_{sol1}	Offline time for obtaining first aro-MPC solution
t_{sol2}	Offline time for obtaining second aro-MPC solution
$\mathbf{u}$	Control action
$\mathbf{u}^L$	Lower bound on control action
$\mathbf{u}^U$	Upper bound on control action
$\mathbf{U}$	Slope associated with linear decision rules for control actions
$\boldsymbol{v}_{t+i}^0$	Intercept associated with linear decision rules for control actions
$v_{SO_2,stream\ 24}$	Volumetric concentration of SO2 in stream 24
V	Volume in tank
$\mathbf{w}$	Objective cost associated with magnitude of control actions
W_{B-101}	Net work of the compressor B-101
$\mathbf{x}$	Process state
$\hat{\mathbf{x}}$	Predicted process state
$\mathbf{X}$	Slope associated with linear decision rules for process states
$\mathbf{x}_t^{\mathrm{Nom}}$	Nominal state of the system at the sampling interval t
$\mathbf{x}^L$	Lower bound on process state
$\mathbf{x}^U$	Upper bound on process state
$\boldsymbol{\chi}_{t+i}^0$	Intercept associated with linear decision rules for process states
$\mathrm{y}^L, \mathrm{y}^U$	Dual variables
$\mathbf{y}$	Process output
$\hat{\mathbf{y}}$	Predicted process output

Chapter 1: Introduction

Chemical engineering systems are typically large, capital intensive projects, that operate over long periods of time. They can have large economic, environmental, and societal impacts on the regions in which they are situated. Thus, it is important that these systems be designed and operated in an optimal fashion. This thesis is composed of two distinct projects which address the issue of optimal operation of large chemical engineering systems.

In the first project a tool is developed to better enable the application of linear MPC to large systems under uncertainty. It is a framework for Explicit Linear Model Predictive Control (MPC). Linear MPC is considered an attractive strategy for achieving optimal control,[1] however its online computational requirements have typically restricted its application.[2] Explicit MPC circumvents this drawback by performing the expensive computation offline thereby reducing online computation to evaluation of a series of algebraic equations.[3] In this work, adjustable robust optimization (ARO) is used to develop an Explicit MPC framework.

The second study involves the simulation and economic optimization of an industrial-scale plant under uncertainty. This work is applicable when demand for the product being manufactured has increased and the operator wishes to identify the maximum profit or output that the plant can achieve given the current design and its associated safety, environmental and productivity restrictions. The use of simulation and optimization tools in this situation is highly advantageous as it can eliminate (or reduce) timely and costly experiments in search of the optimal operating condition. In this work, in collaboration with an industrial partner, a simulation was implemented, and a subsequent economic optimization was carried out to identify the optimal operating

condition for an industrial-scale sulfuric acid plant. Each of the research subjects mentioned above will be discussed next.

1.1 Explicit MPC

MPC has largely been accepted as the solution for optimal control of complex multivariable processes.[4] The key idea in MPC is to compute the sequence of control actions that are expected to maintain the system on target by solving an optimization problem consisting of an internal process model, process constraints, and a user-defined objective function at each sampling interval. Only the first control action is implemented on the process and the procedure is repeated at the following sampling interval.[4] The primary issue raised by this procedure is that a large computational effort may be required to evaluate online an optimization problem thereby limiting its application to slowly varying processes.[2] However, this challenge can be overcome by solving offline the MPC optimization problem in a way that makes the relationship between the control actions and the measured outputs explicit.[3] This is referred to as *Explicit MPC*. The majority of work in the area of Explicit MPC has been accomplished using multi-parametric programming (mp-MPC).[3] Although it addresses the issue associated with online computation, the mp-MPC framework has its limitations. For instance, it is numerically difficult as it involves partitioning the state-space into polyhedral regions while avoiding overlaps in neighboring polyhedra.[5] Also, it does not guarantee that the state variables will remain within their feasible region under deterministic or uncertain conditions.[6,7]

1.2 Modeling and Optimization of an Industrial-Scale Sulfuric Acid Plant

Sulfuric acid is an important industrial chemical because of its direct or indirect involvement in nearly all production industries. The main steps in the sulfuric acid manufacturing process are

combustion of sulfur into SO_2, conversion of SO_2 into SO_3 in a multi-stage packed bed catalytic reactor with inter-stage cooling, and absorption of SO_3 in sulfuric acid. This is referred to as the process gas cycle. An industrial sulfuric acid plant also consists of the process acid cycle, steam and cooling water utilities, and in some cases a scrubbing tower. Although this is a major industrial-scale application, the majority of modeling and optimization work in the literature aimed at sulfuric acid plants has focused solely on the catalytic reactor with very limited works integrating the complete process gas cycle. Moreover, there has only been two models that have been validated using actual plant data.[8,9] Finally, no studies have considered the effect of uncertainty in key model parameters on the economic performance and productivity of the sulfuric acid plant.

1.3 Research Objectives

With respect to Explicit MPC, the aim of this work is to present a novel framework for obtaining the explicit solution to the linear MPC problem using adjustable robust optimization (ARO). This will be referred from heretofore as *aro-MPC*. Two objectives motivate this work: first, it is an alternative method to multi-parametric programming for obtaining the explicit solution to the linear MPC optimization problem; and second, the resulting framework is inherently robust with respect to the state variables, and thus guaranteed to satisfy process constraints without additional considerations. The novelty of this work, and its contribution to the area of optimal control, is the development of a new method for Explicit MPC. It is expected that the aro-MPC framework proposed here may broaden the applicability of Explicit MPC for controlling chemical engineering systems based on its differentiating features from mp-MPC.

In the second research subject, the objective is to develop a comprehensive model for an industrial-scale single absorption sulfuric acid plant with scrubbing tower that includes process utilities. By including the utilities and scrubbing tower, the model can account for more of the interactions between process variables, and thus will capture a more realistic representation of an actual industrial-scale plant. The model will be validated using historical data from an industrial-scale sulfuric acid plant, and thus it can be used to identify economic opportunities based on changes in the current operating conditions. Those opportunities will be identified deterministically and under uncertainty in key parameters to understand the sensitivity of the optimal operating condition and the price of robustness for the plant model. The comprehensive development of this steady-state model is expected to reduce the time and cost associated with identifying the optimal operating condition of the industrial-scale sulfuric acid plant. Moreover, it will enable an improved understanding of the interactions between operating parameters.

1.4 Structure of Thesis

This thesis is organized as follows:

Chapter 2 provides a literature review highlighting the relevant works in the areas of Explicit MPC, ARO, and the design, simulation, and optimization of sulfuric acid plants.

Chapter 3 presents the proposed aro-MPC framework. Three notable computational experiments are included. The first uses a one input, two state system to demonstrate the general features of the framework. The second presents the aro-MPC for a 5x5 system. To the author's knowledge, the largest system for which an Explicit MPC controller has been developed consists of three inputs and four outputs.[10] The third system demonstrates the implementation of the aro-MPC framework on a nonlinear system.

Chapter 4 describes the model used to approximate the industrial-scale sulfuric acid plant and the validation strategy. The model is then used to identify the optimal operating condition under deterministic and uncertain conditions. The content in this chapter has been published in Industrial & Engineering Chemistry Research.[11] This paper was written entirely by myself, and it was edited by my supervisor, Luis Ricardez-Sandoval. Permission has been granted by the publisher to use the published content in this thesis.

Chapter 5 summarizes the methods and results of this thesis and presents conclusions of both works. Recommendations are provided for future work in the areas of aro-MPC and simulation and optimization of industrial-scale sulfuric acid plants.

Chapter 2: Literature Review

This chapter provides detailed literature reviews on the most relevant contributions in the areas of Explicit MPC and ARO as well as the design, simulation, and optimization of sulfuric acid plants. Section 2.1 begins with a brief summary of linear MPC and is followed by a discussion on Explicit MPC and mp-MPC. Afterwards, an overview of ARO is presented. Section 2.2 presents the global importance of sulfuric acid by highlighting its most relevant applications. This is followed by a design overview of industrial-scale sulfuric acid plants and a presentation of the modeling works in the literature relevant to the production of sulfuric acid. A summary on the major findings and gaps identified from the literature review is presented at the end.

2.1 Optimal Control Using MPC

2.1.1 Linear MPC

As discussed in the introduction, MPC is an optimization-based control technique that employs a model of the system to compute the control actions that can minimize plant offsets. When compared to the conventional feedback control schemes such as PID control, MPC poses two key advantages; it can take into account process constraints, e.g. on the states and control actions of a system, and it can drive the controlled variables of the system in such a way that a user-defined objective is optimized.[1] More details about Model Predictive Control can be found elsewhere.[5,12] Linear MPC is typically defined by an optimization problem having linear constraints and a quadratic objective function, i.e.

$$\min_{\substack{\hat{\mathbf{x}}_{t+i}\in\mathbb{R}^{\mathrm{N_x}},\\ \forall i=1,\dots P\\ \mathbf{u}_{t+i}\in\mathbb{R}^{\mathrm{N_u}},\\ \forall i=0,\dots P-1}} \mathbf{q}^{\mathrm{T}}\sum_{i=1}^{P}(\hat{\mathbf{y}}_{t+i}-\mathbf{r}_{t+i})^2+\mathbf{w}^{\mathrm{T}}\sum_{i=1}^{M-1}(\Delta\mathbf{u}_{t+i})^2 \tag{1a}$$

$$\text{s.t.}\quad \hat{\mathbf{x}}_{t+i+1}=\mathbf{A}\hat{\mathbf{x}}_{t+i}+\mathbf{B}\mathbf{u}_{t+i} \qquad \forall i=0,\dots,P-1 \tag{1b}$$

$$\hat{\mathbf{y}}_{t+i}=\mathbf{C}\hat{\mathbf{x}}_{t+i} \qquad \forall i=0,\dots,P \tag{1c}$$

$$\mathbf{u}^L\le\mathbf{u}_{t+i}\le\mathbf{u}^U \qquad \forall i=0,\dots,M-1 \tag{1d}$$

$$\mathbf{x}^L\le\hat{\mathbf{x}}_{t+i}\le\mathbf{x}^U \qquad \forall i=1,\dots,P \tag{1e}$$

$$\mathbf{u}_{t+i}=\mathbf{u}_{t+M-1} \qquad \forall i=M,\dots,P-1 \tag{1f}$$

where $\hat{\mathbf{x}}_{t+i}\in\mathbb{R}^{\mathrm{N_x}}$ is the vector of predicted states, $\hat{\mathbf{y}}_{t+i}\in\mathbb{R}^{\mathrm{N_y}}$ is the vector of predicted outputs, $\mathbf{u}_{t+i}\in\mathbb{R}^{\mathrm{N_u}}$ is the input control vector, $\mathbf{r}_{t+i}\in\mathbb{R}^{\mathrm{N_y}}$ is the vector of user-defined setpoints, and $\Delta\mathbf{u}_{t+i}\in\mathbb{R}^{\mathrm{N_u}}$ is the vector containing the magnitude of the change in process inputs between time interval $t+i-1$ and $t+i$ (i.e. $\Delta\mathbf{u}_{t+i}=\mathbf{u}_{t+i}-\mathbf{u}_{t+i-1}$). The initial condition is the measured output of the process at sampling time t, $\mathbf{y}_t\in\mathbb{R}^{\mathrm{N_y}}$, which replaces $\hat{\mathbf{y}}_{t+i}$ at $i=0$. M and P are the user-defined control and prediction horizons, respectively. Along with the weights on the controlled and manipulated variables (i.e. $\mathbf{q}$ and $\mathbf{w}$), M and P are the tuning parameters of the controller.

Linear MPC is implemented by solving online the MPC optimization problem (1a)-(1f). The general procedure is presented in Figure 1 for a single input single output system. At each time interval, t, the current output of the system y_t is measured and used as an initial condition to identify the sequence of control actions $\mathrm{u}_t,\mathrm{u}_{t+1},\dots,\mathrm{u}_{t+M-1}$ that are expected to drive the future output predictions y_{t+i} towards the user-defined setpoint subject to process constraints. Once solved, the first control action, u_t, is implemented on the process and the remaining are discarded.

Due to model limitations and plant-model mismatch, the predicted output, $\hat{y}_{t+1}$, typically differs from the measured output, y_{t+1}. Hence, feedback is incorporated in the framework by repeating the procedure at the following time interval.

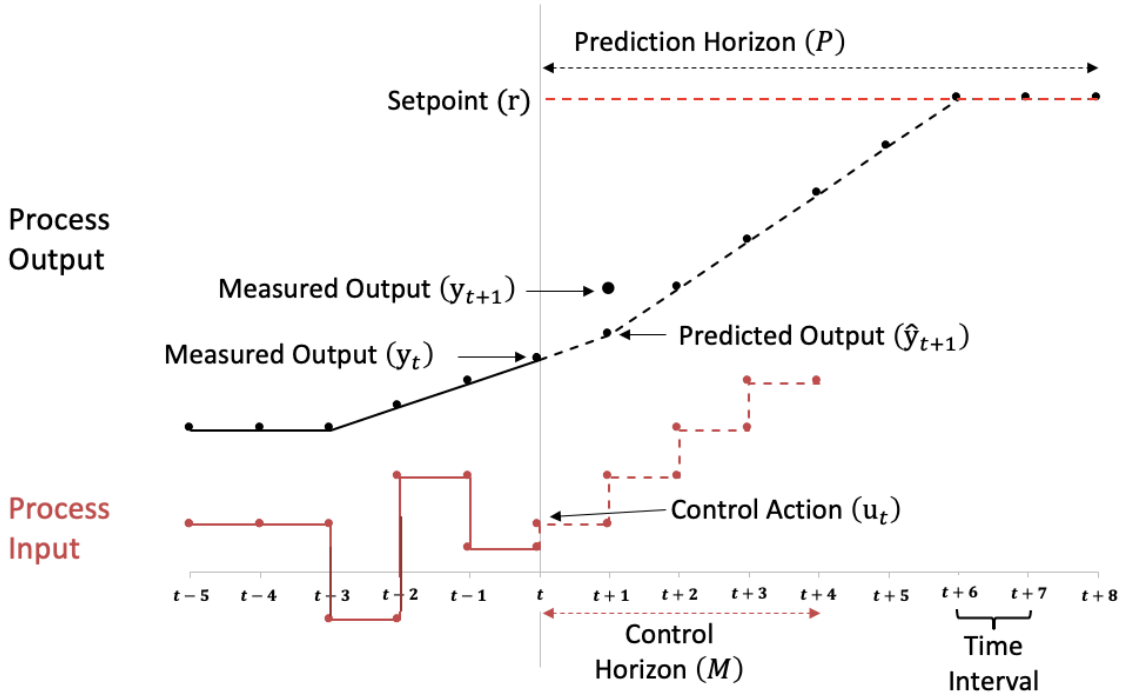

Figure 1. Model predictive control overview[1]

2.1.2 Explicit MPC using Multi-parametric Programming

In Explicit MPC, the MPC optimization problem is solved *a priori* to obtain explicit relationships between the control actions and measured outputs. The most general parametrization takes the following form:

$$\mathbf{u}_{t+i} = \boldsymbol{f}(\mathbf{x}_{t+i}, \mathbf{r}, \boldsymbol{\theta}) \tag{2}$$

such that function $\boldsymbol{f}$ is an algebraic function that is used to evaluate online the control actions $\mathbf{u}_{t+i}$ which are dependent on the process state $\mathbf{x}_{t+i}$, the setpoint $\mathbf{r}$ that was considered when obtaining the parametric solution, and the remaining process model parameters $\boldsymbol{\theta}$. The main feature of this approach is that the online computation of the control actions is reduced to evaluation of the function $\boldsymbol{f}$ instead of solving an MPC optimization formulation at each sampling interval.

As mentioned in section 1.1, the majority of work in the field of Explicit MPC has been accomplished using mp-MPC. This approach involves partitioning the state-space into polyhedral regions such that for each region, an affine control law parametrized by the states of the system is obtained. In addition to evaluating the parametric control law, online implementation of the mp-MPC solution first involves selecting an appropriate control law by identifying the polyhedral region in which the current state measurement lies. Since the seminal work in this area showed the development of a mp-MPC controller for a constrained linear quadratic regulator,[6] the field has received much attention. Multiple studies have considered the topic of mp-MPC under uncertainty.[2,13–16] Uncertain optimization problems are solved using stochastic or robust optimization techniques.[17–25] In the former, the modeler must make an assumption regarding the probability distribution of the uncertain parameter whereas in the latter, no probability distribution is assumed, rather the uncertain parameter is defined by a bounded set. The robust solution is guaranteed to remain feasible over the entire range of uncertain parameter realizations whereas the stochastic solution only provides a probabilistic feasibility guarantee. Studies that have considered mp-MPC under uncertainty have obtained the robust explicit solution for systems with exogenous disturbances and/or model parameter uncertainty in the state-space matrices.[2,13,14] The area of Explicit Stochastic MPC has recently been referred to as an important area of future work.[27] With respect to real-world applications, mp-MPC has been used to solve problems related to the energy

and medical sectors through the control of a PEM fuel cell and an intravenous anaesthesia system, respectively.[10,28] Other chemical engineering applications that have been considered include control of distillation columns and pressure swing absorption systems.[29,30] All of the previous works mentioned have developed the mp-MPC for systems with linear process models; however there has also been a few studies that have developed the mp-MPC for systems described by nonlinear models.[31–33] The main limitation of mp-MPC is the numerical difficulty associated with computing every polyhedron in the state-space while avoiding overlaps and gaps in neighbouring polyhedra.[5] To the author's knowledge, the largest system to which mp-MPC has been successfully applied is the three input, four state PEM fuel cell system.[10] In addition to eliminating the drawback associated with online computation, another advantage of the robust mp-MPC controllers is that they ensure controller feasibility against a user-defined uncertainty set. However, to the author's knowledge, they do not guarantee that the state-space variables will remain within a feasible region in the presence of uncertainty. Although some works have been aimed at reducing the computational complexity associated with solving the mp-MPC optimization problem through the identification of suboptimal solutions using a variety of approximation techniques,[34–40] there has been limited contributions that explore alternative methods of obtaining explicit functions (1) for linear MPC. However, there has been some works that explore the use of machine learning methods to obtain the explicit functions (1) for nonlinear MPC.[41,42] A technique that will be considered in this study to address uncertainty in the Explicit MPC formulation developed in this work is presented next.

2.1.3 Adjustable Robust Optimization

Static robust optimization (SRO) is a method of solving problems subject to uncertainty; however, all decision variables are considered as "here-and-now."[26] The resulting solution is robust

(immune) against a user-defined uncertainty set but the user is unable to incorporate any information that becomes available after the optimization problem is solved without performing re-optimization. ARO has the same advantage of SRO in that the resulting solution is robust against a user-defined uncertainty set; however, the user can select "wait-and-see" decision variables to be adjustable in the ARO framework. In a conventional ARO problem, those variables selected as adjustable are replaced by a user-defined function where the independent variables (i.e. inputs to those functions) are the uncertain parameters. Hence, the coefficients of these functions replace the original variables as the decision variables in the ARO formulation. The resulting expressions are then used to evaluate the adjustable (manipulated) variables at a later point in time when the uncertain parameters have materialized (been observed).

The optimization problem considered to obtain the ARO solution is a deterministic reformulation of the robust multistage optimization problem.[43] This problem is referred to as the adjustable robust counterpart (ARC). For linear optimization problems, it consists of replacing all adjustable variables with their corresponding parametrized functions of the uncertain parameters followed by elimination of the uncertain parameters from all uncertain constraints including the objective function. This is performed by dualization for inequalities constraints and by coefficient matching for equality constraints.

ARO has been applied in the area of process scheduling to develop two-stage and multi-stage robust schedules for batch processing plants.[44–47] With regards to process control, it has been shown that ARO can be used to obtain time-varying control laws for fully linear control problems (i.e. linear objective function and linear constraints) by parametrizing the control action with the measured disturbances rather than the measured states as is done in the multi-parametric programming framework.[26,48] However, online implementation of the control laws is not discussed

beyond stating that the laws are to be implemented in a time-varying fashion nor is their performance evaluated. Although those works focus on the design of optimal linear controllers, they represent the closest attempt to obtaining an explicit solution of the linear MPC problem with a quadratic objective function using ARO.

2.2 Sulfuric Acid Manufacturing Process and Simulation

The most dominant application of sulfuric acid is in the production of phosphate fertilizers, accounting for almost 60% of global consumption in 2009.[49] Other applications include leaching of copper, nickel, and uranium ores, petroleum refining to convert low molecular weight alkenes to alkylates, manufacturing of rubber, plastics, pigments, pulp and paper, and the production of other chemicals and fertilizers.[49] In addition to its application in multiple industries, a secondary benefit of sulfuric acid is that it is mainly produced involuntarily for the purpose of mitigating SO_2 and H_2S.[50] These gases are produced during the processing of metal ores and hydrocarbons, respectively, and are the sources of sulfur for sulfuric acid production. The sulfuric acid production process, also known as the contact process, can directly make use of the SO_2 but H_2S must first be converted into elemental sulfur. Globally, 60% of sulfur used in the production of sulfuric acid comes from hydrocarbons, 30% from metal ores, and the remaining 10% from the decomposition of spent petroleum and polymer sulfuric acid catalyst.[51]

There are two types of manufacturing plants: single and double adsorption. Double absorption plants can operate at SO_2 concentrations as high as 12% and can achieve SO_2 conversion as high as 99.6% whereas single absorption plants can have SO_2 concentrations up to 10% while achieving SO_2 conversion as high as 98.5%.[52] Furthermore, the resulting process gas from a double absorption plant can be directly vented to the atmosphere whereas a downstream scrubbing unit is

required to reduce the concentration of SO_2 in the vent gas from a single absorption column to environmentally acceptable levels.[53] This can be attributed to the inter-stage absorption column that is included between the third and fourth reactor stages for double absorption plants.[54] However, with the aid of the scrubbing unit, single absorption plants produce a vent gas with a concentration lower than 100 ppm SO_2 whereas the double absorption plants produce a vent gas with a concentration of 400-450 ppm SO_2.[53] Moreover, the scrubbing tower makes operation during transient periods such as plant start up significantly easier. While the temperature in the packed beds of the reactor is increasing to the catalyst activation temperature, unreacted SO_2 in the process gas is still being removed so that a vent gas which meets environmental standards is produced.[53,55] For these reasons, single absorption sulfuric acid plants continue to be viable alternatives to the more productive double absorption plants.[56]

Despite its importance, the majority of the theoretical work reported in the literature for this process has been very limited and focused only on modeling the reactor section of the contact process. To the author's knowledge, only one reactor model has been validated using industrial plant data. In that work, a transient model of a multi-stage reactor was created in DYNAM to minimize SO_2 emissions during plant start-up.[8] That work was later extended to include transients during operation when SO_2 concentration in the vent gas from the metallurgical plant may fluctuate.[57] Moreover, other studies have considered the use of alternative reactors, mainly trickle-bed and periodic flow reversal reactors, which eliminate the need for inter-stage cooling. In those works, mechanistic models of the reactors were developed. Those models were validated by comparison with experimental lab data and thereby established the relationships between the design, operating parameters and reactor performance.[58–61] Furthermore, there have been reports that have made use of optimization tools to show potential improvements in the design and

operation of the multi-stage reactor through a reduction in entropy,[62] re-distribution of the catalyst throughout the different stages,[63] and real-time set-point calculation of the first stage inlet temperature for process gas with a fluctuating concentration of SO_2.[64]

To the author's knowledge, there has only been very limited modeling studies in the literature which attempt to model other sections of the contact sulfuric acid plant, in addition to the reactor section. In one of those studies, a single absorption sulfuric acid plant using metallurgical ore roaster gas as the source of SO_2 was simulated at steady state using PROPS.[9] The simulation included the process gas and process acid cycles. To validate the simulation, temperature results from the multiple reactor stages and overall conversion from the model were compared to real plant data. An economic optimization was performed for the plant and it was found that a 0.32% increase in return on investment was possible at the optimal solution. This translated into an annual net earnings increase of $40,000. In that study, the decision variables being considered were the inter-stage heat exchanger outlet temperatures and catalyst loadings in the multiple reactor stages. In another study, a transient model of a double absorption sulfuric acid plant that uses elemental sulfur as the feedstock was completed using gProms.[65] That model also included the complete process gas cycle; however, the process acid cycle only presented the acid streams in the absorption columns. That study suggested that potential SO_2 emissions reductions of up to 40% were possible by optimizing feed flow rates and split fractions. Although there have been studies that aim to minimize the SO_2 emissions from the sulfuric acid plant and maximize its economic performance, there has not been a study that provides insight on the sensitivity of the economic performance of a sulfuric acid plant with respect to the operating conditions. Also, the effect of uncertainty in key model and optimization parameters on economic performance has not been previously considered

for this plant. Furthermore, the cooling water utility and scrubbing tower have not been included in the models reported in the literature.

2.3 Summary

Explicit MPC is an attractive alternative to solving the linear MPC optimization problem online as it significantly reduces the online computational burden. It results in control laws that are parametrized by the measured states of the system and which are evaluated when the process is online. Many works have explored this topic using multi-parametric programming (mp-MPC). Studies in mp-MPC have explored the topics of MPC under uncertainty, MPC for real-world systems such as fuel cells and pressure-swing absorption columns, MPC for nonlinear systems, and approximate explicit solutions to the linear MPC optimization problem. The final topic in the previous list addresses one of the main drawbacks associated with mp-MPC. Namely, the complexity associated with identifying the explicit control laws as a result of the need to partition the state-space while avoiding partition overlaps. Secondly, although mp-MPC under uncertainty has been considered, the resulting control laws have not been shown to be robust with regards to the states of the system. ARO, a method for obtaining robust solutions to uncertain multi-stage optimization problems, is considered a suitable alternative to multi-parametric programming for obtaining the explicit solution to the linear MPC optimization problem. Its benefits are that it is an inherently robust technique and it does not require partitioning the state-space. Within chemical engineering it has mainly been applied to the area of process scheduling. The following chapter presents the proposed framework for aro-MPC.

Sulfuric acid is an important global commodity due to its use in many production processes and its ability to mitigate SO_2 and H_2S. Although the sulfuric acid plant can consist of up to five process

cycles (process gas, process acid, steam utility, cooling water utility, and scrubbing tower) the majority of modeling works in the literature have focused on modeling the catalytic reactor. Of the limited works that develop more comprehensive models by incorporating other major process units, none have developed a complete sulfuric acid plant model. Moreover, the effect of uncertainty in key operating parameters on the plant performance has not been considered. Thus, there is great motivation for developing a comprehensive model that includes all components of the industrial-scale sulfuric acid plant, including its utilities, to explore the economic and environmental benefits of alternative operating conditions. This topic is addressed fully in chapter 4.

Chapter 3: Design of an Explicit Model Predictive Controller using ARO

In this chapter the proposed framework for Explicit MPC using ARO is presented. It begins with the reformulation of the deterministic linear MPC optimization problem presented in Section 2.1.1 into the robust problem that is considered in this work. Afterwards, a detailed description of ARO is provided and is followed by the development of the aro-MPC framework and a comparison to mp-MPC. Finally, computational experiments consisting of three case studies are presented to demonstrate the features of the proposed framework.

3.1 Robust State-Space Model for Linear MPC

The present research work considers only those systems having all states as measurable variables, i.e. $\mathbf{C} \in \mathbb{R}^{\mathrm{N_x x N_x}}$ is an identity matrix. Thus, equation (1c) is not presented in future model formulations to simplify the analysis. Moreover, the following model subject to uncertainty (i.e. robust model) is considered:

$$\hat{\mathbf{x}}_{t+i+1} = \mathbf{A}\hat{\mathbf{x}}_{t+i} + \mathbf{B}\mathbf{u}_{t+i} + \mathbf{D}\mathbf{e}_{t+i+1} \qquad \forall i = 0, \dots, P-1 \quad (3)$$

where $\mathbf{e}_{t+i} \in \mathbb{R}^{\mathrm{N_e}}$ is the vector of uncertain additive time-varying errors between the model and the actual plant, i.e. $\mathbf{e}_{t+i} = \mathbf{x}_{t+i} - \hat{\mathbf{x}}_{t+i}$. Thus, equation (3) replaces equation (1b).

In an online MPC implementation, the newly introduced term above $\mathbf{e}$ is more commonly recognized as a measurable input disturbance $\mathbf{d}$. In the present explicit aro-MPC framework $\mathbf{e}$ is used to capture all sources of error between the state prediction and actual state measurement. This capability has been demonstrated previously in the literature where the additive error was used to represent a variety of modelling uncertainties including nonlinearities and hidden dynamics.[66,67] At the time of obtaining the explicit solution (i.e. solving the ARO problem for the explicit control

laws), $\mathbf{e}_{t+i}$ is assumed to belong to a convex polyhedral set, i.e. $\mathbf{e}^L \leq \mathbf{e}_{t+i} \leq \mathbf{e}^U$. Thus, the modeler is able to estimate *a priori* the bounds on the error between the state predictions obtained from the process model and those measured from the actual plant. When the explicit solution is being implemented online, $\mathbf{e}_{t+i}$ is assumed to be zero in the sampling interval $t+i-1$ when predicting $\hat{\mathbf{x}}_{t+i}$ and its actual realization is evaluated in the sampling interval $t+i$ upon observing the actual state of the system $\mathbf{x}_{t+i}$. This is discussed in further detail in section 3.2.3.

Unlike the typical state-space representation of the input disturbance, which has the same time index as $\mathbf{u}$ (i.e. $\hat{\mathbf{x}}_{t+i+1} = \mathbf{A}\hat{\mathbf{x}}_{t+i} + \mathbf{B}\mathbf{u}_{t+i} + \mathbf{D}\mathbf{d}_{t+i}$), here the time index for the uncertain additive error is the same as the state being predicted, as shown in equation (3). This is done to guarantee that the state predictions of the present aro-MPC formulation are robust estimates for the actual measured states of the process.

Whereas it would act as an initial condition in the online MPC framework, the state of the system $\mathbf{x}_t$ in the present aro-MPC framework will not be observed prior to resolving the problem given that the optimization is being completed offline. Hence, $\mathbf{x}_t$ is also considered as an uncertain (unknown) parameter at the time of solving the explicit aro-MPC problem offline and is assumed to belong to a convex polyhedral uncertainty set: $\mathbf{x}^L \leq \mathbf{x}_t \leq \mathbf{x}^U$.

Equations (1) and (3) with the exception of (1b) are referred to as the robust linear MPC optimization problem. The following section develops the aro-MPC framework out of the robust

linear MPC optimization problem and presents a control policy for online implementation of the explicit solution.

3.2 Framework for Linear Explicit MPC using ARO (aro-MPC)

This section begins with a general overview of ARO and its use in solving uncertain multistage optimization problems. Afterwards, the necessary components for solving the robust linear MPC optimization problem using ARO are presented and they are used to develop the adjustable robust counterpart (ARC), which is a necessary step in the ARO formulation. The procedure for implementing the aro-MPC framework is discussed at the end of this section.

3.2.1 Handling Uncertainty in Linear MPC

There are three approaches to handling uncertainty in MPC.[4,5] The first involves ignoring the uncertainty in the closed loop nominal MPC and accepting its inherent, but limited, robustness. In the second approach referred to as open loop min-max MPC, uncertainty is taken into consideration by identifying a sequence of control actions for a known initial state and uncertainty set such that the states will remain feasible for any disturbance sequence that materializes. In the last approach, feedback min-max MPC considers the system as a closed loop subject to realizations of the uncertain parameter and optimization occurs over a sequence of control laws rather than control actions. In pursuing the latter approach, the robust linear MPC optimization problem can be considered as a multistage optimization problem. In this work, adjustable robust optimization (ARO) is used to obtain the feedback min-max MPC solution offline. As with the change from open loop to feedback min-max MPC,[4] searching for the robust solution using ARO as opposed to SRO reduces its conservativeness, which makes the present aro-MPC approach attractive.

3.2.2 Developing the ARC for the Robust Linear MPC Optimization Problem

As it applies to the robust linear MPC optimization problem the key decisions that the modeler must make to solve the problem using ARO are:

- Identify the uncertain parameters and their corresponding uncertainty set.
- Define the parametric representation for the "wait-and-see" decision variables.

As mentioned above, the parameters in the uncertain linear MPC optimization problem being considered as uncertain are the initial state of the system $\mathbf{x}_t$ and the additive time-varying uncertain error $\mathbf{e}_{t+i}$. Those uncertain parameters are recast as functions of primitive uncertain parameters $\boldsymbol{\xi}_{t+i} \in \mathbb{R}^{n_F}$ referred to as factors. The formal definitions for the factor representations of the original uncertain parameters are as follows:

$$\mathbf{x}_t = \mathbf{x}_t^{\mathrm{Nom}} + \boldsymbol{\Phi}_0 \boldsymbol{\xi}_t \tag{4}$$

$$\mathbf{e}_{t+i} = \boldsymbol{\Phi}_1 \boldsymbol{\xi}_{t+i} \quad \forall i = 1, \dots, P \tag{5}$$

where $\mathbf{x}_t^{\mathrm{Nom}} \in \mathbb{R}^{N_x}$ is the vector of expected values for the states of the process in the first sampling interval, whereas matrices $\boldsymbol{\Phi}_0 \in \mathbb{R}^{N_x \times N_F}$ and $\boldsymbol{\Phi}_1 \in \mathbb{R}^{N_e \times N_F}$ contain user-defined constants relating the primitive factors to the uncertain parameters.

The uncertain factors $\boldsymbol{\xi}$ are assumed to be represented by a bounded factor model. This definition of the uncertainty set has two attractive features when considering application of the framework proposed here to large, real-world systems. Firstly, the factors can capture non-trivial parameter correlations that can readily be identified from historical data.[68] Secondly, the uncertainty set is

polyhedral; thus, it can be easily accommodated into linear ARO. The description of the uncertainty set is as follows:

$$\boldsymbol{\varsigma} = \left\{ \begin{array}{c} \left\{\mathbf{x}_t \in \mathbb{R}^{\mathrm{N_x}}: \mathbf{x}_t = \mathbf{x}_t^{\mathrm{Nom}} + \boldsymbol{\Phi}_0 \boldsymbol{\xi}_t \text{ for some } \boldsymbol{\xi}_t \in \Xi_t; \mathbf{x}^{\mathrm{L}} \leq \mathbf{x}_t \leq \mathbf{x}^{\mathrm{U}}\right\} \\ \left\{\mathbf{e}_{t+i} \in \mathbb{R}^{\mathrm{N_e}}: \mathbf{e}_{t+i} = \boldsymbol{\Phi}_1 \boldsymbol{\xi}_{t+i} \text{ for some } \boldsymbol{\xi}_{t+i} \in \Xi_{t+i}; \mathbf{e}^{\mathrm{L}} \leq \mathbf{e}_{t+i} \leq \mathbf{e}^{\mathrm{U}}\right\} \quad \forall i = 1, \dots, P \\ \text{where } \Xi_{t+i} \text{ is defined as:} \\ \Xi_{t+i} = \left\{\boldsymbol{\xi}_{t+i} \in \mathbb{R}^{\mathrm{N_F}}: \boldsymbol{\xi}_{t+i} \in [-\mathbf{ez}, +\mathbf{ez}], \mathbf{ez}^{\mathrm{T}} \boldsymbol{\xi}_{t+i} \in [-\beta \mathrm{F}, +\beta \mathrm{F}], \beta \in [0,1]\right\} \quad \forall i = 0, \dots, P \end{array} \right\} \tag{6}$$

where $\mathbf{ez} \in \mathbb{R}^{\mathrm{N_F}}$ denotes the vector of ones, F is the number of factors, and the scalar β is a user defined constant in addition to the previously introduced matrices $\boldsymbol{\Phi}_0$ and $\boldsymbol{\Phi}_1$. Thus, the range of the individual primitive factors is limited to $|1|$ and additional information regarding their interdependencies can be used to further reduce their range by reducing the value of β, as shown in (6). Note that the convex polyhedral bounds for $\mathbf{x}_t$ and $\mathbf{e}_{t+i}$ introduced in section 3.1 have also been explicitly included in the uncertainty set description (6). A description of how the uncertainty set is defined is presented in Section 3.3.1.

The control actions are the primary decision variables of interest to be adjustable to the uncertain time-varying error $\mathbf{e}$. However, to maintain equality of the constraints (3) when adjusting the control action based on different realizations of the uncertain parameters, it is necessary to also define the predicted process states as adjustable variables. Several alternative representations for the parametrized function have been proposed by various researchers when developing an ARO framework.[69–71] Affine relationships are often considered in the interest of numerical tractability.[26] Affine functions are used to represent the adjustable variables in this work and they are defined as

follows:

$$\mathbf{u}_{t+i} \leftarrow \boldsymbol{v}_{t+i}^{0} + \sum_{j=t}^{t+P-1} \mathbf{U}_{t+i,j}\boldsymbol{\xi}_{j} \quad \forall i = 0, \dots, P-1 \tag{7}$$

$$\hat{\mathbf{x}}_{t+i} \leftarrow \boldsymbol{\chi}_{t+i}^{0} + \sum_{j=t}^{t+P} \mathbf{X}_{t+i,j}\boldsymbol{\xi}_{j} \quad \forall i = 1, \dots, P \tag{8}$$

where the vectors $\boldsymbol{v}_{t+i}^{0} \in \mathbb{R}^{\mathrm{N_u}}$ and $\boldsymbol{\chi}_{t+i}^{0} \in \mathbb{R}^{\mathrm{N_x}}$ represent the intercepts whereas the elements in the matrices $\mathbf{U}_{t+i} \in \mathbb{R}^{\mathrm{N_u} \times \mathrm{N_F}}$ and $\mathbf{X}_{t+i} \in \mathbb{R}^{\mathrm{N_x} \times \mathrm{N_F}}$ represent the slopes of the respective affine expressions. Thus, the variables $\boldsymbol{v}_{t+i}^{0}$ and $\mathbf{U}_{t+i}$ as well as $\boldsymbol{\chi}_{t+i}^{0}$ and $\mathbf{X}_{t+i}$ replace the original variables $\mathbf{u}_{t+i}$ and $\hat{\mathbf{x}}_{t+i}$, respectively, as the decision variables of the robust MPC optimization problem.

To reduce the conservativeness of the control laws, full recourse is considered in the aro-MPC framework. That is, the adjustable variables are not restricted to be functions of the most recent realizations of the uncertain parameters but rather are allowed to be a function of all previously observed values of uncertainty. Thus, the control action $\mathbf{u}_{t+i}$ and the predicted process state $\hat{\mathbf{x}}_{t+i}$ are both defined as explicit functions of the primitive factors $\boldsymbol{\xi}_{t}, \dots, \boldsymbol{\xi}_{t+i}$. This is reflected in the present framework by including the following non-anticipativity restrictions:

$$\mathbf{U}_{ij} = \mathbf{0} \quad \forall j > i \tag{9}$$

$$\mathbf{X}_{ij} = \mathbf{0} \quad \forall j > i \tag{10}$$

In typical ARO applications a subset of the decision variables is designated as “here-and-now”. In

this work, the ARO method is adapted for the aro-MPC framework so that the first control actions can be computed as affine functions of the first observed state of the process, $\mathbf{x}_t$. Note that the mp-MPC framework is the same in that all control actions are evaluated using measured states of the process. In the present aro-MPC formulation, this is accomplished by solving all of the original decision variables ($\mathbf{u}_{t+i}\ \forall i = 0, \dots P-1$, $\hat{\mathbf{x}}_{t+i}\ \forall i = 1, \dots P$) as adjustable variables, and thus having no "here-and-now" decisions.

3.2.2.1 Formulating ARC

For the robust linear MPC optimization problem defined by equations (1) and (3), excluding (1b), the full ARC is formulated by replacing the adjustable variables with their affine expressions, equations (7) and (8), considering the non-anticipativity restrictions, equations (9) and (10), and incorporating the uncertainty set description (6) to reformulate the uncertain equality and inequality constraints by coefficient matching and dualization, respectively. Note that the adjustable variables in the objective function are only replaced by their respective intercepts and not the complete affine functions. Hence, the resulting solution is robust in its satisfaction of the process constraints, but the objective function is reflective of the expected

rather than the worst-case realization of the uncertain parameters. This was done to avoid the need to dualize the nonlinear objective function which is left for future studies.

Based on the above, the following is the ARC for the equality constraint (3) after coefficient matching:

$$\boldsymbol{\chi}_{t+1}^{0} = \mathbf{A}\mathbf{x}_{t}^{\mathrm{Nom}} + \mathbf{B}\boldsymbol{v}_{t}^{0} \tag{11a}$$

$$\mathbf{X}_{t+1,t} = \mathbf{A}\boldsymbol{\Phi}_{\mathbf{0}} + \mathbf{B}\mathbf{U}_{t,t} \tag{11b}$$

$$\boldsymbol{\chi}_{t+i+1}^{0} = \mathbf{A}\boldsymbol{\chi}_{t+i}^{0} + \mathbf{B}\boldsymbol{v}_{t+i}^{0} \qquad \forall i = 1, \dots, P-1 \tag{11c}$$

$$\mathbf{X}_{t+i+1,j} = \mathbf{A}\mathbf{X}_{t+i,j} + \mathbf{B}\mathbf{U}_{t+i,j} \qquad \forall j = t, \dots, t+i \tag{11d}$$

$$\forall i = 1, \dots, P-1$$

$$\mathbf{X}_{t+i+1,t+i+1} = \mathbf{D}\boldsymbol{\Phi}_{1} \qquad \forall i = 0, \dots, P-1 \tag{11e}$$

Similarly, the following is the ARC for each row $n = 1, \dots, \mathrm{N_x}$ of the lower bound of the uncertain inequality constraint (1e) after dualization:

$$\sum_{j=t}^{t+i} \mathbf{ez}_{\mathrm{F}}^{\mathrm{T}} \mathbf{p}_{t+i,n,j}^{U} + \sum_{j=t}^{t+i} \mathbf{ez}_{\mathrm{F}}^{\mathrm{T}} \mathbf{p}_{t+i,n,j}^{L} + \sum_{j=t}^{t+i} \beta \mathrm{Fy}_{t+i,n,j}^{U} + \sum_{j=t}^{t+i} \beta \mathrm{Fy}_{t+i,n,j}^{L} + \left(\mathbf{x}^{U} - \mathbf{x}_{t}^{\mathrm{Nom}}\right) \mathbf{r}_{t+i,n,t}^{U} + \left(\mathbf{x}_{t}^{\mathrm{Nom}} - \boldsymbol{x}^{L}\right) \mathbf{r}_{t+i,n,t}^{L} + \sum_{j=t+1}^{t+i} \mathbf{e}^{U} \mathbf{r}_{t+i,n,j}^{U} + \sum_{j=t+1}^{t+i} \mathbf{e}^{L} \mathbf{r}_{t+i,n,j}^{L} \leq \boldsymbol{x}_{t+i(n)}^{0} - \mathbf{x}_{(n)}^{L} \qquad \forall i = 1, \ldots, P \qquad (12a)$$

$$\mathbf{p}_{t+i,n,t}^{U} - \mathbf{p}_{t+i,n,t}^{L} + \mathrm{y}_{t+i,n,t}^{U} \mathbf{ez}_{\mathrm{F}} - \mathrm{y}_{t+i,n,t}^{L} \mathbf{ez}_{\mathrm{F}} + \boldsymbol{\Phi}_{0}^{\mathrm{T}} \mathbf{r}_{t+i,n,t}^{U} - \boldsymbol{\Phi}_{0}^{\mathrm{T}} \mathbf{r}_{t+i,n,t}^{L} = -\mathbf{X}_{t+i,t(n)}^{\mathrm{T}} \qquad \forall i = 1, \ldots, P \qquad (12b)$$

$$\mathbf{p}_{t+i,n,j}^{U} - \mathbf{p}_{t+i,n,j}^{L} + \mathrm{y}_{t+i,n,j}^{U} \mathbf{ez}_{F} - \mathrm{y}_{t+i,n,j}^{L} \mathbf{ez}_{F} + \boldsymbol{\Phi}_{1}^{\mathrm{T}} \mathbf{r}_{t+i,n,j}^{U} - \boldsymbol{\Phi}_{1}^{\mathrm{T}} \mathbf{r}_{t+i,n,j}^{L} = -\mathbf{X}_{t+i,j(n)}^{\mathrm{T}} \qquad \forall j = t+1, \ldots, t+i \quad \forall i = 1, \ldots, P \qquad (12c)$$

$$\mathbf{p}_{t+i,n,j}^{U}, \mathbf{p}_{t+i,n,j}^{L}, \mathbf{r}_{t+i,n,j}^{U}, \mathbf{r}_{t+i,n,j}^{L} \geq \mathbf{0} \qquad \forall j = t, \ldots, t+i \quad \forall i = 1, \ldots, P \qquad (12d)$$

$$\mathrm{y}_{t+i,n,j}^{U}, \mathrm{y}_{t+i,n,j}^{U} \geq 0 \qquad \forall j = t, \ldots, t+i \quad \forall i = 1, \ldots, P \qquad (12e)$$

where $\mathbf{p}_{t+i,n,j}^{U}, \mathbf{p}_{t+i,n,j}^{L} \in \mathbb{R}^{\mathrm{N_F}}$, $\mathbf{r}_{t+i,n,j}^{U}, \mathbf{r}_{t+i,n,j}^{L} \in \mathbb{R}^{\mathrm{N_y}}$, and $\mathrm{y}_{t+i,n,j}^{U}, \mathrm{y}_{t+i,n,j}^{L} \in \mathbb{R}$, $\forall n = 1, \ldots, \mathrm{N_x}$, $\forall j = t, \ldots, t+i$, $\forall i = 1, \ldots, P$. In equations (12a) to (12e), $\mathbf{a}_{(n)}$ and $\mathbf{A}_{(n)}$ are general representations used to denote the n[th] element of vector $\mathbf{a}$ (a scalar) and the n[th] row of a matrix $\mathbf{A}$ (a row vector), respectively. The complete ARC for the robust linear MPC optimization problem can be found in Appendix A. For a complete description on formulating the ARC the reader is referred to other sources.[47]

3.2.3 aro-MPC Framework Implementation

The full ARC of the robust optimization problem defined by equations (1) and (3), excluding (1b),

is solved offline. In this work, the optimization solver IPOPT was used to identify the optimal solution. Note that the process is assumed to be in continuous operation. Thus, the state of the system is not explicitly considered at the time of solving the ARC to obtain the explicit control laws. Rather, any known state of the system at the time of solving the ARC is only implicitly considered since it is used as an estimate for $\mathbf{x}_t^{\mathrm{Nom}}$. The inputs to solve the ARC are $\mathbf{x}_t^{\mathrm{Nom}}$, the typical information required to solve the deterministic optimization problem defined by equations (1) with the exception of the initial state of the system, i.e. M, P, $\mathbf{q}$, $\mathbf{w}$, $\mathbf{A}$, $\mathbf{B}$, $\mathbf{C}$, and $\mathbf{D}$, and a fully defined uncertainty set $\boldsymbol{\varsigma}$, as shown in (6).

A timeline for solving offline the full ARC and implementing the explicit solution is presented in Figure 2. The sampling interval in which the first control law of the explicit solution is to be implemented is defined as t. The modeler must begin solving the ARC at an offline time t_{sol1} where the requirement is that the difference between t_{sol1} and t be greater than or equal to the time required to solve the ARC. At t_{sol1} an estimate of $\mathbf{x}_t^{\mathrm{Nom}}$ is required. The estimate can be obtained using the current state of the system. The number of affine expressions obtained as control laws, equations (7), is the same as the control horizon (M) defined by the modeler. Moreover, the control laws are implemented in sequence in a time-varying manner. Thus, at sampling interval $t + M - 1$ the final control law is implemented and another explicit solution is required to continue controlling the process at sampling interval $t + M$. Therefore, the ARC must be solved once again

at an offline time t_{sol2} before $t + M$, as shown in Figure 2.

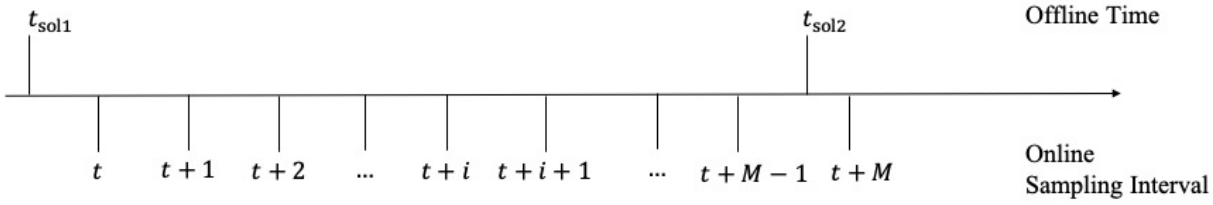

Figure 2. Key timepoints for the aro-MPC framework: $\boldsymbol{t_{sol1}}$ and $\boldsymbol{t_{sol2}}$, offline times for obtaining the explicit solution, $\boldsymbol{t}$ and $\boldsymbol{t + M}$, the sampling intervals for implementing the first control law in the sequence, and $\boldsymbol{t + M - 1}$ the sampling interval for implementing the final control law in the sequence.

The online implementation of the resulting control laws is presented in Table 1. It is assumed that the control laws for time interval t to $t + M - 1$ are available by solving the full ARC formulation at t_{sol1}, referred to as ARC Solution 1. Thus, at the sampling interval t the state of the system $\mathbf{x}_t$ is measured and compared to the expected state $\mathbf{x}_t^{\text{Nom}}$ to obtain the factor realization $\boldsymbol{\xi}_t$ using equations (4). The control action $\mathbf{u}_t$ and the predicted state of the system $\hat{\mathbf{x}}_{t+1}$ are calculated using their respective affine functions, equations (7) and (8), as obtained in ARC Solution 1. For the latter, $\boldsymbol{\xi}_{t+1}$ is assumed to be 0 as it has not yet materialized. $\hat{\mathbf{x}}_{t+1}$ can be seen to be a function of $\boldsymbol{\xi}_{t+1}$ as per equation (11e) where the slope $\mathbf{X}_{t+i+1,t+i+1}$ has not been eliminated by the non-anticipativity restriction, equation (10). This occurs as a result of the uncertain time-varying error having the same time index as the state being predicted in the original robust model as shown in equation (3). The procedure for the sampling intervals $t + 1$ to $t + M - 1$ is the same with the exception that comparison of the actual and predicted states of the system, $\mathbf{x}_{t+i}$ and $\hat{\mathbf{x}}_{t+i}$, respectively, is performed using equations (5) instead of (4). As discussed in Section 3.2.2, full recourse is considered in the present aro-MPC framework. Thus, the control law is a function of

all uncertain parameters materializing, starting from the first sampling interval in which the current ARC Solution was applied. Before the systems reaches $t + M$, a second ARC formulation needs to be resolved at time t_{sol2} (referred to as ARC Solution 2). Accordingly, when implementing ARC Solution 2 in sampling interval $t + M$, the first control law in the sequence is only a function of the uncertain factor $\boldsymbol{\xi}_{t+M}$, as shown in Table 1.

Table 1. Online implementation of the aro-MPC solution

ARC Solution	1				2
Sampling Interval	t	$t+1$	...	$t+M-1$	$t+M$
Measure	$\mathbf{x}_t$	$\mathbf{x}_{t+1}$		$\mathbf{x}_{t+M-1}$	$\mathbf{x}_{t+M}$
Compare To	$\mathbf{x}_t^{\text{Nom}}$	$\hat{\mathbf{x}}_{t+1}$		$\hat{\mathbf{x}}_{t+M-1}$	$\mathbf{x}_{t+M}^{\text{Nom}}$
Calculate	$\mathbf{u}_t = \boldsymbol{f}(\boldsymbol{\xi}_t)$ $\hat{\mathbf{x}}_{t+1} = \boldsymbol{f}(\boldsymbol{\xi}_t, \boldsymbol{\xi}_{t+1})$	$\mathbf{u}_{t+1} = \boldsymbol{f}(\boldsymbol{\xi}_t, \boldsymbol{\xi}_{t+1})$ $\hat{\mathbf{x}}_{t+2} = \boldsymbol{f}(\boldsymbol{\xi}_t, \boldsymbol{\xi}_{t+1}, \boldsymbol{\xi}_{t+2})$		$\mathbf{u}_{t+M-1} = \boldsymbol{f}(\boldsymbol{\xi}_t, \dots, \boldsymbol{\xi}_{t+M-1})$ $\hat{\mathbf{x}}_{t+M} = \boldsymbol{f}(\boldsymbol{\xi}_t, \dots, \boldsymbol{\xi}_{t+M-1}, \boldsymbol{\xi}_{t+M})$	$\mathbf{u}_{t+M} = \boldsymbol{f}(\boldsymbol{\xi}_{t+M})$ $\hat{\mathbf{x}}_{t+M+1} = \boldsymbol{f}(\boldsymbol{\xi}_{t+M}, \boldsymbol{\xi}_{t+M+1})$

A novel feature of the present aro-MPC framework is that it is guaranteed to remain feasible for any sequence of uncertain parameters of length M belonging to the pre-defined uncertainty set $\boldsymbol{\varsigma}$. Thus, the calculated control laws are such that the observed states of the system over the control horizon M will remain within their bounds, equations (1d). This is a direct consequence of the ARO method and the resulting decision rules for adjustable variables being fully robust for realizations of the uncertain parameter within the user-defined uncertainty set.[26]

3.2.4 Comparison to mp-MPC

Although the mp-MPC and aro-MPC frameworks yield explicit feedback control laws to the linear MPC optimization problem, there are some key differences between the two approaches. The main advantage of the mp-MPC framework is the optimization problem does not have to be resolved for a new explicit solution after an elapsed number of time intervals. Both the aro-MPC and mp-

MPC frameworks require re-optimization if the setpoints of the system change or the modeller wishes to update the uncertainty set. However, to guarantee feasibility, the time-varying nature of the aro-MPC controls laws results in required re-optimization when the sequence of control laws is exhausted, even if the system is at steady-state. In addition to not having to partition the state-space into polyhedral regions, another advantage of the present aro-MPC framework is that controller feasibility is guaranteed, i.e. when evaluated, the control laws are guaranteed to maintain the states of the system within their feasible region for any sequence of uncertain parameters materializing within the user-defined uncertainty set.

3.3 Results

This section presents three case studies that demonstrate the capabilities of the proposed aro-MPC framework. The first case study highlights the effects of the size of the uncertainty set and the length of the control horizon on the CPU time required to obtain the control laws and the resulting controller performance. This is followed by a comparison to online MPC for four disturbance sequences. The second case study considers a 5x5 system to highlight the applicability of the framework to larger systems. In the final case study a linear model is used to approximate a nonlinear plant to demonstrate that the uncertain additive time-varying error can capture error resulting from plant-model mismatch.

3.3.1 Case Study 1

The following single input two state system has been adapted from the seminal work on mp-MPC:[6]

$$\mathbf{x}_{t+i+1} = \begin{bmatrix} 0.7326 & -0.0861 \\ 0.1722 & 0.9909 \end{bmatrix} \mathbf{x}_{t+i} + \begin{bmatrix} 0.0609 \\ 0.0064 \end{bmatrix} \mathrm{u}_{t+i} + \begin{bmatrix} 0.1 & 0 \\ 0 & 0.07 \end{bmatrix} \mathbf{d}_{t+i} \quad \forall i \geq 0 \tag{13a}$$

$$\mathbf{x}_{t+i} \geq -0.5 \qquad \forall i \geq 0 \qquad (13b)$$

$$-10 \leq \mathrm{u}_{t+i} \leq 10 \qquad \forall i \geq 0 \qquad (13c)$$

$$\begin{bmatrix}-0.11\\-0.11\end{bmatrix} \leq \mathbf{d}_{t+i} \leq \begin{bmatrix}0.11\\0.11\end{bmatrix} \qquad \forall i \geq 0 \qquad (13d)$$

The aro-MPC solution is obtained for the above system under the assumption that the plant defined by equations (13a) can be perfectly modeled with the exception of the unmeasurable disturbance **d**. Thus, the following equations are used as a robust model for the plant equations (13a):

$$\hat{\mathbf{x}}_{t+i+1} = \begin{bmatrix}0.7326 & -0.0861\\0.1722 & 0.9909\end{bmatrix}\hat{\mathbf{x}}_{t+i} + \begin{bmatrix}0.0609\\0.0064\end{bmatrix}\mathrm{u}_{t+i} + \begin{bmatrix}1 & 0\\0 & 1\end{bmatrix}\mathbf{e}_{t+i+1} \qquad \forall i = 0, \dots, P-1 \qquad (14)$$

As in the original mp-MPC work, the objective is to regulate the system to the origin. The robust linear MPC optimization problem for this system has the following objective function:

$$PM = \sum_{i=1}^{P}\left(\hat{\mathrm{x}}_{1,t+i}^2 + \hat{\mathrm{x}}_{2,t+i}^2\right) + \sum_{i=1}^{M-1}(\Delta \mathrm{u}_{t+i})^2 \qquad (15)$$

The bounded factor uncertainty set at t_{sol1} has the following representation:

$$F = 2, \beta = 1, \mathbf{\Phi}_0 = \mathbf{\Phi}_1 = \begin{bmatrix}1 & 0\\0 & 1\end{bmatrix}, \ \mathbf{x}_{\mathrm{t}}^{\mathrm{Nom}} = \begin{bmatrix}1\\1\end{bmatrix}$$

Note the definition of $\mathbf{x}_{\mathrm{t}}^{\mathrm{Nom}}$ above only applies to the ARC Solution obtained at t_{sol1}. For future ARC Solutions the final predicted state of the system was used to define $\mathbf{x}_{\mathrm{t}}^{\mathrm{Nom}}$. Thus, $\hat{\mathbf{x}}_{t+M}$ was used as an estimate for the initial state of the system in the first time interval of ARC Solution 2, $\mathbf{x}_{\mathrm{t+M}}^{\mathrm{Nom}}$.

In the three case studies presented in this work, the $\mathbf{\Phi}$ matrices have been considered as identity

matrices. However, it is possible to consider nonzero entries in the off-diagonal elements. This represents the case where there is interaction between the process disturbances and their effects on the system states. As compared to the aro-MPC that does not consider interaction in the process disturbances, for the same uncertainty set, one that considers interaction may require less restriction on the input variables (i.e. relaxed constraints) to achieve a feasible solution.

The remaining parameters for the uncertainty set remained constant for all ARC Solutions.

To explore the effect of the size of the uncertainty set on the controller performance the bounds for $\mathbf{x}_t$ and $\mathbf{e}_{t+i}$ are varied using the parameter $\propto$. For $\mathbf{x}_t$, $\propto$ defines the range around $\mathbf{x}_0^{\mathrm{Nom}}$ whereas for $\mathbf{e}_{t+i}$ this parameter defines the absolute-value norm. Thus, for $\propto = 0.05$, $\mathbf{x}^L = \begin{bmatrix}0.95\\0.95\end{bmatrix}$, $\mathbf{x}^U = \begin{bmatrix}1.05\\1.05\end{bmatrix}$, $\mathbf{e}^L = \begin{bmatrix}-0.05\\-0.05\end{bmatrix}$, and $\mathbf{e}^U = \begin{bmatrix}0.05\\0.05\end{bmatrix}$.

3.3.1.1 aro-MPC Performance Subject to Nominal Disturbance Sequence

Figure 3a demonstrates the effects of controller horizon (*M*) and size of the uncertainty set on the performance of the resulting explicit controller as defined by the Performance Metric (*PM*) which is evaluated using equation (15). Thus, *PM* is evaluated *a posteriori*, i.e. at the end of the period under consideration using the actual measured states of the system and implemented control actions rather than when obtaining the explicit solution. The period under consideration consists of 100 time intervals. Note that the results presented in this case study initially assumed that the disturbance is assumed to materialize at its nominal value in each time interval. Consequently, the uncertain primitive factors also materialize at their nominal value. Figure 3b presents the average CPU time needed to solve the ARC of the robust linear MPC optimization problem (i.e. for the

controller having a control horizon (M) of 2, the optimization problem was solved 50 times in order to obtain 100 total time varying control laws).

In Figure 3a, it can be observed that for $\propto = 0.05$ the *PM* is reduced by 42.8% by increasing the control horizon from 2 to 20, respectively. Beyond a control horizon of 20, the improvement in performance is negligible as the *PM* only reduces by a further 1.3% at a control horizon of 50. For the $\propto$ values of 0.1, 0.2, and 0.3 the minimum *PM* occurs at control horizons (M) of 8, 2, and 2, respectively. Thus, the existence of an optimal control horizon for a particular size of the uncertainty set is expected. Figure 4 presents a sample comparison of two aro-MPC controllers, both with $\propto = 0.1$. This figure aims to highlight the cause of increasing *PM* value when the control horizon is increased beyond that resulting in the minimum *PM*. Figure 4a and Figure 4b show the state trajectory and sequence of control actions for the aro-MPC with $M = 8$ whereas Figure 4c and Figure 4d are for the aro-MPC with $M = 10$. As shown in these figures, the former controller achieves the minimum *PM*. Figure 4a demonstrates that the former aro-MPC is able to achieve the setpoint within the 100 time intervals whereas Figure 4b shows that the manipulated variable reaches a new steady-state under a nominal disturbance. For the aro-MPC with $M = 10$ a steady-state offset for the second state (x_2) results as shown in Figure 4c. The cause of this is the additional uncertainty that the solution must accommodate when the control horizon is extended by two additional time periods (i.e. the change from $M = 8$ to $M = 10$) in the aro-MPC formulation, which results in the control actions not achieving a steady-state value of 0 as shown in Figure 4d. Hence, the increasing *PM* when the control horizon is increased beyond the value resulting in the minimum *PM* can be interpreted as the price of robustness. In order to guarantee constraint satisfaction under uncertainty in the system states, the aro-MPC must admit a degree of offset.

However, the controllers with steady-state offset still have the advantage of the aro-MPC framework in that the resulting explicit solutions are guaranteed to remain feasible for any realization in the bounded set of the states.

As shown in Figure 3b, the average CPU time to solve the ARC of the robust linear MPC optimization problem increases as a function of the control horizon and the size of the uncertainty set. The effect of the control horizon on the offline CPU time is expected because the number of constraints and decision variables in the ARC formulation increases as the control horizon increases.

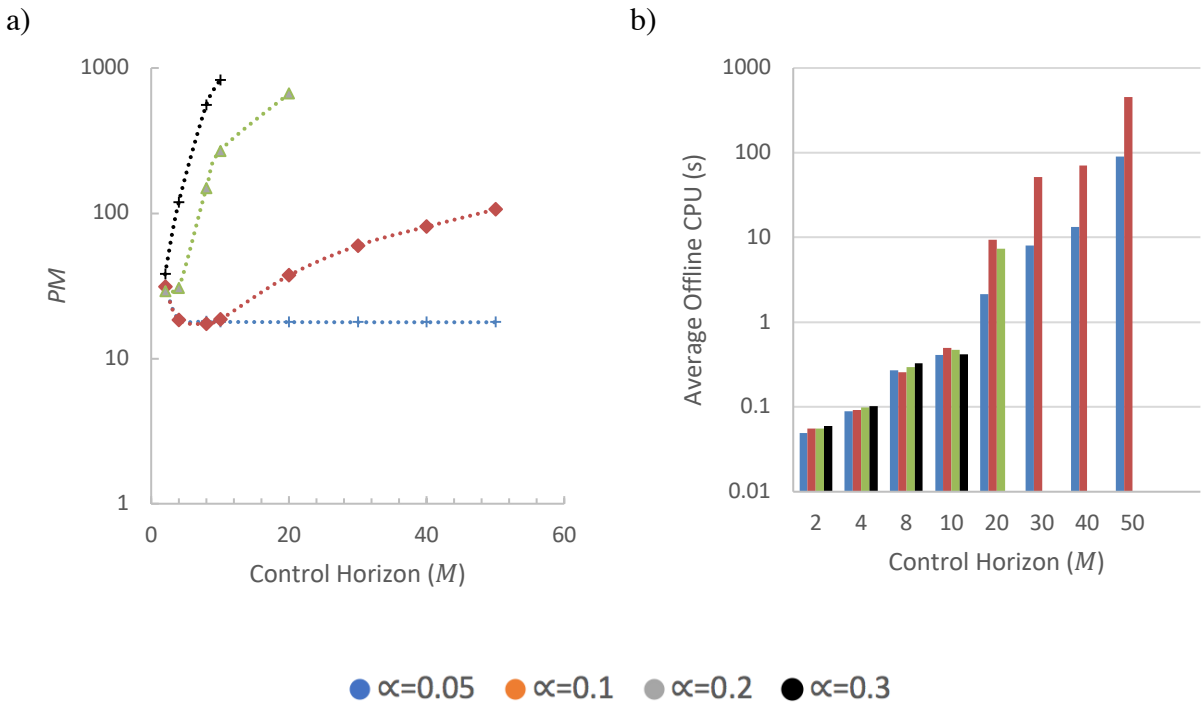

Figure 3. aro-MPC controller for Case Study 1 results for a range of control horizons and uncertainty set sizes: a) PM between the observed states and the setpoint, and b) average offline CPU (s) required to obtain the sequence of control laws.

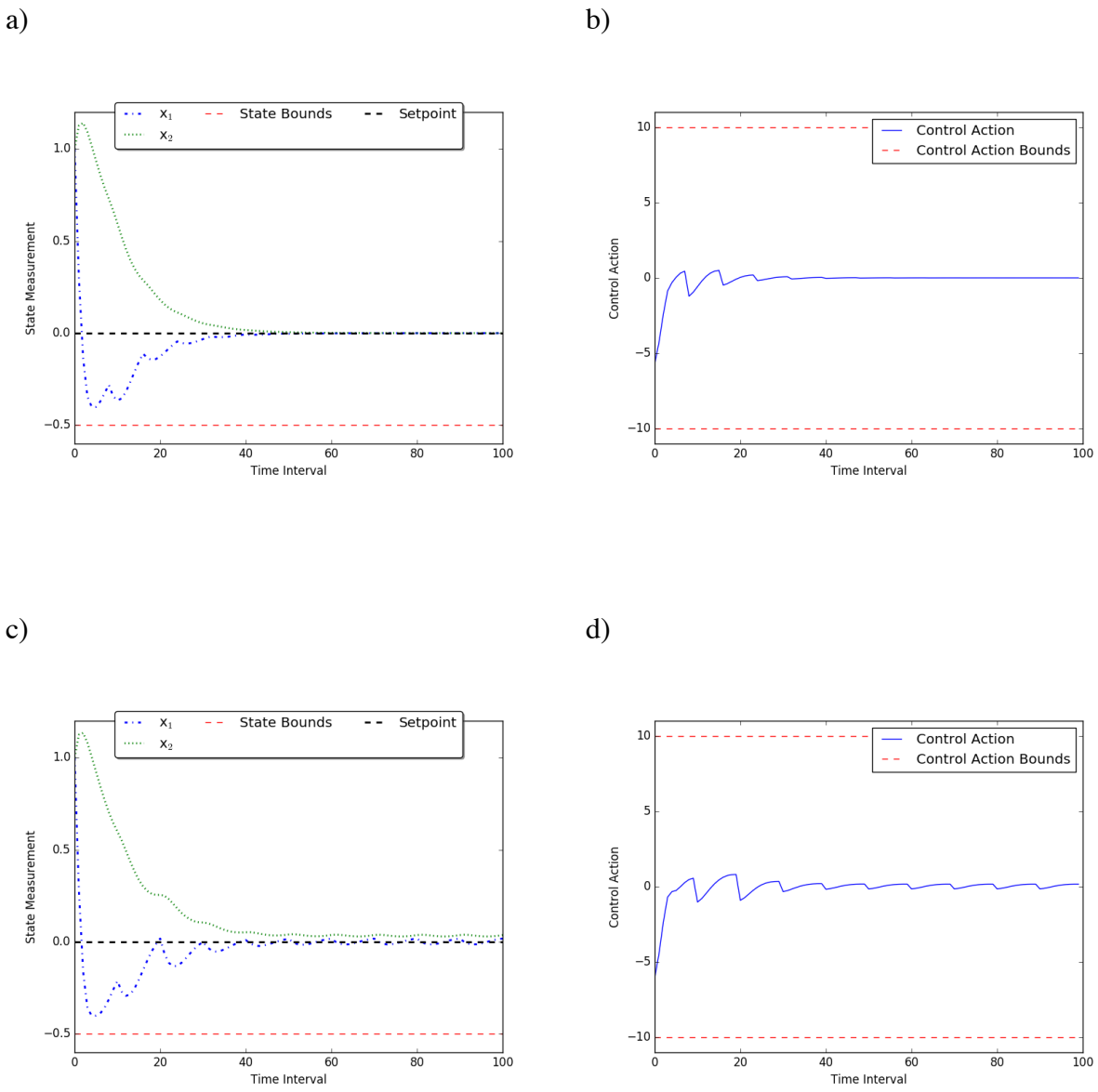

Figure 4. Case study 1: aro-MPC performance ($\propto = 0.1$). a) state trajectory and b) control action profile ($M = 8$); c) state trajectory and d) control action profile ($M = 10$).

3.3.1.2 aro-MPC Disturbance Rejection and Robustness

Unlike Section 3.3.1.1, the scenarios considered in this section did not assume that the complete disturbance sequence materialized at its nominal value. Rather, a variety of disturbance sequences were considered to explore the disturbance rejection capabilities and robustness of the aro-MPC

controller. Table 2 presents the CPU times and objective value for two controllers: an aro-MPC controller with a control horizon of 50 and uncertainty set defined by $\propto = 0.05$ and a standard online MPC controller with a control horizon of 50. Both controllers where simulated under five different disturbance scenarios, as shown in Table 2. The simulation period was set to 100 time intervals. The offline CPU time for the aro-MPC controller is the total computation time required to obtain the explicit solution for the entire period under consideration, i.e. for the aro-MPC controller with $M = 50$, the CPU time that is required to solve the optimization problem twice. For both controllers, the online CPU times are totals for the period under consideration. Thus, for the aro-MPC framework it is the time required to evaluate the complete sequence of control actions whereas for the online MPC it is the cumulative time required to solve the linear MPC optimization problem in each of the 100 time intervals.

Table 2 highlights two key results. Firstly, the aro-MPC controller achieves the desired result of significantly reducing the online CPU time associated with linear MPC. The online CPU time for the aro-MPC is nearly 2 orders of magnitude smaller than that of the standard online MPC. Secondly, the loss in performance in restricting the control actions to be affine and obtaining their coefficients offline is minimal and in some cases results in an improved objective value (i.e. Sc3 and Sc4 in Table 2). As in Section 3.3.1.1, PM is used to evaluate the performance of the resulting controller. As shown in Table 2, for Sc1 and Sc2 a maximum percent improvement of 2.14% is achieved in the online MPC but for Sc3 and Sc4 the aro-MPC improves closed-loop performance by 5.89% approximately. In Sc4, the online MPC experiences a state violation as a result of the linear MPC controller not being robust.

The main feature of the aro-MPC is highlighted in Sc5 that considers random realizations in the disturbances. Closed-loop simulations for Sc5 are shown in Figure 5. For this scenario, 20 random 100-period disturbance sequences are uniformly sampled from the bounded disturbance set shown in equation (13d) and applied to the system in closed-loop. Moreover, the initial states are also randomly sampled from the bounded uncertainty set defined by $\propto = 0.05$. Figure 5a presents the state trajectories when the system is controlled by the online MPC with $M = 50$. As expected, the enlarged section of Figure 5a focusses on time intervals 3 to 10 where the system experiences state violations in 16 out of 20 scenarios. However, Figure 5b demonstrates that when the system is controlled by the aro-MPC with $M = 50$ and $\propto = 0.05$ no state violations occur. Moreover, the average PM improvement achieved by the online MPC as compared to the aro-MPC for the random realizations considered is only 1.70% though it does not comply with state bounds. Thus, the aro-MPC framework proposed here can be considered as a promising alternative to online MPC.

Table 2. CPU time and PM for an aro-MPC with $\propto = \mathbf{0.05}$ and $\boldsymbol{M = 50}$ and an Online MPC with $\boldsymbol{M = 50}$ subject to a variety of disturbance sequences over a 100-period time interval

Scenario	Disturbance Sequence	aro-MPC			Online MPC			Percent Difference PM
		Total Offline CPU (s)	Online CPU (s)	PM	Online CPU (s)	PM	Constraint Violation	
Sc1	Nominal Disturbance	30.93	<0.1	17.77	7.36	17.39	No	2.14%
Sc2	Upper Bounded Disturbance	31.62	<0.1	20.43	6.90	20.00	No	2.10%
Sc3	Low Frequency	31.27	<0.1	19.40	6.97	20.21	No	-4.18%

	(1 time interval) Bounded Disturbance									
Sc4	High Frequency (10 time intervals) Bounded Disturbance	31.47	<0.1	18.66		7.25	19.76*	Yes		-5.89%
Sc5	Random Disturbance Sequences	31.32	<0.1	18.19		7.12	17.88*	Yes		1.70%

*State violation

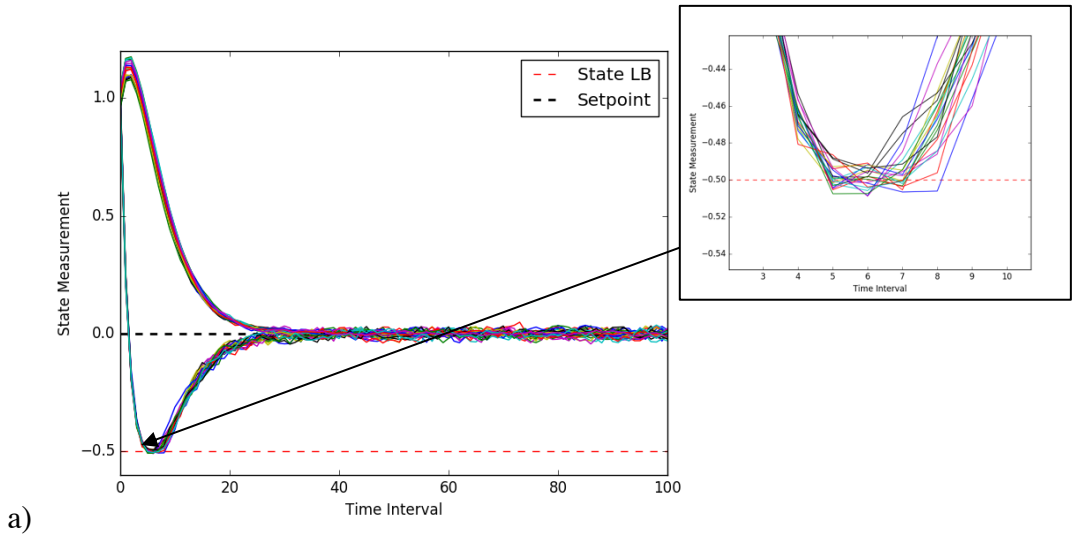

a)

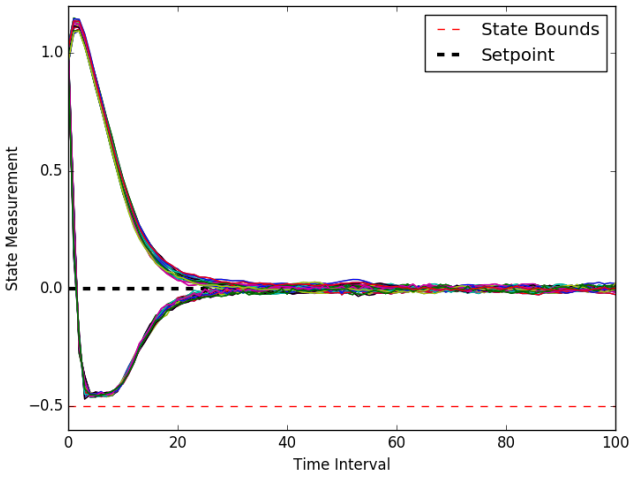

b)

Figure 5. State trajectories for 20 random disturbance sequences. a) online MPC with $\boldsymbol{M = 50}$, with focus on time intervals 3 to 10 to highlight time region where state violations occur, and b) aro-MPC with $\boldsymbol{M = 50}$ and $\boldsymbol{\propto = 0.05}$.

3.3.2 Case Study 2

As in the previous case study, the present case study assumes that the model used to obtain the aro-MPC solution is a perfect approximation of the plant with the exception that the disturbance

is considered to be unmeasurable. The proposed 5x5 plant under consideration is defined by the following robust model and constraints:

$$\hat{\mathbf{x}}_{t+i+1} \qquad \forall i = 0, \dots, P-1 \qquad (16a)$$

$$= \begin{bmatrix} 0.7326 & -0.0861 & 0.0009 & 0.0010 & -0.0385 \\ 0.1722 & 0.9909 & 0.0700 & -0.1500 & 0.0300 \\ 0.0900 & 0.0300 & 0.8500 & 0.0200 & 0.0100 \\ 0.1000 & 0.0500 & -0.0600 & 0.9000 & 0.1300 \\ 0.0200 & 0.0900 & 0.0100 & 0.3000 & 0.7700 \end{bmatrix} \hat{\mathbf{x}}_{t+i}$$

$$+ \begin{bmatrix} 0.70 & -0.08 & 0.01 & 0.20 & -0.04 \\ 0.01 & 0.70 & 0.01 & 0.02 & -0.30 \\ 0.10 & 0.02 & 0.80 & 0.02 & 0.01 \\ 0.05 & -0.02 & 0.15 & 0.90 & -0.04 \\ 0.01 & 0.02 & -0.02 & -0.01 & 0.5 \end{bmatrix} \mathbf{u}_t$$

$$+ \begin{bmatrix} 1 & 0 & 0 & 0 & 0 \\ 0 & 1 & 0 & 0 & 0 \\ 0 & 0 & 1 & 0 & 0 \\ 0 & 0 & 0 & 1 & 0 \\ 0 & 0 & 0 & 0 & 1 \end{bmatrix} \mathbf{e}_{t+1}$$

$$-0.5 \leq \hat{\mathbf{x}}_{t+i} \leq 10 \qquad \forall i = 0, \dots, P \qquad (16b)$$

$$-1.5 \leq \mathrm{u}_{t+i} \leq 1.5 \qquad \forall i = 0, \dots, P-1 \qquad (16c)$$

The purpose of this case study is to test the performance of the aro-MPC by observing how the offline CPU time changes as the system becomes larger and its ability to drive the system states to their respective setpoints. When obtaining the ARC Solution, the uncertain additive error is bounded by the uncertainty set. However, in the present analysis, only the nominal disturbance sequence is considered. The objective in this case study is to drive the states to the setpoint, $\mathbf{r}^{\mathrm{T}} = [0 \quad 1 \quad 0 \quad 0.73 \quad 0.5]$ the weights in the performance function (PM) are $\mathbf{q}^{\mathrm{T}} = [1 \quad 1 \quad 1 \quad 1 \quad 1]$ and $\mathbf{w}^{\mathrm{T}} = [0.1 \quad 0.1 \quad 0.1 \quad 0.1 \quad 0.1]$. The uncertainty set for the above system is defined as follows:

$$F = 5,\ \beta = 1,\ \mathbf{\Phi}_0 = \mathbf{\Phi}_1 = \begin{bmatrix} 1 & 0 & 0 & 0 & 0 \\ 0 & 1 & 0 & 0 & 0 \\ 0 & 0 & 1 & 0 & 0 \\ 0 & 0 & 0 & 1 & 0 \\ 0 & 0 & 0 & 0 & 1 \end{bmatrix},\ \mathbf{x}_t^{\mathrm{Nom}} = \begin{bmatrix} 5 \\ 5 \\ 1 \\ 5 \\ 1 \end{bmatrix}$$

The parameter $\propto$ and M are set to 0.05 and 50, respectively. Note that the nominal measured states ($\mathbf{x}_t^{\mathrm{Nom}}$) considered for this test are significantly far from their corresponding set-points (**r**). Figure 6a demonstrates that the control laws for the present aro-MPC successfully drive the system to the setpoint when the disturbance sequence attains its nominal value. In Figure 6b the average online CPU times for this larger system (CS2) are compared to those of Case Study 1 (CS1) for the same size uncertainty set (i.e. $\propto$=0.05) and control horizons. As shown in this figure, the CPU times for CS2 are larger than CS1 as expected. However, for the largest control horizon considered, the CPU time remains below 200 seconds for CS2. Furthermore, although for the smaller control horizons considered the CPU time was as much as 17 times larger for CS2 as compared to CS1, for the aro-MPC with $M = 50$ the increase in CPU time from CS1 to CS2 was approximately two-fold. The optimization problem under consideration for CS2 was significantly larger than CS1. The former consisted of 161,876 constraints and 639,501 decision variables whereas the latter only involved 16,001 constraints and 60,001 decision variables. Thus, these results show that the proposed aro-MPC framework is attractive to address large-scale systems.

a) b)

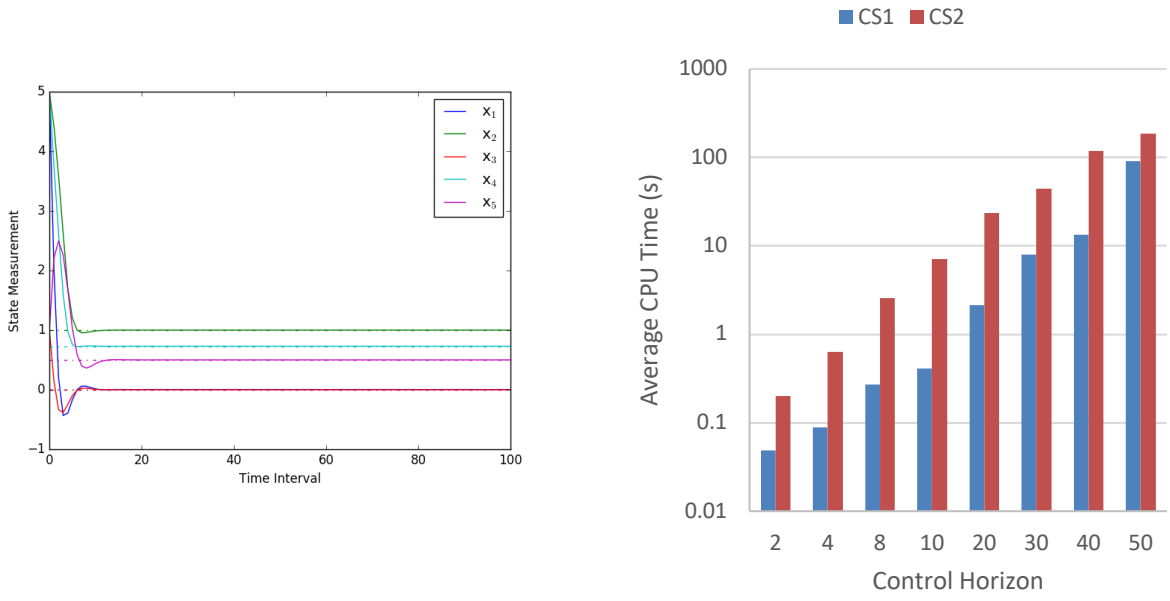

Figure 6. Case Study 2 ($\propto = 0.05$). a) state trajectory over a 100-period time interval, and b) comparison of average CPU times for aro-MPC controllers of varying control horizons for Case Study 1 (CS1) and Case Study 2 (CS2).

3.3.3 Case Study 3

To further demonstrate the implementation of the present framework to an actual application, the performance of the aro-MPC was tested under plant-model mismatch. To perform this test, the following nonlinear plant that describes the changes in the liquid hold-up in a mixing tank with two inlet streams and one outlet stream has been adapted from literature:[72]

$$\frac{dV}{dt} = F_h + F_c - \sqrt{V} \tag{17a}$$

$$0.05\,m^3/h \leq F_h \leq 0.15\,m^3/h \tag{17b}$$

$$0.4925\,m^3/h \leq F_c \leq 1.4925\,m^3/h \tag{17c}$$

$$\mathrm{V} \geq 0.9\ \mathrm{m}^3 \tag{17d}$$

where $\mathrm{F_h}$ represents the flowrate of the hot inlet stream which is an additive disturbance, $\mathrm{F_c}$ is the flowrate of the cold inlet stream, a manipulated variable used for control, and V is the volume of the tank, the state variable. The plant defined by equation (17a) is linearized around the nominal point $\mathrm{V} = 1.19\ \mathrm{m}^3$, $\mathrm{F_c} = 0.9925\ \mathrm{m}^3/\mathrm{h}$, and $\mathrm{F_h} = 0.1\ \mathrm{m}^3/\mathrm{h}$. To implement the aro-MPC framework, $\mathrm{F_h}$ is replaced with e to yield the following linearized discrete process model:

$$\mathrm{V}'_{t+1} = \mathrm{e}_t \Delta t + \mathrm{F}'_{\mathrm{c},t} \Delta t + \mathrm{V}'_t \left(1 - \frac{1}{2\sqrt{\mathrm{V}_0}} \Delta t\right) \tag{18}$$

where Y'_t is the variable Y_t in deviation variables whereas Y_0 represents the variables' nominal point; Δt is the time interval. In addition to capturing the effects of the additive disturbance $\mathrm{F}_{\mathrm{h},t}$, e_t is able to capture the plant-model mismatch resulting from the use of equation (18) to model the plant defined by equation (17a) in the aro-MPC framework.

The ARC is developed for the robust linear MPC optimization problem defined by equations (17c) to (17d) and (18) and has the following objective function:

$$PM_V = \sum_{i=1}^{P} (\widehat{\mathrm{V}}_{t+i})^2 + \sum_{i=1}^{M-1} (\Delta \mathrm{F}_{\mathrm{c},t+i})^2 \tag{19}$$

The uncertainty set for this case study is defined as follows:

$$F = 1,\ \beta = 1,\ \mathbf{\Phi}_0 = \mathbf{\Phi}_1 = [1],\ \mathbf{x}_{\mathrm{t}}^{\mathrm{Nom}} = [1]$$

Thus, the initial state of the plant is assumed to be different from the nominal condition around which the linear model was obtained. To capture the plant-model mismatch, the bounds for e_t are

estimated using the steady-state error between the equations (17a) and (18) after a bounded step change in the control action (F_c) based on the feasible range defined by equations (17b). Thus, to accommodate additional error between the nonlinear plant and the linear model that may result from the uncertain parameter attaining its upper or lower bound, the parameter $\propto$ is set to a value of 0.4.

As was done in Section 3.3.1.2, Figure 7 presents the state trajectories for two controllers subjected to 20 random disturbance sequences and initial state realizations sampled from equation (17b) and the uncertainty set, respectively. Figure 7a presents the results for the online MPC with $M = 25$ and Figure 7b for the aro-MPC with $M = 25$ and $\propto = 0.4$. The average CPU time required to obtain the ARC Solution is 1.05 seconds. The aro-MPC is able to maintain the system in close proximity to the setpoint under a continuous disturbance sequence in F_h. Moreover, it can be seen that the online MPC experiences larger oscillations around the setpoint. This leads to a significant performance improvement in the aro-MPC as measured by PM_V, averaging 17.1% over the 20 sequences considered.

Figure 8 demonstrates the effectiveness of the aro-MPC framework for controlling the nonlinear plant when it is subjected to a series of setpoint changes. As expected, the plant-model mismatch increases as the setpoint deviates farther from the nominal operating point. This can be seen in Figure 8a where the uncertain primitive factor ξ achieves increasing steady-state values, 0.11, 0.12, and 0.22 corresponding to the three setpoints in Figure 8c, 1.5, 1.7, and 2.2, respectively. Moreover, the performance of the controller deteriorates as the offset between the plant and the setpoint increases with each of the setpoint changes. Furthermore, from Figure 8b and Figure 8c it can be seen that the control actions and the state variables always remain within their bounds.

Moreover, the former remained at its upper bound for a small time period when the setpoint changed from 1.7 to 2.2.

Many chemical engineering applications are defined by nonlinear models. Thus, the results of this case study are particularly promising as they indicate that the aro-MPC framework can be applied to nonlinear systems. Moreover, to obtain an explicit controller that performs well, the user must identify a linear model that captures the plant behaviour around a nominal condition.

a) b)

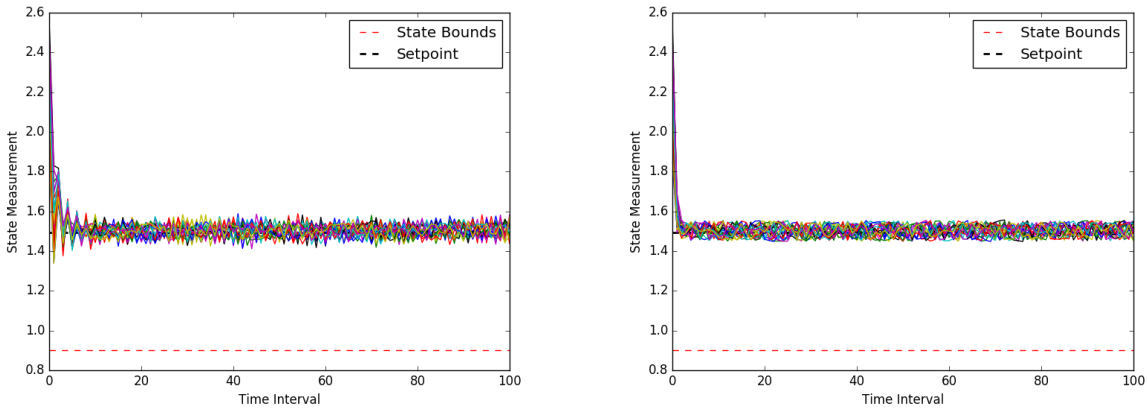

Figure 7. State trajectories for 20 random disturbance sequences. a) online MPC with $M = 25$, and b) aro-MPC with $M = 25$ and $\propto = 0.4$.

a) b)

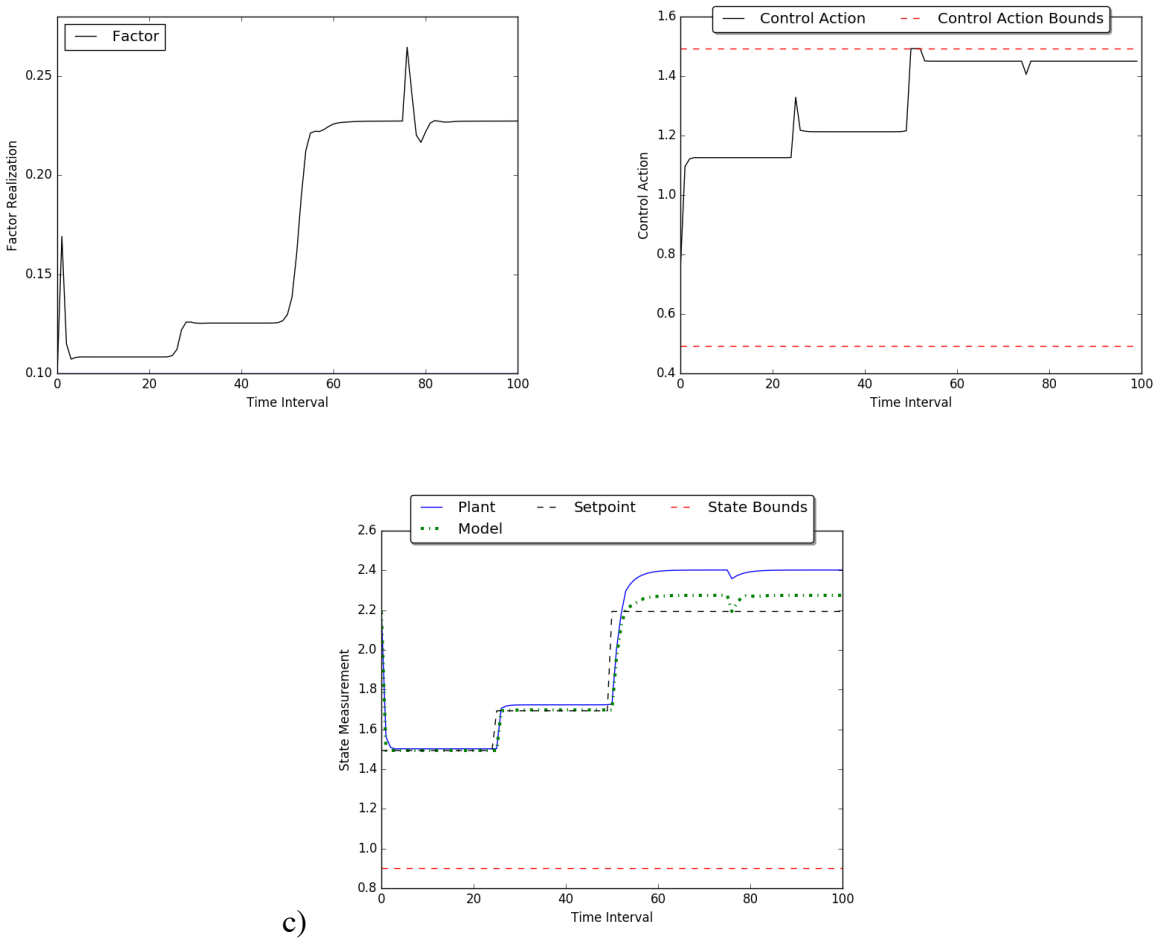

c)

Figure 8. Case Study 3; a) factor realizations and disturbance sequence, b) control action sequence, and c) plant and model state trajectories as well as the user-defined setpoint.

3.4 Summary

The aro-MPC framework is a novel method for Explicit MPC. Its major feature is that the resulting parametrized relationships for the manipulated variables (control inputs) are inherently robust and guaranteed to maintain the state variables within their feasible region without additional considerations. The deterministic linear MPC optimization problem is adapted for the aro-MPC

framework by replacing the input disturbance with an uncertain additive time-varying error. In this framework, the future control actions and predicted states are solved as adjustable variables which are defined as linear functions of the uncertain parameters. The uncertain parameters, the initial state of the system and the additive error, are recast as functions of uncertain primitive factors defined by a bounded factor uncertainty set. By incorporating the definitions of the adjustable variables, the uncertain parameters, and the uncertainty set into the robust linear MPC optimization problem, the user is able to define the full ARC. Performance of the aro-MPC framework was determined to be a function of the control horizon and the size of the uncertainty set. Moreover, the resulting controller was shown to experience a negligible loss in performance as compared to Online MPC with the added benefit of being robust against the user-defined uncertainty set. The final two case studies highlight that the aro-MPC framework CPU time scales well for larger systems and that it is applicable to nonlinear systems.

Chapter 4: Economic Optimization of an Industrial-scale Sulfuric Acid Plant Under Uncertainty

This chapter presents the modeling and economic optimization of an industrial-scale sulfuric acid plant under uncertainty. It begins with a description of the five plant sections that have been incorporated into the process flowsheet model of the single absorption sulfuric acid plant with scrubbing tower. The method used to achieve overall convergence of the flowsheet and the thermodynamic models that were used are also described. The model is validated by comparison with historical plant data and a sensitivity analysis is carried out to identify key process parameters. This culminates in an economic optimization to determine the combination of process parameters that maximizes the daily profit and an uncertainty analysis to understand profit variability.

4.1 Sulfuric Acid Plant Model

The 200-metric ton per day industrial sulfuric acid plant with scrubbing tower, from here on referred to as the *Sulfuric Acid plant*, that was modeled in this study consists of five process flowsheets that are connected as shown in Figure 9. The design and operating specifications of the key process units are defined in Table 3. The main purpose of the process gas flowsheet is to generate SO_3 which is absorbed by the process acid flowsheet in the absorption towers and converted into H_2SO_4. The scrubbing tower reduces the concentration of SO_2 in the vent gas stream from the process gas flowsheet to environmentally acceptable levels by reacting it with NaOH and producing a sellable stream of sodium bisulfite (SBS). Heat is dissipated from the process gas flowsheet via steam generation and from the process acid flowsheet using cooling water.

Sections 4.1.1 to 4.1.5 present a detailed description of each of the plant flowsheets and how they were implemented in Aspen Plus. Section 4.1.6 presents the convergence strategy that was used whereas section 4.1.7 presents the thermodynamic package details.

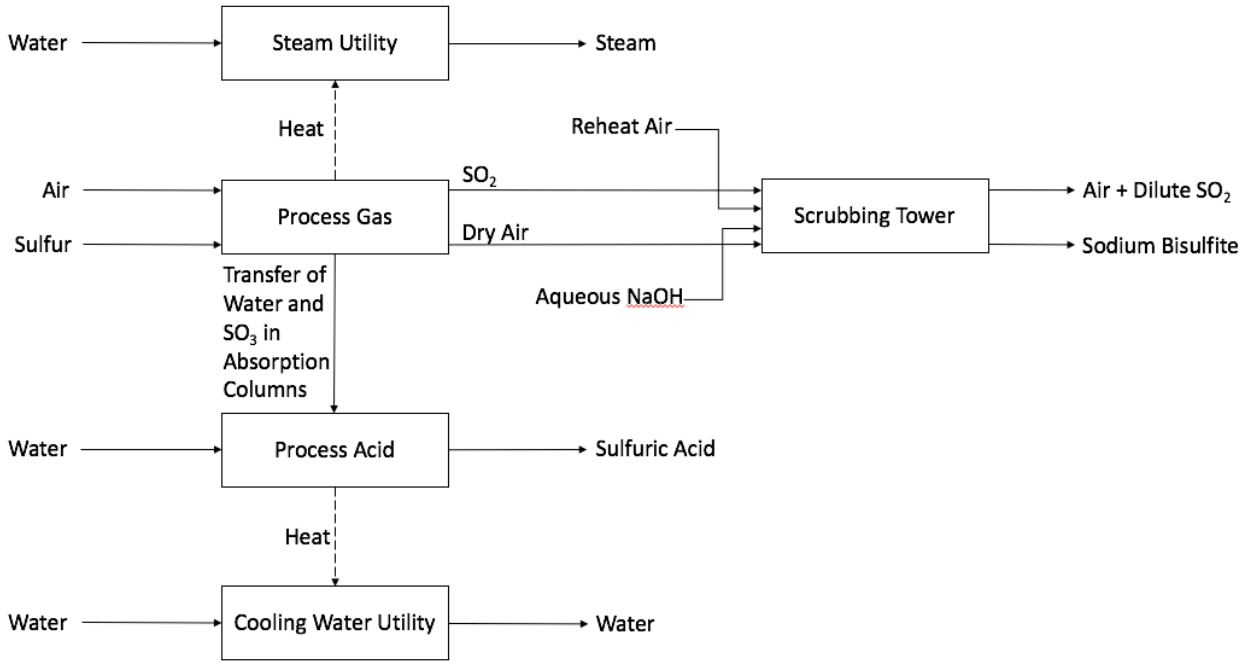

Figure 9. Block flow diagram of the Sulfuric Acid plant.

Table 3. Nominal operating conditions for the main units in the Sulfuric Acid plant

Flowsheet	Equipment Label	Type	Specifications
Process Gas	C-101	absorption column	packing type = raschig ring, raschig torus-saddle, raschig torus-saddle packing size = 75 mm, 50 mm, 25 mm packing height = 0.25 m, 5.49 m, 0.30 m P = 125.49 kPa
	C-102	absorption column	packing type = raschig torus-saddle, raschig super-pak packing size = 50 mm, 250mm packing height = 3.66 m, 0.10 m

			P = 107.30 kPa		
	C-103	absorption column	packing type = raschig ring packing size = 75 mm packing height = 5.13 m P = 104.81 kPa		
	R-101	multi-stage catalytic packed bed reactor	stage	catalytic activity	catalyst volume (L)
			1	2	4800
			2	2.2	6400
			3	8	10000
			4	0.16	9100
	H-101	furnace	P = 122.50 kPa heat duty = 0 kW		
	E-103	heat exchanger	T = 710.93 K P = 117.02 kPa		
	E-104	heat exchanger, hot side	T = 710.93 K P = 113.78 kPa		
	E-105	heat exchanger, hot side	T = 463.71 K P = 108.80 kPa		
Process Acid	E-106	heat exchanger, hot side	T = 310.93 K P = 342.64 kPa		
	E-107	heat exchanger, hot side	T = 327.60 K P = 342.64 kPa		
	E-108	heat exchanger, hot side	T = 325.49 K P = 342.64 kPa		
Scrubbing Tower	E-24	absorption column	packing type = raschig torus-saddle packing size = 50 mm packing height = 3.05 m P = 104.81 kPa pumparound flowrate = 0.57 m^3/min		
	E-25	absorption column	packing type = raschig torus-saddle packing size = 50 mm packing height = 3.05 m p = 101.33 kPa pumparound flowrate = 0.57 m^3/min		
Steam Utility	E-104	heat exchanger, cold side	T = 561.76 K P = 1495.47 kPa		
	E-105	heat exchanger, cold side	T = 469.84 K P = 1447.90 kPa		
	Boiler	Boiler	T = 471.36 K		

			P = 1495.47 kPa
	E-109	Deaerator	T = 388.71 K
Cooling Water Utility	E-106, cold side	heat exchanger, cold side	T = 308.89 K
	E-107, cold side	heat exchanger, cold side	T = 321.88 K
	E-108, cold side	heat exchanger, cold side	T = 303.03 K
	E-110	heat exchanger	T = 300 K

4.1.1 Process Gas Flowsheet

As shown in Figure 10, the process gas flowsheet for the plant consists of a feed preparation step (B-101 and C-101), followed by combustion of sulfur (H-101), then reaction of SO_2 in the multi-stage catalytic packed bed reactor (R-101-1, R-101-2, R-101-3, R-101-4), and absorption of the SO_3 using oleum and concentrated sulfuric acid (C-103 and C-102).

The conversion reaction of SO_2 proceeds as follows:[52]

$$SO_2 + \frac{1}{2}O_2 \leftrightarrow SO_3\,; \qquad \Delta H = -99\frac{\text{kJ}}{\text{mol}} \tag{20}$$

The heat exchangers E-101, E-103, and E-104 cool the process gas thus improving the conversion of SO_2. Similarly, the absorption of SO_3 by sulfuric acid occurs as follows:[50]

$$SO_3 + H_2O \rightarrow H_2SO_4; \qquad \Delta H = -130\frac{\text{MJ}}{\text{kg mol } H_2SO_4} \tag{21}$$

This reaction is highly exothermic and produces fuming sulfuric acid. In order to avoid significant production of this component, a portion of the SO_3 is first absorbed by H_2SO_4 thereby creating oleum:[52,73]

$$H_2SO_4 + SO_3 \rightarrow H_2S_2O_7; \qquad \Delta H = -84 \frac{\text{MJ}}{\text{kg mol } H_2SO_4} \tag{22}$$

The heat exchanger E-105 cools the process gas to improve the absorption of SO_3. More details on this process can be found elsewhere.[50,52]

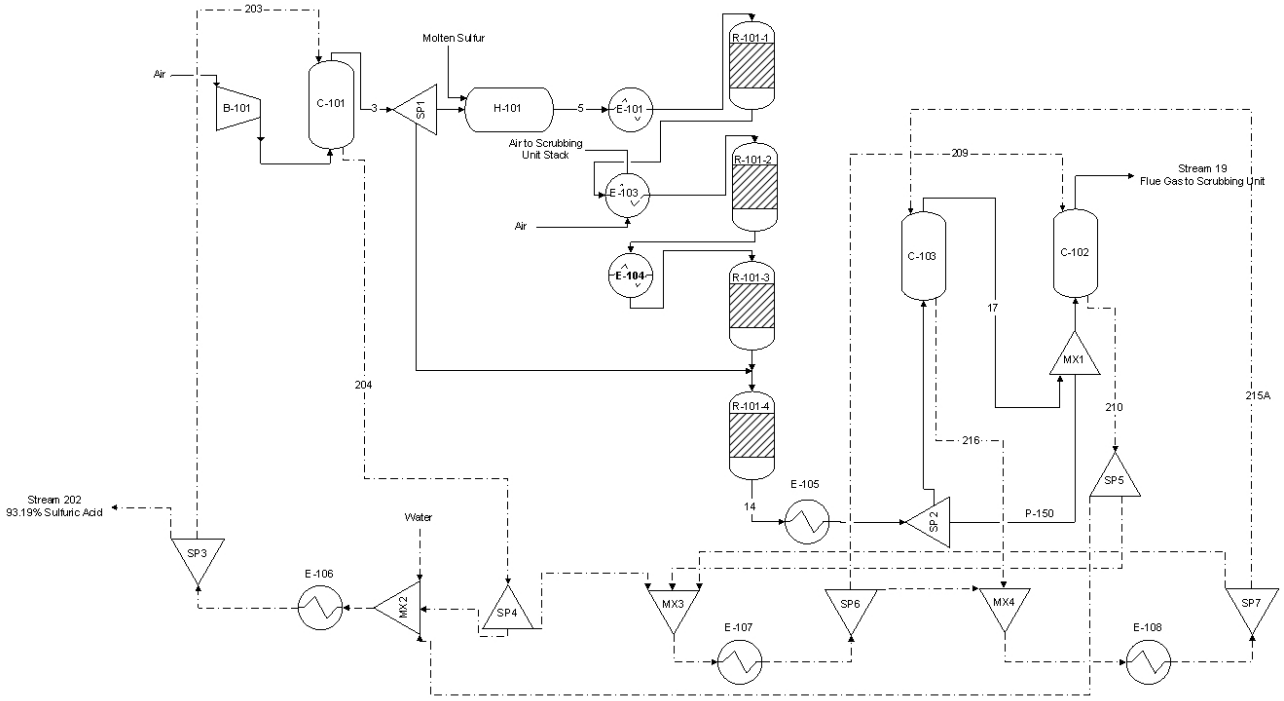

Figure 10. Flowsheet for process gas (solid lines) and process acid (dashed lines).

When compared to the double absorption sulfuric acid plant presented by Bhat et al.,[74] the absorption columns in this work are modeled using the rate-based model as it is known that these provide a more realistic representation of the system behavior as compared to the equilibrium based models.[74,75] The correlation by Bravo and Fair was selected as the mass transfer coefficient method and the Chilton and Colburn correlation was selected as the heat transfer coefficient method.[76,77] The type and quantity of packing in the absorption columns was selected so as to match the industrial sulfuric acid plant for which the present model was developed. The other key

units in the flowsheet shown in Figure 10 are the blower (B-101), the furnace (H-101), and the multi-stage packed bed catalytic reactor (R-101-1, R-101-2, R-101-3, R-101-4). These units were implemented in the same manner as described in the study performed by Bhat et al.[74] The catalytic activity for the different reactor sections was estimated using confidential data provided by the industrial partner.

The highest molar concentration of SO_2 is found at the outlet of H-101 and is referred to as the gas strength. At the nominal operating condition, the gas strength in the Sulfuric Acid plant is maintained at 11.5% by adjusting the sulfur flow rate based on the air flow rate. Although not necessary during the model development process, a design specification was created in Aspen Plus to maintain a gas strength of 11.5% by adjusting the molar flow rate of sulfur when the air flow rate was changed.

4.1.2 Process Acid Flowsheet

The process acid flowsheet for the plant is shown in Figure 10. It is composed of three circuits;[52] the sales acid (C-101, T-101, and E-106), the concentrated sulfuric acid (C-102, T-102, and E-107), and the oleum (C-103, T-103, and E-108). In C-101, the sales acid becomes diluted by the absorption of water from the process gas whereas in C-102 and C-103, the concentrated sulfuric acid and oleum become more concentrated by the absorption of SO_3 from the process gas. To maintain a constant concentration in each circuit they are connected as shown in Figure 10, and a water makeup stream is added. A fraction of the sales acid circuit is continuously sent to the sales acid storage tank. When the acid and oleum streams pass through their respective absorption tower,

their temperature increases. Thus, the heat exchangers E-106, E-107, and E-108 are used for cooling the acid streams prior to entering their respective absorption tower.

4.1.3 Scrubbing Tower Flowsheet

The scrubbing tower flowsheet for the Sulfuric Acid plant is shown in Figure 11. In the absorption tower (E-24 and E-25), the SO_2 in the tail gas from the sulfuric acid plant is absorbed by an aqueous mixture of NaOH as follows:[78]

$$SO_2 + 2OH^- \rightarrow SO_3^{2-} + H_2O \quad (23)$$

$$SO_3^{2-} + H_2O \leftrightarrow OH^- + HSO_3^- \quad (24)$$

The SO_2 in the vapor is further diluted in the exhaust stack (MX4) by mixing with the air from the heat exchanger E-103 and vented to the atmosphere. The liquid product is a sellable stream of SBS.

The absorption column has been modeled as two absorption columns to represent the two sections of identical packing that are separated inside the Sulfuric Acid plant column. Both E-24 and E-25 have individual pumparounds to recycle liquid to the top of the respective packing section. As it was performed for the absorption columns in the process gas flowsheet, the two columns in the scrubbing tower flowsheet are modeled using the rate-based models with the same heat and mass transfer coefficient methods as previously mentioned. The quantity and type of packing was

selected to match the actual plant column's specifications. A calculator was used in Aspen Plus to set the flowrate of NaOH into the scrubbing tower equal to the flowrate of SO_2 entering the column.

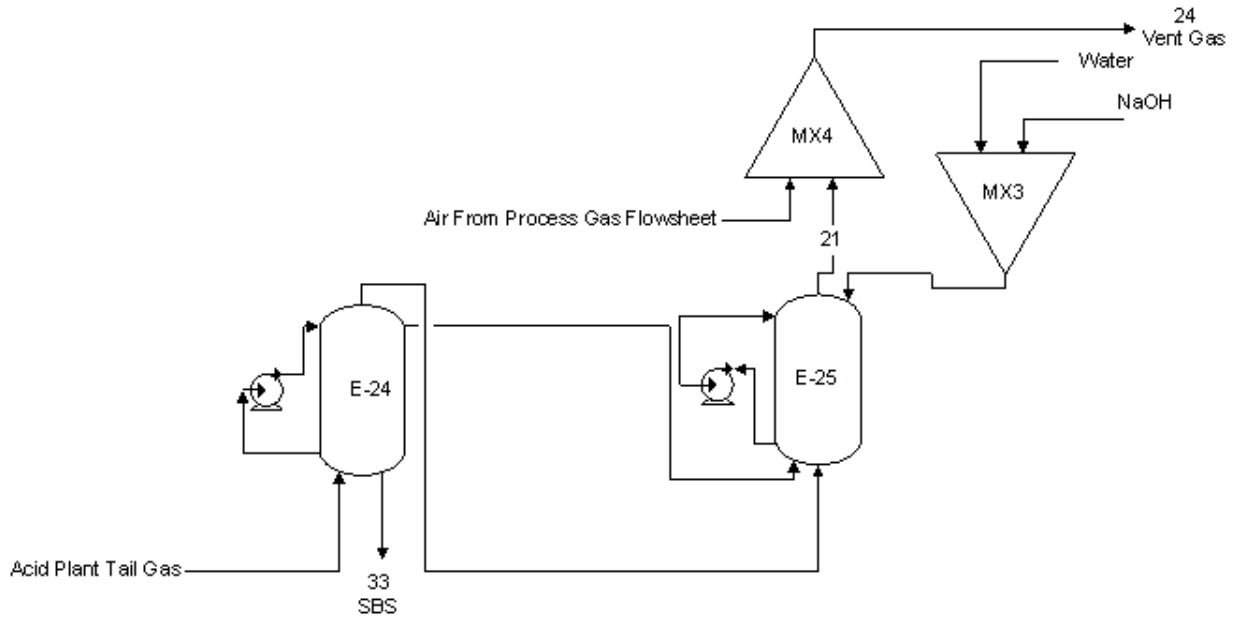

Figure 11. Scrubbing tower flowsheet.

4.1.4 Steam Utility flowsheet

As shown in Figure 12, the main units in the steam utility flowsheet for the Sulfuric Acid plant are the economizer (E-105), the boiler (Boiler), the superheater (E-104), and the deaerator (E-109). In the economizer the boiler feed water is preheated by cooling the process gas stream after exiting the fourth stage of the catalytic packed bed reactor; a small amount of the boiler feed water is vaporized in this process unit. In order to generate saturated steam from the boiler, it was necessary to create a design specification in Aspen Plus which manipulates the flowrate in the makeup water stream so as to achieve a vapor fraction of 0.99 in stream S101B; at the nominal operating condition the makeup water flowrate was 9,105 kg/hr. In the superheater, the steam is superheated by cooling the process gas stream between the second and third stage of the catalytic packed bed

reactor. The purpose of the deaerator is to remove O_2 and CO_2 and to condense a portion of the steam by combining it with condensate and makeup water. As the water in the model was pure, the only purpose for the deaerator was to blend the liquid and vapor stream to produce a stream that is liquid. This was achieved by using a heat exchanger.

The steam that is generated using the heat released by the reactions in the process gas flowsheet is sold elsewhere or used to serve a variety of purposes in the plant, e.g. it is used to power the pump P-109, cool the sulfur gun inside the furnace H-101, recycled for use in the deaerator E-109, and heat the sulfur pit, plant offices, and the oleum storage. A makeup stream of water is required due to losses, such as by degradation or steam sales.

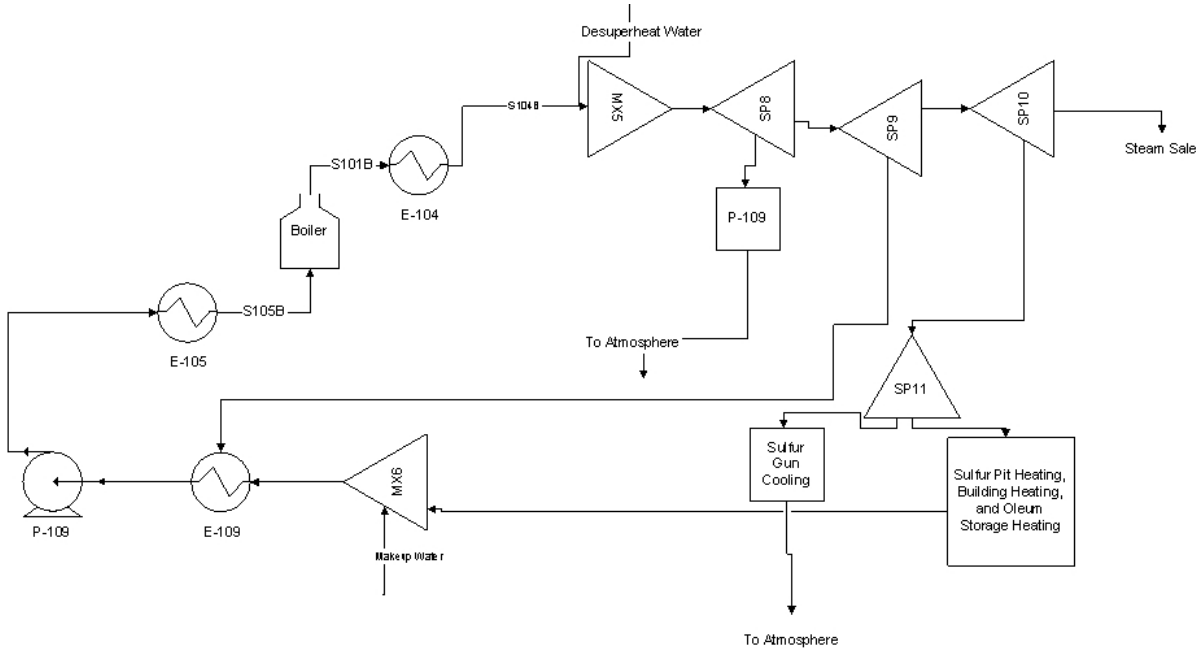

Figure 12. Steam utility flowsheet.

4.1.5 Cooling Water Utility Flowsheet

As shown in Figure 13, the cooling water utility flowsheet for the plant consists of a discharge pump for increasing the pressure of the water (P-110A), the three heat exchangers previously presented in the process acid flowsheet (E-106, E-107, and E-108), and a heat exchanger to reduce the temperature of the cooling water for reuse (E-110). In the Sulfuric Acid plant, E-110 is a cooling tower that uses ambient air as the coolant. A cooling tower can be approximated in Aspen Plus using an absorption column as suggested in previous studies, however due to insufficient air data (temperature and humidity), it was modeled as a heat exchanger.[79] E-110 has a maximum heat duty of 4.39 MW. The make-up water stream is used to replace the water that is released as blowdown, and in the case of the industrial plant, the water that is evaporated in the cooling tower.

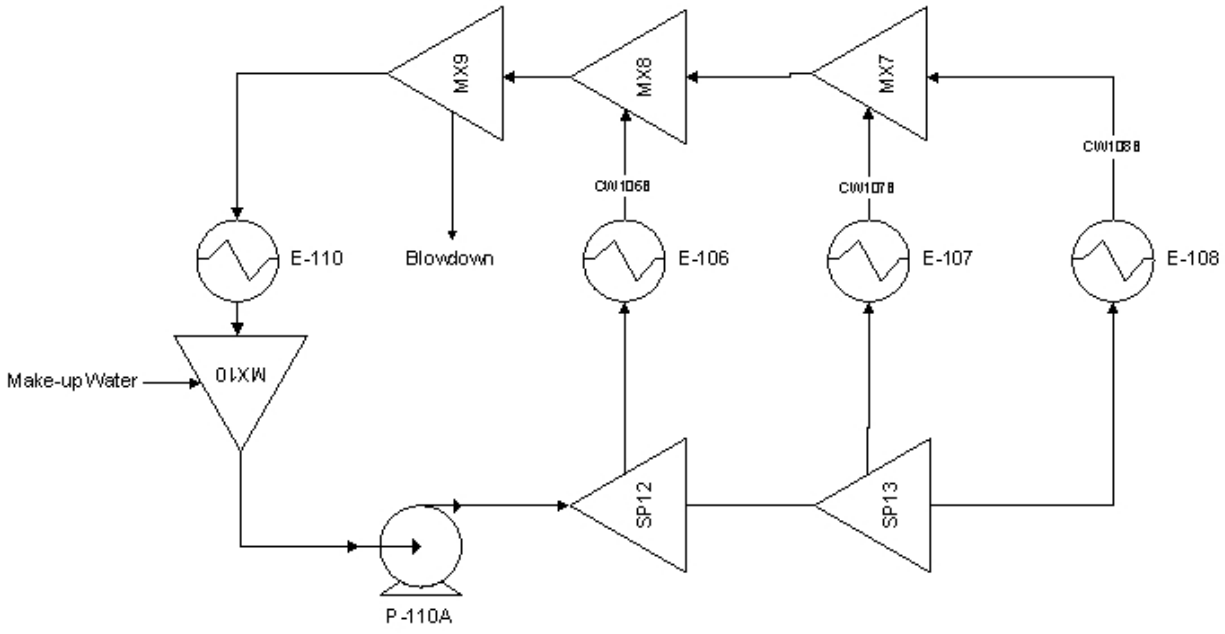

Figure 13. Cooling water utility flowsheet.

4.1.6 Process Flowsheet Implementation

The complete process flowsheet of the Sulfuric Acid plant presented above was developed in Aspen Plus. The plant flowsheet contains many process units, with a significant number of them involving complex solution chemistry. Thus, a strategic approach must be taken in order to achieve complete model convergence. In this work, the first section that was implemented was the process gas flowsheet. That flowsheet cannot be developed independently of the process acid flowsheet as the gas and acid streams are in contact in the absorption columns C-101, C-102, and C-103, as shown in Figure 10. Initially, the only acid streams that were included were those at the inlet and outlet of those columns. Moreover, the absorption columns were first made to converge using an equilibrium-based model available on Aspen Plus.

When the process acid flowsheet was being extended to include the remaining streams and units, it was important to create this highly coupled section one unit at a time in order to establish suitable initial conditions for the connected flowsheet. It was not until this section was fully connected and converged that the model for the absorption columns was switched to a rate-based model in Aspen Plus. This was done so that the equilibrium-based solution could be used as a suitable (educated) initial condition for the more rigorous rate-based model.

The scrubbing tower flowsheet was then added into the plant flowsheet. The two absorption columns E-24 and E-25 also result in a closed loop system so they were first developed in an open loop using the equilibrium-based model. When the section had been fully coupled and made to converge, the model was switched to the rate-based model.

The steam and cooling water utility flowsheets were the final flowsheets to be developed and connected to the plant model. There are no reactions taking place in these flowsheets, therefore it was only necessary to converge the units of each flowsheet in open loop prior to closing the loop.

4.1.7 Thermodynamic Package

Data regarding the thermodynamic properties of the water-sulfuric acid-sulfur trioxide system is widely available in the literature.[80,81] In a previous study, Que et al. combined the results of all these works to develop a comprehensive thermodynamic model for this system by correlating the data over the entire concentration range using the symmetric electrolyte non-random two-liquid (NRTL) model.[82] This is the thermodynamic package used for the sulfuric acid plant developed in this work and it uses the Redlich-Kwong equation of state to model the gas phase. The solution chemistry presented in the work of Que et al. was also adopted in the present analysis and is as follows:

$$H_2SO_4 + H_2O \leftrightarrow HSO_4^- + H_3O^+ \tag{25}$$

$$HSO_4^- + H_2O \leftrightarrow SO_4^{2-} + H_3O^+ \tag{26}$$

$$SO_3 + H_2O \leftrightarrow H_2SO_4 \tag{27}$$

$$SO_3 + H_2SO_4 \leftrightarrow H_2S_2O_7 \tag{28}$$

The liquid phase of the scrubbing tower section does not involve the water-sulfuric acid-sulfur trioxide system but instead an ionic solution, aqueous NaOH. For this section, the thermodynamic model used for the liquid phase was the electrolyte NRTL model and the Redlich-Kwong equation

of state for the gas phase. This model was selected because it is recommended to model ionic systems.[83]

4.2 Results

The accuracy of the Aspen Plus flowsheet model presented in section 4.1 was evaluated during model fitting and validation by comparison with various data points collected from an industrial-scale Sulfuric Acid plant. This was followed by a sensitivity analysis on the design and operating conditions of the plant model to identify those parameters that present the greatest impact on key output variables. An economic optimization was then performed to maximize the daily profit of the Sulfuric Acid plant. Furthermore, the coefficients of the objective function and the catalytic activities in the multi-stage reactor were considered as uncertain variables to evaluate the conditions under which the optimal solution changes.

4.2.1 Model Fitting

Data from the Sulfuric Acid plant were available at three operating conditions; plant configurations that resulted in the highest H_2SO_4 production (OP1), low H_2SO_4 production (OP2), and the production setting for which the plant was originally designed (OPD). The operating condition OPD was used for model fitting because it was the most complete dataset containing the composition, temperature, pressure, and total flowrate of nearly every stream in the plant. The operating conditions OP1 and OP2 were used in section 4.2.2 to validate the model by examining its prediction capabilities.

The catalytic activity in the multistage reactor was used for model fitting. Unlike the design and operating specifications of the plant that are fixed, the expected value for this parameter is not known but it has an acceptable range as outlined by the industrial sponsor. Hence, its true

(expected) value is uncertain. As shown in section 4.2.5, the present plant model is optimized under uncertainty and one of the parameters considered as uncertain is the catalytic activity.

The aim of the steady-state plant model was to capture the Sulfuric Acid plant behavior with reasonable accuracy; this was measured by evaluating the percent error between the Sulfuric Acid plant data at OPD and the model results. Due to the large number of streams in the Sulfuric Acid plant, only percent errors greater than 10% were further analyzed and only the percent error for key streams associated with each process flowsheet are presented in Table 4. Note that blank entries in Table 4 indicate that the particular data point was not available in the Sulfuric Acid plant data or, in the case of the component flowrates for the steam utility and cooling water utility flowsheets, the data points were not required because the streams are pure water.

For the process gas, process acid, and scrubbing tower flowsheets, the key streams were chosen as those exiting a reactor vessel or absorption column. Those units involve changes in temperature and chemical reactions whereas the other process units are limited to changes in temperature, e.g. E-101. The additional complexity of the reactor vessels and absorption columns makes them the most likely to result in errors in the process streams. The only data point available for the liquid in the scrubbing tower flowsheet was the amount of SBS produced. That liquid data and the reactions shown in equations (23) and (24) were used to estimate the amount of NaOH solution used for scrubbing. Due to the incompleteness of the liquid data in the scrubbing tower flowsheet, the percent errors are only calculated for the gas streams. In the steam utility and cooling water utility flowsheets, the key streams were selected as those exiting the heat exchangers where the utility is in thermal contact with the process streams.

As shown in Table 4, there are several streams for which a component flowrate resulted in an error greater than 10%, i.e. the H_2O in streams 210 and 21. In streams 210 and 21 the error in the H_2O content is 15.87% and 10.77% below that reported in the data, respectively. This is caused by water making up a small fraction of each of these streams and the streams being overall low in total flowrate, 210 was 2.57% too low and 21 was 2.35%. In all those cases where there was an error in stream composition larger than 10%, the maximum impact on total stream flowrate was 3.17%. Although an appropriate percent error could not be obtained for the SO_3 flowrate in streams 17 and 19, i.e. the entry for these values in Table 4 is DNA*, the results for these particular data points were validated by the industrial sponsor through their collection of actual plant measurements. The errors in stream composition were deemed acceptable for the purposes of this study as it was assumed that they may not significantly impact the model prediction capabilities, as it is shown in the next sections.

The error in the temperature of streams 204, 210, and 216 had an absolute value between 12.89% and 19.16%. This error can most likely be attributed to the complexity of the solution chemistry as well as the highly coupled nature of the process acid flowsheet. Other areas of the plant model that may be affected by temperature error in the process acid streams are the process gas streams and cooling water utility streams. The only errors in the process gas streams that were larger than 10% were compositional errors and these were identified as insignificant because the impact on overall stream flowrate was no larger than 0.61%. The errors in the temperature of the cooling water were no larger than 5.89%, which was also considered acceptable.

In addition to the previously discussed compositional errors in the scrubbing tower flowsheet, a 9.75% error is observed in the temperature of stream 21. For this stream, the most important data

point is the amount of SO_2 as this will be vented to the atmosphere. The temperature error in stream 21 did not affect the amount of SO_2 in this stream significantly as the error was 1.98%. Furthermore, the error in temperature was reduced to -1.89% after combining with the heated air from the heat exchanger E-103. For these reasons, the temperature error in stream 21 was considered acceptable.

The model shows a few errors that are greater than 10%. Further model fitting cannot be done as this would require adjusting design and operating specifications thereby reducing the validity of the plant model. However, the key results (H_2SO_4 flowrate in stream 202 and SO_2 in streams 21 and 24) are low in error, and thus the overall model is considered to capture the key processing characteristics of the actual Sulfuric Acid plant.

Table 4. Model testing: Sulfuric Acid plant (percent error)

Flowsheet	Stream	Flowrate	Temperature	Pressure	Component Flowrates				
Process Gas (molar)					SO_3	SO_2	O_2	N_2	H_2O
	3	0.00	0.00	0.00	-0.09	0.00	-0.08	2.36	0.00
	5	0.00	-0.66	0.64	-0.09	0.00	-0.08	-2.34	0.00
	14	-0.61	-1.74	1.88	-0.09	0.00	-0.05	0.11	0.00
	17	DNA*	-1.76	1.72	-0.24	0.00	-0.04	3.60	0.00
	19	DNA*	-1.97	3.61	0.31	0.00	0.61	1.91	0.00
Process Acid (mass)					SO_3		H_2SO_4	H_2O	
	202	-2.28	0.00		0.00		-0.32	-1.10	
	204	-2.37	12.89		0.00		-0.42	-1.06	
	210	-2.57	-19.16		0.00		-0.41	-15.87	
	216	-3.17	13.25		-3.10		-4.15	0.00	
Scrubbing Tower (molar)					SO_3	SO2	O2	N2	H2O
	21	0.00	1.98	1.95	-0.10	-10.77	1.95	-0.10	10.77
	24	0.00	1.98	0.36	-0.05	-6.84	0.36	-0.05	6.84

Steam Utility (mass)									
	S101B	-3.22	0.83	3.73					
	S104B	-3.22	3.17	-3.73					
	S105B	0.01	1.54	7.14					
Cooling Water Utility (volumetric)									
	CW106 B	0.29	0.89						
	CW107 B	0.69	0.46						
	CW108 B	0.17	4.92						

DNA*: Data not applicable. The available data were confirmed by the industrial sponsor to be incorrect based on collection of actual plant measurements.

4.2.2 Model Validation

The plant flowsheet model was validated by comparison with the data obtained from the two operating conditions OP1 and OP2. The model validation is presented in Table 5. Due to the non-disclosure agreement with the industrial sponsor the normalized data is presented here along with the associated relative error when compared to the model results.

To simulate the plant at an operating point different from that presented in section 4.2.1, the raw material flowrates and operating conditions need to be adjusted accordingly. For the operating points OP1 and OP2, the flowrate of air entering the furnace was used to set the air flowrate of stream 1. The other raw materials were then adjusted accordingly based on the design specifications discussed in section 4.1. That is, sulfur flowrate was determined based on the 11.5% gas strength, NaOH flowrate in the scrubbing tower was set equal to the incoming flowrate of SO_2 in stream 19, and the flowrate of boiler feed water was set so that the stream at the outlet of the boiler was saturated. For the operating points OP1 and OP2, the temperatures of the process gas at

the inlets of the second and third catalyst packed beds were used to set the outlet temperatures on the process side of the heat exchangers E-103 and E-104, respectively.

The catalytic activities were re-calibrated using the data for OP1 and OP2 so that the model was able to capture the current plant state. The catalytic activities were set so that the packed bed outlet temperatures when simulating OP1 matched the recorded values while ensuring that the range remained reasonable as per the confidential data provided by the industrial sponsor previously mentioned in section 4.1. The catalytic activities remained unchanged when simulating OP2 with the expectation being that the packed bed outlet temperatures will closely resemble the recorded values.

The re-calibrated catalytic activities were good approximations because the outlet temperatures of the first three stages were very similar to those in the data of OP1 and OP2; for OP1 the errors are 0% and this was expected as these temperatures were used to calibrate the catalytic activities but for OP2 the errors are no larger than 1%. The errors entering and leaving the fourth stage are larger at 8% and 4% for OP1 and 4% and 2% for OP2, respectively. This can be attributed to the air in stream 12 insufficiently cooling the process gas at the outlet of the 3rd stage of the reactor. The 10% error in the temperature of superheated steam exiting the heat exchanger E-104 for OP1 and OP2 is related to the outlet temperature of the process gas from the second stage of the reactor. This was considered acceptable because the process side temperatures are the key variables.

The errors in temperature at the midpoint and top of the scrubbing column were between 11% and 21%. The key variable in the scrubbing column is the SO_2 concentration in the vent stream. The industrial sponsor estimates that the SO_2 concentration is below 50 ppm at all operating conditions

based on periodic measurements of this variable offline. This condition was satisfied by the model at operating conditions OP1 and OP2 as the SO_2 concentrations in the vent stream were 37 ppm and 29 ppm, respectively. Based on the above, the model suitably predicts the operation of the Sulfuric Acid plant.

Table 5. Model validation

	Normalized Data		Relative Error	
	OP1	OP2	OP1	OP2
Air Flowrate into Furnace	0.94	0.72	0%	0%
Stage 1 Inlet Temperature	0.44	0.44	-4%	-6%
Stage 1 Outlet Temperature	0.59	0.59	0%	0%
Stage 2 Inlet Temperature	0.43	0.43	0%	1%
Stage 2 Outlet Temperature	0.51	0.51	0%	0%
Stage 3 Inlet Temperature	0.43	0.43	0%	0%
Stage 3 Outlet Temperature	0.47	0.47	0%	1%
Stage 4 Inlet Temperature	0.44	0.45	8%	4%
Stage 4 Outlet Temperature	0.47	0.47	4%	2%
Stream 19 Temperature	0.07	0.07	2%	6%
Temperature of Gas Leaving E-24	0.04	0.04	16%	15%
Temperature of Gas Leaving E-25	0.04	0.04	21%	11%
Production Rate of H_2SO_4	1.00	0.84	-3%	-6%
E-104 Steam Temperature	0.28	0.28	10%	10%

4.2.3 Sensitivity Analysis

The purpose of the sensitivity analysis was to identify the process operating conditions that most affect the flowrate of raw materials, products, and the SO_2 flowrate exiting the vent stack. Excluding air, all other products and raw materials were considered as responding variables during the analysis. Unlike the amount of sulfur and water consumed by the process, which respond based on their respective design specifications in the model, the air consumption is a user decision

variable and does not respond based on changes to other operating conditions. Hence, it was considered as an input during the sensitivity analysis. The NaOH flowrate was not observed during the sensitivity analysis as there are no side reactions involving sodium, and thus the flowrate of NaOH is equivalent to the flowrate of SBS.

For the sensitivity analysis, 13 process operating conditions were considered as inputs and they are listed in Table 6. Each input was varied over six levels between -15% and +15% of its nominal value in increments of 5% to observe any nonlinear interactions between the input and responding variables. The nominal operating condition for the sensitivity analysis was taken to be the midpoint between OP1 and OP2. Although OPD represents the design operating condition of the plant, it does not represent the current nominal operating condition for this plant. The condition of the plant is known to fluctuate between OP1 and OP2, and hence the selection of the nominal operating condition. Note HX34T implies that the outlet temperature on the process side of the heat exchangers E103 and E104 were varied simultaneously. This was done to ensure that the process gas stream remained as the hot stream in both of these heat exchangers. For example, in the case that the outlet temperature of E-103 is reduced to 643 K, the heat generated in the second reactor stage only increases the process gas temperature to 703 K. If the outlet temperature from E-104 remained constant at 711 K, the process gas stream would be heated rather than cooled in that heat exchanger, thus violating its purpose.

Table 6. Process variables considered in the sensitivity analysis

Category	Process Variables	Acronym
Flow Rate	Air Flow	AF
Design Specifications	Gas Strength	GS
	E-24 Recirculation pH	pH

Process Side Outlet Temperature	E-103 and E-104	HX34T
	E-105	HX5T
	E-106	HX6T
	E-107	HX7T
	E-108	HX8T
Packing Height	C-101	PK101
	C-102	PK102
	C-103	PK103
	E-24	PK24
	E-25	PK25

The change in each responding variable with respect to each input variable is shown in Figure 14a to Figure 14. With the exception of the air flow in Figure 14, for all other response lines that cannot be distinguished, the input variables had a near zero effect on the respective responding variables. The only design variable that affected the plant performance was PK25, the packing height in the absorption column E-25. According to the model, the absorption in this column is not as efficient as the other four absorption columns in the plant, and thus changing the packing height has a direct impact on the concentration of SO_2 in the vent stream. As shown in Figure 14f, in the range of -10% to +5% of the design variable PK25 the effect on the SO_2 concentration in the vent stream is insignificant. At a -15% change in PK25 the SO_2 concentration increases in the vent stream and beyond an increase of +10% only minor reductions in SO_2 concentration are observed. The responding variables were insensitive to the other input variables in the packing height category as well as the pH, HX7T, and HX8T. Moreover, HX6T only affected the steam flowrate whereas HX5T affected both the water and steam flowrates. The effect of the input variables on the daily profit of the plant as calculated using (10) is shown in Figure 14g. Based on the results shown in Figure 14a to Figure 14f and subsequently in Figure 14g, the daily profit, the key input variables that were identified in the sensitivity analysis that affect the process performance and process

economics were AF, GS, and HX34T (see Table 6). AF and GS induced a response in all responding variables whereas the sulfur flowrate was the only output that was insensitive to HX34T.

As shown in Figure 14a and Figure 14e, the key input variables have a direct correlation with the water flowrate required and subsequently the steam produced. This is a result of the condition specified in section 4.1.4 that the water flowrate should be such that the stream leaving the boiler has a vapor fraction of 0.99. In Figure 14b it can be observed that the sulfur flowrate is only affected by AF and GS based on the gas strength condition specified in section 4.1.1. As mentioned above, the results for AF in Figure 14b does not indicate that no response was caused in the sulfur flowrate but rather the same response as GS. For the H_2SO_4 and SBS flowrates, Figure 14c and Figure 14d, respectively, AF causes a direct response whereas GS and HX34T result in nonlinear responses. Increases in GS larger than +10% result in no additional H_2SO_4 production but rather an exponential increase in the amount of SBS produced. At a value of HX34T 5% below the nominal there exists a maxima in the H_2SO_4 production and a minima in the SBS produced. The concentration of SO2 vented also resulted in nonlinear responses to the input variables AF, GS, HX34T, and PK25. Due to limited relevant data at the operating conditions considered in the model validation stage, it was not possible to further validate the results presented in Figure 14f. As indicated in section 4.2.2, only periodic offline measurements are taken for this variable. However, at the nominal condition considered for the sensitivity analysis, the concentration of SO2 vented was 18 ppm. From Figure 14f it can be observed that the greatest increase in the concentration of SO2 vented is 5 ppm as a result of reducing GS by 5% from its nominal value. This increases the concentration of SO2 vented to 23 ppm, which is significantly below the 100 ppm maximum limit.

a)

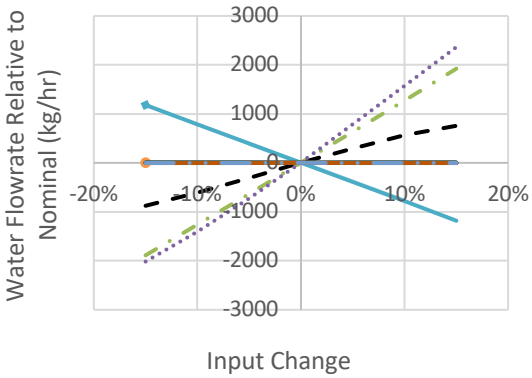
Water Flowrate Relative to Nominal (kg/hr)
3000
2000
1000
0
-1000
-2000
-3000
-20%
-10%
0%
10%
20%
Input Change

b)

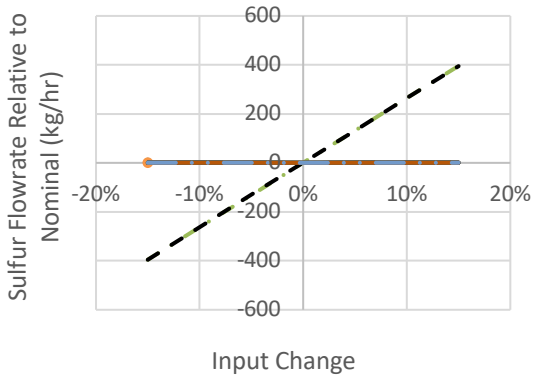
Sulfur Flowrate Relative to Nominal (kg/hr)
600
400
200
0
-200
-400
-600
-20%
-10%
0%
10%
20%
Input Change

c)

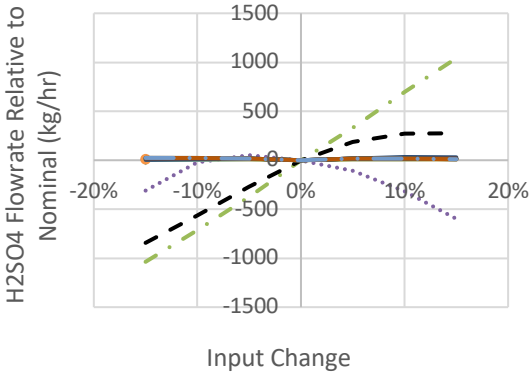
H2SO4 Flowrate Relative to Nominal (kg/hr)
1500
1000
500
0
-500
-1000
-1500
-20%
-10%
0%
10%
20%
Input Change

d)

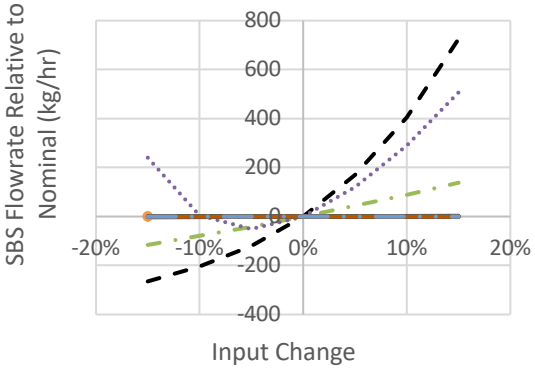
SBS Flowrate Relative to Nominal (kg/hr)
800
600
400
200
0
-200
-400
-20%
-10%
0%
10%
20%
Input Change

e)

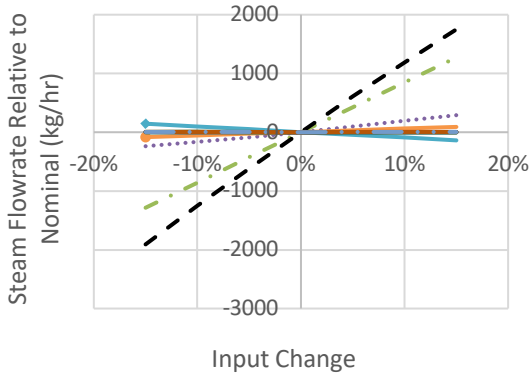
Steam Flowrate Relative to Nominal (kg/hr)
2000
1000
0
-1000
-2000
-3000
-20%
-10%
0%
10%
20%
Input Change

f)

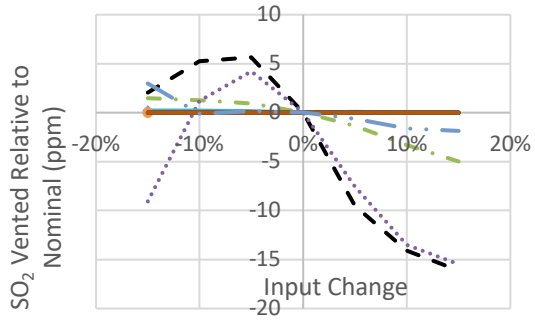
SO2 Vented Relative to Nominal (ppm)
10
5
0
-5
-10
-15
-20
-20%
-10%
0%
10%
20%
Input Change

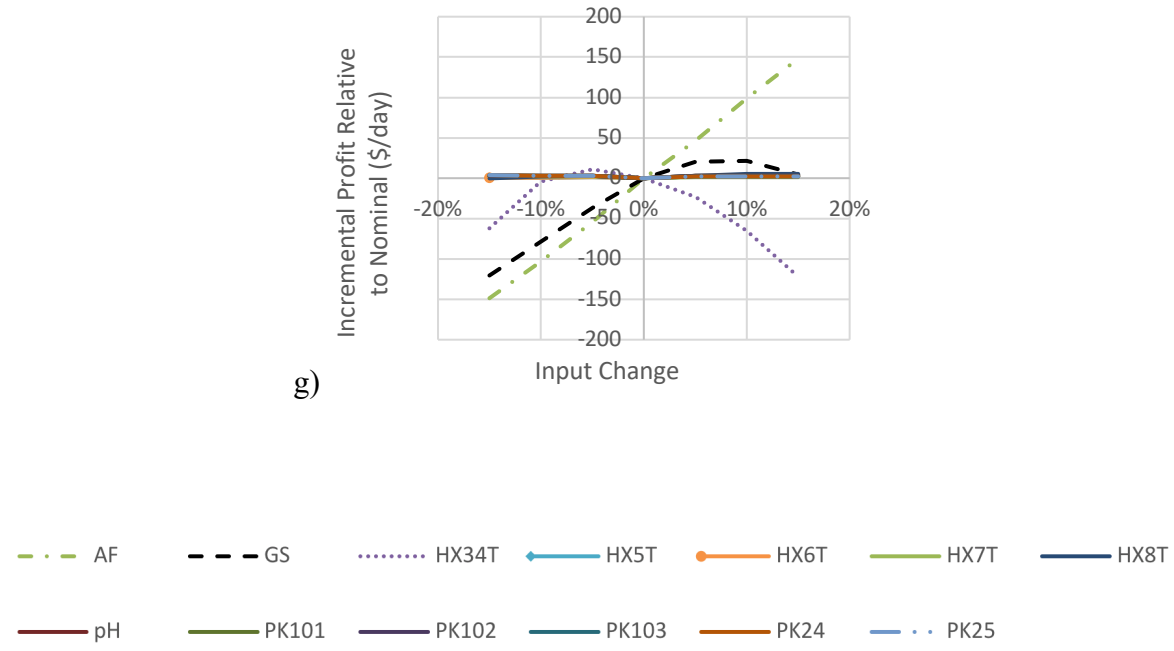

Figure 14. Changes in responding variables with respect to changes in the input variables.

4.2.4 Economic Optimization

The aim of this section is to formulate an optimization problem that can provide insights as to how the key input variables identified from the sensitivity analysis can be adjusted to improve the process economics of this plant. Hence, the objective function aims to maximize the daily profit of the plant by considering the difference in expenses and revenues from raw materials and products, respectively. Note that the objective function considered in this work resembles how the industrial sponsor measures daily profit; other objective functions that take into account other factors can be considered for different applications. The prices of raw materials and products are shown in Table 7.

Table 7. Prices of raw materials and products

Component	Price

H_2SO_4 ($/kg)	0.16
SBS ($/kg)	0.21
Steam ($/kg)	0.014
Sulfur ($/kg)	0.065
NaOH ($/kg)	0.65
Water ($/kg)	0.002

The key input variables identified from the sensitivity analysis are the decision variables of the problem, i.e. AF, GS, and HX34T. The constraints of the optimization problem are the key design and operational limitations of the actual plant, namely the net energy requirement of the blower B-101, the net heat duty of the cooling tower E-110, and the concentration of the SO_2 in stream 24. The blower and cooling tower constraints are based on the design limitation of the respective process unit. The constraint on SO_2 emission concentration is a corporate mandate to which the industrial sponsor adheres in order to produce in an environmentally sustainable manner. Based on the above, the optimization problem considered in this work is as follows:

$$\max_{\xi} \quad \text{Daily Profit} \tag{29}$$

$$= p_{H_2SO_4}\dot{M}_{H_2SO_4} + p_{SBS}\dot{M}_{SBS} + p_{steam}\dot{M}_{steam} - p_{sulfur}\dot{M}_{sulfur} - p_{NaOH}\dot{M}_{NaOH} - p_w\dot{M}_w$$

$$\text{s.t.} \quad \text{Plant Model} \tag{30}$$

$$v_{SO_2,stream\ 24} < 100 \text{ ppm} \tag{31}$$

$$Q_{E-110} < 4.61 \text{ MW} \tag{32}$$

$$W_{B-101} < 0.261 \text{ MW} \tag{33}$$

$$\xi^{LB} < \xi < \xi^{UB} \tag{34}$$

Where:

p_z: price of raw material or product z ($/kg)

$\dot{M}_z$: mass flowrate of raw material or product z (kg/day)

$v_{SO_2,stream\ 24}$: volumetric concentration of SO_2 in stream 24 (ppm)

Q_{E-110}: heat duty of the cooling tower E-110 (MW)

W_{B-101}: net work of the compressor B-101 (MW)

ξ: the set of decision variables, i.e. ξ ={AF, GS, HX34T}

z: component with associated cost (H_2SO_4, SBS, steam, sulfur, NaOH, water)

An alternative objective function considered based on the plant's production target is related to the maximization of the production rate of H_2SO_4 (i.e. MaxProd). To account for this condition, the optimization formulation shown in (29)-(34) can be reformulated by replacing the Daily Profit objective function shown in (29) with the following function:

$$\text{MaxProd} = \quad \dot{M}_{H_2SO_4} \tag{35}$$

The large size of the model led to convergence times on the order of 30 minutes; although considered, Aspen Plus' optimization capabilities may result in highly intensive calculations. Hence, it was necessary to consider solvers outside of the Aspen environment. The implementation of other gradient based optimization methods may be challenging since the explicit plant model equations are not available, i.e. the plant can be considered as a black-box model. Conventional derivative free optimization methods, specifically genetic algorithms (GA), were therefore considered. Difficulties associated with model convergence were encountered as a result of the randomness with which GA selects candidate solutions within the search space; particular combinations of the decision variables may be infeasible for the plant model. Based on these limitations, the generalized pattern search method (GPS)[84] was employed to find a local optimal solution to this problem. This method involves enumerating over the entire search space to identify the locally optimal solution out of the set of candidate solutions. The discrete realizations of the decision variables considered in the sensitivity analysis were used as a basis to define the initial

mesh considered in the optimization. For each of the operating conditions defined by the mesh, the Aspen plant model was simulated, and the relevant data required to evaluate the objective function and process constraints was gathered. The data collected for all the operating conditions were used to perform the GPS optimization.

Figure 15a and Figure 15b show the objective function values at the locally optimal solution for the Daily profit and the MaxProd optimization problems, respectively. The locally optimal operating conditions for both Daily profit and MaxProd are identified as OBJ1 and OBJ2, respectively. Also included is the result for the operating condition OP1 which is considered by the plant operators to be the operating condition that results in the highest production rate of H_2SO_4. The operating condition OBJ1 occurs at GS = 12.075, air flowrate = 2,416 kg/hr, and HX34T = 700 K; the daily profit was $29,985. The operating condition OBJ2 occurs at GS = 12.65, air flowrate = 2,416 kg/hr, and HX34T = 705 K. The figures clearly illustrate that OBJ1 and OBJ2 are local optima for their respective optimization problems. The current maximum daily profit of the plant is $28,989 at the operating condition OP1, ie. AF = 2,373 kg/hr, GS = 11.5, HX34T = 713 K. Changing the operating condition to OBJ1 results in a 3.3% increase in profit. Conversely, if it is desired to achieve maximum plant productivity (i.e. MaxProd), then the operating condition OBJ2 can be selected. At this setting, the profit and the H_2SO_4 production rate are 2.3% and 4.3% higher than at OP1, respectively.

Based on the above, changes are therefore required to move the operating condition of the plant from OP1 to OBJ1 or OBJ2. In order to operate at OBJ1, the air flowrate must be increased by 43 kg/hr, GS must be increased by 0.575 and HX34T must be reduced by 13 K. In addition to increasing the air flowrate by 43 kg/hr, GS must also be increased by 1.15 to move the operating

condition of the plant to OBJ2. This is an indication that the model has good prediction capabilities as the optimal operating points that were identified are relatively close to the best operating condition already observed for this plant. Although this analysis identified that the plant is operating at near optimal conditions (OP1), a more economically optimal operating point can be selected (OBJ1 or OBJ2) for the industrial-scale plant. The improvement in annual profits as compared to the current nominal operating condition is in the order of $243,820 (OBJ2) to $363,540 (OBJ1).

Figure 16 shows the constraint values at the optimal air flowrate. The constraints were fully satisfied in the range of optimal solutions. The net energy requirement of the blower B-101 was 0.208 MW at OP1 and 0.212 MW at all other operating conditions shown. That occurred because the net energy requirement is a direct function of the air flowrate. The optimal air flowrate was the highest that was considered, and thus the constraint is also satisfied at the sub-optimal air flowrates.

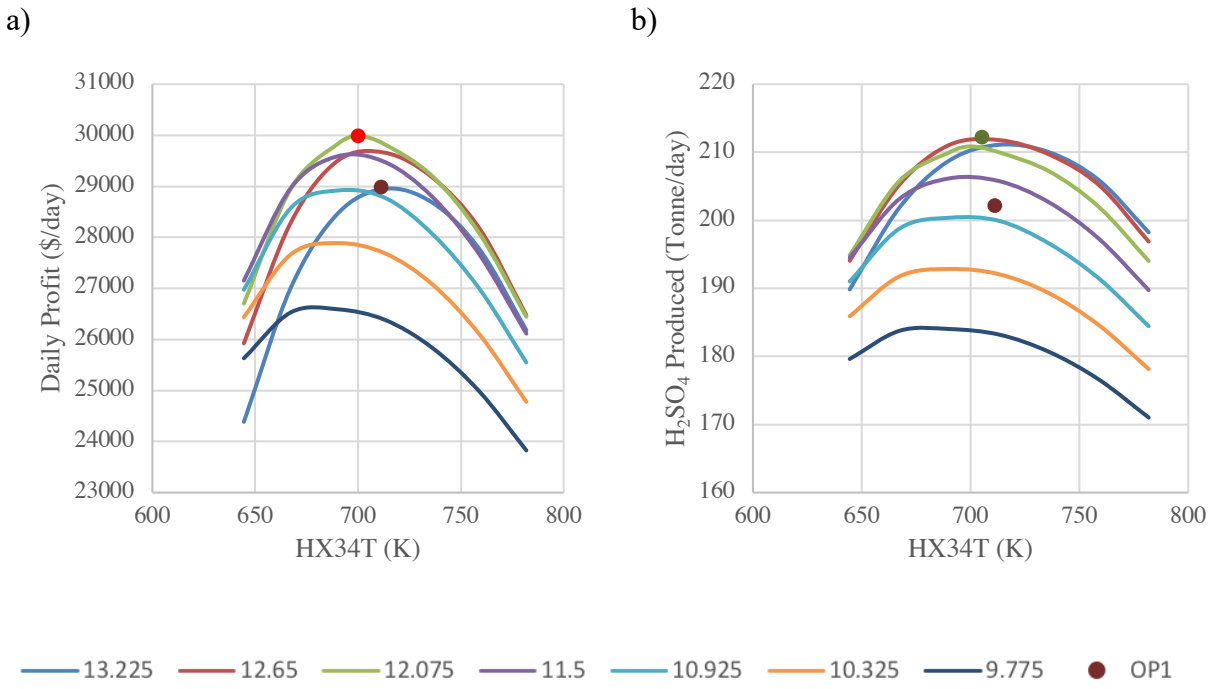

Figure 15. Daily Profit and H_2SO_4 production rate near the optimal point at AF = 2,416 kg/hr, OBJ1 is shown in red and OBJ2 in green; the daily profit obtained at operating condition OP1 has also been included. The different colored trend lines are used to distinguish the gas strengths (GS) evaluated at different operating points.

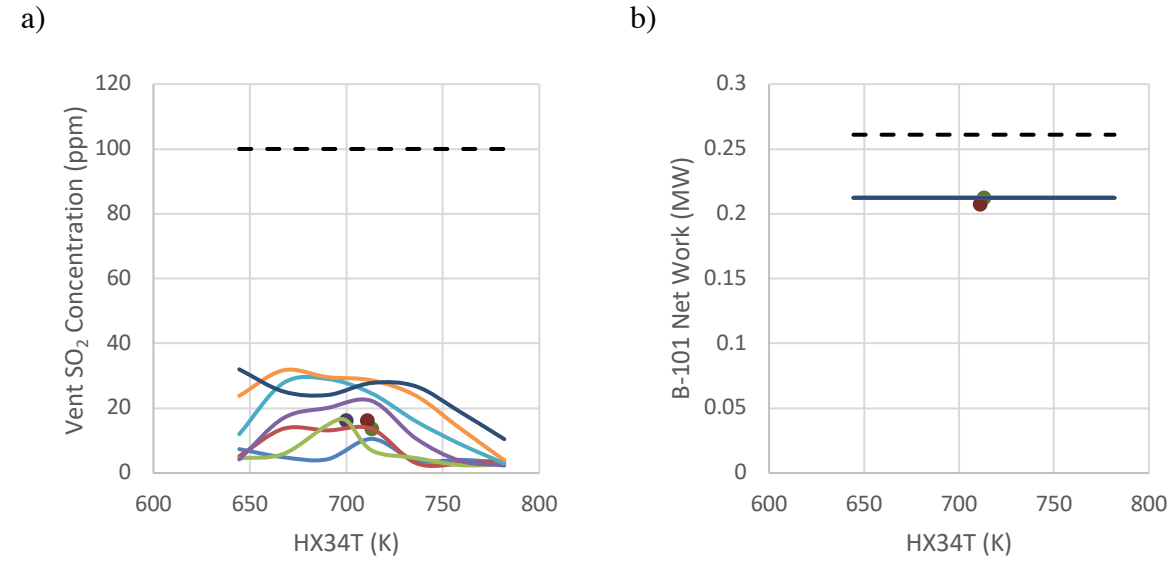

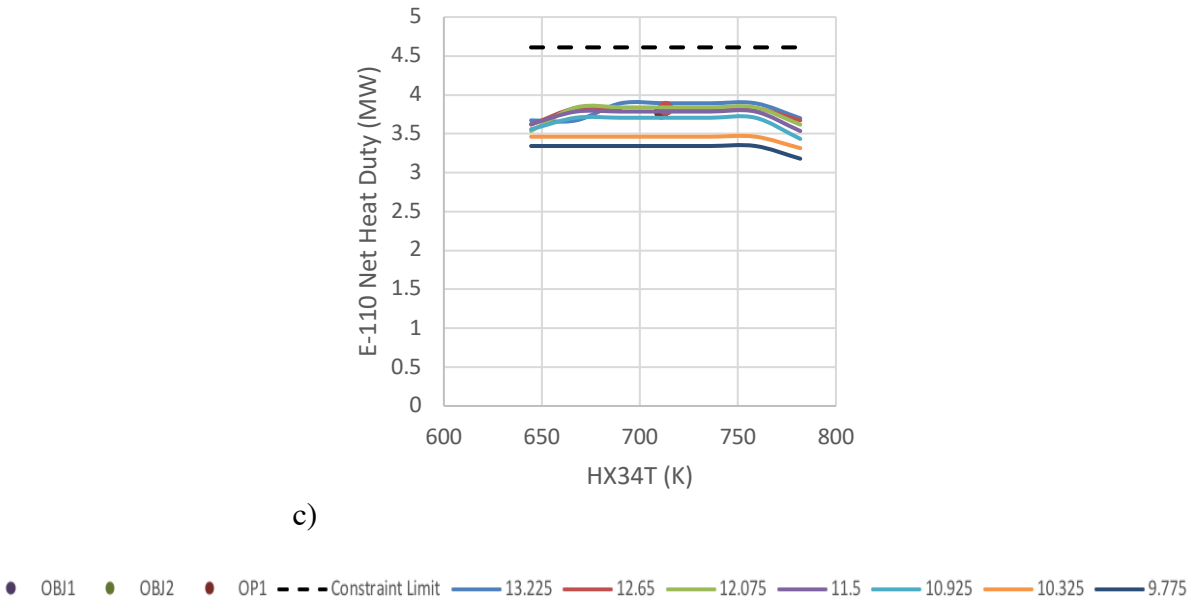

Figure 16. Evaluation of the process constraints. The different colored trend lines are used to distinguish the gas strengths (GS) at different operating points.

4.2.5 Uncertainty Analysis

The aim of this section is to identify the operating conditions that result in the maximum expected value and minimum standard deviation (i.e. minimum variability) when the plant is subjected to uncertainty in key process model and economic parameters. Understanding the variability of the optimal operating condition to uncertainty provides insight into how the operating condition of the plant needs to be adjusted to remain optimal in the presence of uncertainty. Moreover, the price of robustness gives an estimate for the expected profit loss associated with narrowing the spread of the daily profit and may be desirable under highly uncertain conditions so that a smaller range of profits can be guaranteed.

The uncertain parameters that were considered in the present analysis are shown in Table 8. Sulfur and sulfuric acid are both commodities that experience price fluctuation based on their supply and

demand in the markets. The nominal price of NaOH is more than twice as large as that of any other raw material or product, and thus a change in its price can have a large impact on the daily profit of the plant. During model development, all operating conditions were defined explicitly except for the catalytic activities in the four stages of the packed bed reactor. As previously described in sections 4.2.1 and 4.2.2, the catalytic activities were used for model fitting and validation. Although over the catalyst cycle the catalytic activity will decrease monotonically, the precise value is unknown. Furthermore, the catalytic activity is a key plant variable as it has a significant impact on the conversion of SO_2, and subsequently the production of H_2SO_4 and SBS. Hence, the precise values of those seven parameters may be unknown or fluctuating at any period in time, and thus are suitable for an uncertainty analysis.

For each of the 7 uncertain variables a normal distribution was assumed with mean equal to the nominal value and standard deviation equal to 15% of the mean, as shown in Table 8. A normal distribution was selected given that it is the most accepted type of distribution for most engineering applications.[85] Two optimization problems similar to that presented in section 4.2.4 are considered, in this case, however, the objectives are maximize the expected daily profit, and minimize the standard deviation in daily profit under uncertainty in the model parameters. Each of these problems is solved using the GPS method for a set of 5,000 scenarios (realizations) in the uncertain parameters; thus, the process constraints and a modification of the cost function shown in problem (29), i.e. maximum expectation and minimum standard deviation, were evaluated at each discrete realization in the uncertain parameters. The uncertainty set scenarios were obtained by random sampling from the normal distributions of the 7 uncertain parameters considered in the analysis. The daily profit distributions for the two scenarios are shown in Figure 17. For comparison the

daily profit distribution obtained under uncertainty at the operating condition OP1 is also presented in this figure.

Table 8. Uncertainty descriptions

Uncertain Variable	Mean	Standard Deviation
Sulfur Price	0.065	9.75×10^{-2}
NaOH Price	0.65	9.75×10^{-1}
H_2SO_4 Price	0.16	2.4×10^{-2}
Stage 1 Catalytic Activity	1.3	0.195
Stage 2 Catalytic Activity	1.4	0.210
Stage 3 Catalytic Activity	1.5	0.225
Stage 4 Catalytic Activity	1	0.150

As shown in Figure 18, the process constraint on SO_2 emitted from the vent stack is immune (insensitive) to uncertainty in the catalyst activity. Similarly, the process constraints, equations (32)-(33), i.e. the net energy requirement of the blower B-101 and the net heat duty of the cooling tower E-110, showed no variability to the uncertainty in catalyst activity. These results indicate that the locally optimal solution is insensitive to uncertainty since none of the constraints considered in the problem are active at the locally optimal solution. Therefore, the locally optimal operating condition for the maximum expected daily profit scenario remained unchanged from that identified under deterministic conditions as OBJ1. Accordingly, the operating condition of the plant does not have to be adjusted for variation in the uncertain parameters within the range considered. For this operating condition, the mean daily profit was $29,985. Although the local optimal point did not change with respect to the Daily Profit optimization problem, the daily variability in profits is significant at a value of $5,218. This represents 17.4% of the daily plant profit.

On the other hand, the operating condition that achieved the local minimum standard deviation was at AF = 1,785 kg/hr, GS = 10.35, and HX34T = 781 K. At that operating condition the mean daily profit was $18,510 and the standard deviation was $3,359. This shows that the price of robustness for this plant is high as the expected reduction in daily profit is $11,461 for a reduction in standard deviation of $1,859. Furthermore, the change in the plant operating condition to transfer from the maximum expected value condition to the minimum standard deviation condition is large; the air flowrate must be reduced by 26%, the gas strength must be reduced by 14%, and the outlet temperature of the heat exchangers E-103 and E-104 must be increased by 21%.

At the operating condition OP1 the expected daily profit and standard deviation were $28,989 and $4,950, respectively. As was discussed in section 4.2.4, the operating condition of the plant can be changed from OP1 to OBJ1 by making changes in the air flowrate, gas strength, and outlet temperature of the heat exchangers E-103 and E-104. This results in a more economically optimal operating point with increased annual profits in the order of $363,540.

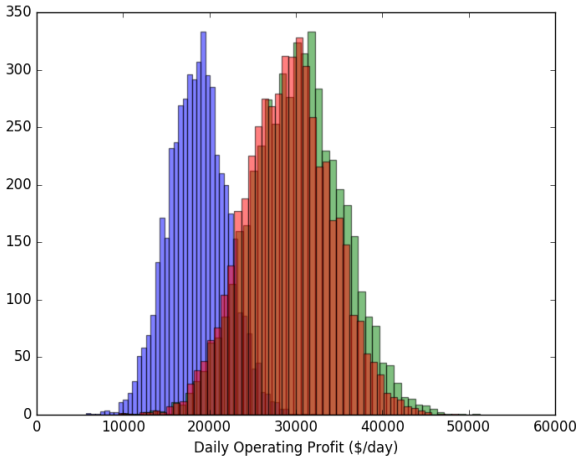

Figure 17. Histogram for the two scenarios: minimum standard deviation (purple) and maximum expected value (green); also shown is the distribution at the operating condition OP1 (red).

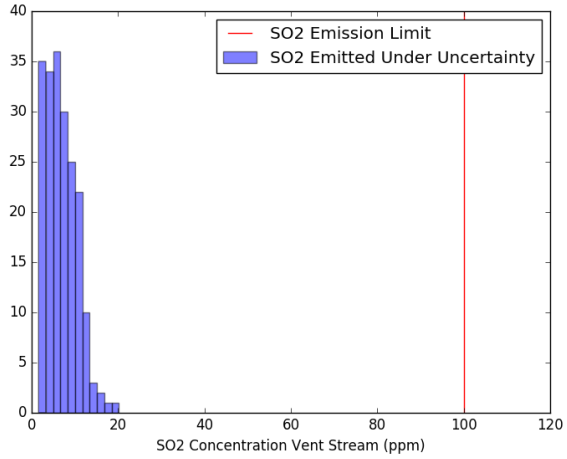

Figure 18. Histogram for the SO_2 concentration in the vent stream under uncertainty in the catalytic activity; also shown is the SO_2 emission limit.

4.3 Summary

The industrial-scale single absorption sulfuric acid plant with scrubbing tower under consideration consisted of five process flowsheets: process gas used to generate SO_3, process acid to absorb SO_3 into H_2SO_4, scrubbing tower for reducing the SO_2 concentration in the vent stream, steam cycle

for cooling the process gas cycle, and cooling water cycle to remove heat from process acid cycle. As the aim of this research was to develop a comprehensive plant model, all of the flowsheets were included in the Aspen Plus simulation.

The resulting Aspen flowsheet model was fitted using the catalytic activities in the multi-stage reactor as tuning parameters and by comparison to a historical operating point OPD. Afterwards, the prediction capabilities of the model were confirmed by comparison to two additional historical operating points that represented high and low operating conditions, respectively.

The resulting Aspen flowsheet model was then used to perform a sensitivity analysis. Three process parameters were identified which most greatly influenced the quantities of raw materials and products and they were subsequently used to carry out optimization for economic and productivity objective functions. Optimal operating conditions were identified which could increase daily profit and the H_2SO_4 production rate. Moreover, the relevant process parameters at the locally optimal operating conditions were found to be well within their respective range as defined by the process constraints.

Furthermore, the economic optimization was repeated under uncertainty in the catalytic activities and the prices of sulfur, NaOH, and H_2SO_4. It was found that the local optimal solution under deterministic conditions remain unchanged for the uncertainty set considered. However, it did result in a large amount of variability. Moreover, the price of robustness to minimize the variability was found to be a significant portion of the daily operating profit.

Chapter 5: Conclusions and Recommendations

5.1 aro-MPC

The advantages of the proposed method are that it is inherently robust. A sequence of time-varying control laws is obtained for the present aro-MPC controller and their performance was determined to be a function of the control horizon and the uncertainty set. The aro-MPC framework presented in this work is applicable to systems with additive input disturbance that can be described by a linear state-space model. In the aro-MPC framework the input disturbance is replaced with an additive time-varying error. The error term is the source of feedback and can accommodate mismatch in the states between the model and the actual plant resulting from unmeasurable disturbances (Case Study 1 and 2, sections 3.3.1 and 3.3.2, respectively) as well as nonlinearities (Case Study 3, section 3.3.3). When solving the robust optimization problem, the additive error is only known to belong to a bounded set, however during online implementation its realizations become known through feedback and are used to evaluate the control laws. A comparison to online MPC demonstrated that for the system under consideration the loss in performance of the aro-MPC was negligible (section 3.3.1.1). Moreover, it was shown that the aro-MPC can be applied to larger systems (section 3.3.2) as well as to nonlinear systems (section 3.3.3). Based on these results, the present aro-MPC framework is considered a promising approach for applying MPC to large-scale, real world systems.

5.2 Simulation and Economic Optimization of an Industrial-Scale Sulfuric Acid Plant under Uncertainty

As stated in the introduction section, the second study conducted in this thesis sought to address the issue of understanding the maximum operating capacity of an industrial-scale plant given the current design and its associated safety, environmental and productivity restrictions. In this study

the complete flowsheet (consisting of 5 sub-flowsheets) for an industrial-scale single absorption sulfuric acid plant with scrubbing tower was presented. The resulting plant flowsheet model was fully validated using historical plant data and it was found to have suitable prediction capabilities; some errors in stream composition and temperature were large but justified, however the error in total flowrate of any particular stream was no larger than 6%. This enabled its use to gain insight on the sensitivity of key response variables with respect to the operating parameters of the plant. That analysis showed that the air flowrate, gas strength, and outlet temperatures of the heat exchangers following the second and third passes of the multi-stage reactor where the most sensitive variables in the plant. An optimization using those three variables as the decision variables was performed to identify the operating point that resulted in the maximum daily profit of the plant and the maximum H_2SO_4 production rate. As compared to the current best operating condition of the plant, the operating conditions identified during the optimization showed that improvements of 3.3% and 4.3% can be achieved in the daily profit of the plant and H_2SO_4 production rate, respectively. The economic optimization problem was repeated under uncertainty in the prices of key raw materials and products as well as the catalytic activities in the multi-stage reactor. The optimal operating condition did not change significantly from that obtained under deterministic conditions and the price of robustness associated with minimizing the standard deviation in daily profits was found to be nearly 38% of the expected profit.

5.3 Future Work

In the area of aro-MPC, future works include implementing the aro-MPC on larger scale nonlinear systems, likely starting with a small multi-unit plant and proceeding to a large-scale industrial plant. As it would be necessary to use linear models that closely approximate the nonlinear plants, these studies may be an opportunity to explore the implementation of multiple aro-MPC controllers

on a single chemical system. That is, when the system enters a different operating region, a different explicit solution can take over which is based on a different linear model so as to minimize the degree of mismatch. Alternatively, the aro-MPC framework can be modified to accommodate nonlinear objective functions and nonlinear constraints. The main challenge with considering nonlinearities in the aro-MPC framework is the need to dualize uncertain constraints and objectives in formulating the ARC.[86] Hence, a simplification was made in the current framework to optimize the nominal rather than the worst-case realization of uncertainty. Furthermore, an alternative method of accommodating variable recourse (non-deterministic A and B state-space matrices, equations (3)) should be explored. The framework presented here grouped the input disturbance and model parameter uncertainty (i.e. unknown mismatch between the nonlinear plant and linear model) into the additive time-varying error term due to the fact that ARO is restricted to deterministic recourse.[26] However, it is likely that separating how the different model uncertainties are considered in the aro-MPC framework may lead to improvements in the formulation and therefore process performance.

As it applies to the industrial-scale sulfuric acid plant developed in this work, the highest priority future work is to develop a dynamic model. This type of model would enable the study of plant controllability as well as a flexibility analysis under common disturbances such as weather conditions and market demands. However, as it applies to the broader field of simulation and optimization of large multi-unit processes at steady-state, the demand is for general frameworks for each stage of the analysis. Those stages are plant simulation, model convergence, model validation, and model optimization. Given the large human and computational time expenditures associated with each of these vital steps in the process, a robust framework would most surely benefit widespread application of these techniques.

Letter of Copyrights Permission

Title: Optimization and Modeling of an IndustrialScale Sulfuric Acid Plant under Uncertainty

Author: Manuel TejedaIglesias, Jason Szuba, Ron Koniuch, et al

Publication: Industrial & Engineering Chemistry Research

Publisher: American Chemical Society
Date: Jun 1, 2018

PERMISSION/LICENSE IS GRANTED FOR YOUR ORDER AT NO CHARGE

This type of permission/license, instead of the standard Terms & Conditions, is sent to you because no fee is being charged for your order. Please note the following:

- Permission is granted for your request in both print and electronic formats, and translations.
- If figures and/or tables were requested, they may be adapted or used in part.
- Please print this page for your records and send a copy of it to your publisher/graduate school.
- Appropriate credit for the requested material should be given as follows: "Reprinted (adapted) with permission from (COMPLETE REFERENCE CITATION). Copyright (YEAR) American Chemical Society." Insert appropriate information in place of the capitalized words.
- One-time permission is granted only for the use specified in your request. No additional uses are granted (such as derivative works or other editions). For any other uses, please submit a new request.

Appendix A

The decision variables of the ARC for the robust linear MPC optimization problem are the intercepts and slopes of the affine functions ($\boldsymbol{v}_{t+i}^0, \boldsymbol{\chi}_{t+i}^0, \mathbf{U}_{t+i}, \mathbf{X}_{t+i}$) and the dual variables that are introduced when dualizing the inequality constraints. The dual variables have all been grouped together in equation (A1) and are represented by DL. DL consists of $\mathbf{p}_{t+i,n,j,k}^U, \mathbf{p}_{t+i,n,j,k}^L \in \mathbb{R}^{\mathrm{N_F}}$, $\mathbf{r}_{t+i,n,j,k}^U, \mathbf{r}_{t+i,n,j,k}^L \in \mathbb{R}^{\mathrm{N_x}}$, and $\mathrm{y}_{t+i,n,j,k}^U, \mathrm{y}_{t+i,n,j,k}^L \in \mathbb{R}$, $\forall n = 1, \dots, \mathrm{N_x}$, $\forall j = t, \dots, t+i$, $\forall i = 1, \dots, P$, $\forall k = 1,2,3,4$. The following is the complete ARC for the robust linear MPC optimization problem where references have been made to the original constraints of the robust problem. For the equation (1a):

$$\min_{\substack{\boldsymbol{v}_{t+i}^0 \in \mathbb{R}^{\mathrm{N_u}}, \mathbf{U}_{t+i} \in \mathbb{R}^{\mathrm{N_u} \times \mathrm{N_F}} \\ \forall i = 0, \dots, P-1, \\ \boldsymbol{\chi}_{t+i}^0 \in \mathbb{R}^{\mathrm{N_x}}, \mathbf{X}_{t+i} \in \mathbb{R}^{\mathrm{N_x} \times \mathrm{N_F}} \\ \forall i = 1, \dots, P \\ \mathrm{DL}}} \mathbf{q}^{\mathrm{T}} \sum_{i=1}^{P} (\boldsymbol{\chi}_{t+i+1}^0 - \mathbf{r}_{t+i})^2 + \mathbf{w}^{\mathrm{T}} \sum_{i=1}^{M-1} (\Delta \boldsymbol{v}_{t+i}^0)^2 \tag{A1}$$

For the equations (3):

$$\begin{aligned}
\boldsymbol{\chi}_{t+1}^0 &= \mathbf{A}\mathbf{x}_t^{\mathrm{Nom}} + \mathbf{B}\boldsymbol{v}_t^0 \\
\mathbf{X}_{t+1,t} &= \mathbf{A}\boldsymbol{\Phi}_{\mathbf{0}} + \mathbf{B}\mathbf{U}_{t,t} \\
\boldsymbol{\chi}_{t+i+1}^0 &= \mathbf{A}\boldsymbol{\chi}_{t+i}^0 + \mathbf{B}\boldsymbol{v}_{t+i}^0 && \forall i = 1, \dots, P-1 \\
\mathbf{X}_{t+i+1,j} &= \mathbf{A}\mathbf{X}_{t+i,j} + \mathbf{B}\mathbf{U}_{t+i,j} && \forall j = t, \dots, t+i \quad \forall i = 1, \dots, P-1 \\
\mathbf{X}_{t+i+1,t+i+1} &= \mathbf{D}\boldsymbol{\Phi}_1 && \forall i = 0, \dots, P-1
\end{aligned} \tag{A2}$$

Note in equations (A3) to (A6), $\mathbf{a}_{(n)}$ and $\mathbf{A}_{(n)}$ denote the n$^{\mathrm{th}}$ element of vector $\mathbf{a}$ (a scalar) and the n$^{\mathrm{th}}$ row of a matrix $\mathbf{A}$ (a row vector), respectively. For the lower bound of the equations (1d):

$$
\begin{aligned}
&\sum_{j=t}^{t+i} \mathbf{ez}_{\mathrm{F}}^{\mathrm{T}} \mathbf{p}_{t+i,n,j,1}^{U} + \sum_{j=t}^{t+i} \mathbf{ez}_{\mathrm{F}}^{\mathrm{T}} \mathbf{p}_{t+i,n,j,1}^{L} + \sum_{j=t}^{t+i} \beta \mathrm{Fy}_{t+i,n,j,1}^{U} \qquad \forall i = 1, \dots, P \\
&\quad + \sum_{j=t}^{t+i} \beta \mathrm{Fy}_{t+i,n,j,1}^{L} \\
&\quad + \left(\mathbf{x}^{U} - \mathbf{x}_{t}^{\mathrm{Nom}}\right) \mathbf{r}_{t+i,n,t,1}^{U} \\
&\quad + \left(\mathbf{x}_{t}^{\mathrm{Nom}} - \boldsymbol{x}^{L}\right) \mathbf{r}_{t+i,n,t,1}^{L} \\
&\quad + \sum_{j=t+1}^{t+i} \mathbf{e}^{U} \mathbf{r}_{t+i,n,j,1}^{U} \\
&\quad + \sum_{j=t+1}^{t+i} \mathbf{e}^{L} \mathbf{r}_{t+i,n,j,1}^{L} \leq \boldsymbol{\upsilon}_{t+i(n)}^{0} - \mathbf{u}_{(n)}^{L}
\end{aligned}
\tag{A3}
$$

$$
\begin{aligned}
&\mathbf{p}_{t+i,n,t,1}^{U} - \mathbf{p}_{t+i,n,t,1}^{L} + \mathrm{y}_{t+i,n,t,1}^{U} \mathbf{ez}_{\mathrm{F}} - \mathrm{y}_{t+i,n,t,1}^{L} \mathbf{ez}_{\mathrm{F}} \qquad \forall i = 1, \dots, P \\
&\quad + \boldsymbol{\Phi}_{0}^{\mathrm{T}} \mathbf{r}_{t+i,n,t,1}^{U} - \boldsymbol{\Phi}_{0}^{\mathrm{T}} \mathbf{r}_{t+i,n,t,1}^{L} \\
&\quad = -\mathbf{U}_{t+i,t(n)}^{\mathrm{T}}
\end{aligned}
$$

$$
\begin{aligned}
&\mathbf{p}_{t+i,n,j,1}^{U} - \mathbf{p}_{t+i,n,j,1}^{L} + \mathrm{y}_{t+i,n,j,1}^{U} \mathbf{ez}_{F} - \mathrm{y}_{t+i,n,j,1}^{L} \mathbf{ez}_{F} \qquad \forall j = t+1, \dots, t+i \\
&\quad + \boldsymbol{\Phi}_{1}^{\mathrm{T}} \mathbf{r}_{t+i,n,j,1}^{U} - \boldsymbol{\Phi}_{1}^{\mathrm{T}} \mathbf{r}_{t+i,n,j,1}^{L} \qquad \forall i = 1, \dots, P \\
&\quad = -\mathbf{U}_{t+i,j(n)}^{\mathrm{T}}
\end{aligned}
$$

$$
\mathbf{p}_{t+i,n,j,1}^{U}, \mathbf{p}_{t+i,n,j,1}^{L}, \mathbf{r}_{t+i,n,j,1}^{U}, \mathbf{r}_{t+i,n,j,1}^{L} \geq \mathbf{0} \qquad \forall j = t, \dots, t+i \quad \forall i = 1, \dots, P
$$

$$
\begin{aligned}
&\mathrm{y}_{t+i,n,j,1}^{U}, \mathrm{y}_{t+i,n,j,1}^{U} \geq 0 \qquad \forall j = t+1, \dots, t+ \\
&\qquad\qquad\qquad\qquad\qquad\qquad\qquad\qquad\qquad\qquad\qquad\qquad\qquad\qquad\qquad\qquad \forall i = 1, \dots, P
\end{aligned}
$$

For the upper bound of the equations (1d):

$$\sum_{j=t}^{t+i} \mathbf{ez}_{\mathrm{F}}^{\mathrm{T}} \mathbf{p}_{t+i,n,j,2}^{U} + \sum_{j=t}^{t+i} \mathbf{ez}_{\mathrm{F}}^{\mathrm{T}} \mathbf{p}_{t+i,n,j,2}^{L} + \sum_{j=t}^{t+i} \beta \mathrm{Fy}_{t+i,n,j,2}^{U} \qquad \forall i = 1, \dots, P$$

$$+ \sum_{j=t}^{t+i} \beta \mathrm{Fy}_{t+i,n,j,2}^{L}$$

$$+ \left(\mathbf{x}^{U} - \mathbf{x}_{t}^{\mathrm{Nom}}\right) \mathbf{r}_{t+i,n,t,2}^{U}$$

$$+ \left(\mathbf{x}_{t}^{\mathrm{Nom}} - \boldsymbol{x}^{L}\right) \mathbf{r}_{t+i,n,t,2}^{L}$$

$$+ \sum_{j=t+1}^{t+i} \mathbf{e}^{U} \mathbf{r}_{t+i,n,j,2}^{U} + \sum_{j=t+1}^{t+i} \mathbf{e}^{L} \mathbf{r}_{t+i,n,j,2}^{L}$$

$$\leq -\boldsymbol{v}_{t+i(n)}^{0} + \mathbf{u}_{(n)}^{U}$$

$$\mathbf{p}_{t+i,n,t,2}^{U} - \mathbf{p}_{t+i,n,t,2}^{L} + \mathrm{y}_{t+i,n,t,2}^{U} \mathbf{ez}_{\mathrm{F}} - \mathrm{y}_{t+i,n,t,2}^{L} \mathbf{ez}_{\mathrm{F}} \qquad \forall i = 1, \dots, P \qquad \text{(A4)}$$

$$+ \boldsymbol{\Phi}_{0}^{\mathrm{T}} \mathbf{r}_{t+i,n,t,2}^{U} - \boldsymbol{\Phi}_{0}^{\mathrm{T}} \mathbf{r}_{t+i,n,t,2}^{L}$$

$$= \mathbf{U}_{t+i,t(n)}^{\mathrm{T}}$$

$$\mathbf{p}_{t+i,n,j,2}^{U} - \mathbf{p}_{t+i,n,j,2}^{L} + \mathrm{y}_{t+i,n,j,2}^{U} \mathbf{ez}_{F} - \mathrm{y}_{t+i,n,j,2}^{L} \mathbf{ez}_{F} \qquad \forall j = t+1, \dots, t+i$$

$$+ \boldsymbol{\Phi}_{1}^{\mathrm{T}} \mathbf{r}_{t+i,n,j,2}^{U} - \boldsymbol{\Phi}_{1}^{\mathrm{T}} \mathbf{r}_{t+i,n,j,2}^{L} \qquad \forall i = 1, \dots, P$$

$$= \mathbf{U}_{t+i,j(n)}^{\mathrm{T}}$$

$$\mathbf{p}_{t+i,n,j,2}^{U}, \mathbf{p}_{t+i,n,j,2}^{L}, \mathbf{r}_{t+i,n,j,2}^{U}, \mathbf{r}_{t+i,n,j,2}^{L} \geq \mathbf{0} \qquad \forall j = t, \dots, t+i \quad \forall i = 1, \dots, P$$

$$\mathrm{y}_{t+i,n,j,2}^{U}, \mathrm{y}_{t+i,n,j,2}^{U} \geq 0 \qquad \forall j = t+1, \dots, t+$$

$$\forall i = 1, \dots, P$$

For the lower bound of the equations (1e):

$$\sum_{j=t}^{t+i} \mathbf{ez}_{\mathrm{F}}^{\mathrm{T}} \mathbf{p}_{t+i,n,j,3}^{U} + \sum_{j=t}^{t+i} \mathbf{ez}_{\mathrm{F}}^{\mathrm{T}} \mathbf{p}_{t+i,n,j,3}^{L} + \sum_{j=t}^{t+i} \beta \mathrm{Fy}_{t+i,n,j,3}^{U} \qquad \forall i = 1, \dots, P$$

$$+ \sum_{j=t}^{t+i} \beta \mathrm{Fy}_{t+i,n,j,3}^{L}$$

$$+ \left(\mathbf{x}^{U} - \mathbf{x}_{t}^{\mathrm{Nom}}\right) \mathbf{r}_{t+i,n,t,3}^{U}$$

$$+ \left(\mathbf{x}_{t}^{\mathrm{Nom}} - \boldsymbol{x}^{L}\right) \mathbf{r}_{t+i,n,t,3}^{L}$$

$$+ \sum_{j=t+1}^{t+i} \mathbf{e}^{U} \mathbf{r}_{t+i,n,j,3}^{U} + \sum_{j=t+1}^{t+i} \mathbf{e}^{L} \mathbf{r}_{t+i,n,j,3}^{L}$$

$$\leq \boldsymbol{x}_{t+i(n)}^{0} - \mathbf{x}_{(n)}^{L}$$

$$\mathbf{p}_{t+i,n,t,3}^{U} - \mathbf{p}_{t+i,n,t,3}^{L} + \mathrm{y}_{t+i,n,t,3}^{U} \mathbf{ez}_{\mathrm{F}} - \mathrm{y}_{t+i,n,t,3}^{L} \mathbf{ez}_{\mathrm{F}} \qquad \forall i = 1, \dots, P \qquad \text{(A5)}$$

$$+ \boldsymbol{\Phi}_{0}^{\mathrm{T}} \mathbf{r}_{t+i,n,t,3}^{U} - \boldsymbol{\Phi}_{0}^{\mathrm{T}} \mathbf{r}_{t+i,n,t,3}^{L}$$

$$= -\mathbf{X}_{t+i,t(n)}^{\mathrm{T}}$$

$$\mathbf{p}_{t+i,n,j,3}^{U} - \mathbf{p}_{t+i,n,j,3}^{L} + \mathrm{y}_{t+i,n,j,3}^{U} \mathbf{ez}_{F} - \mathrm{y}_{t+i,n,j,3}^{L} \mathbf{ez}_{F} \qquad \forall j = t+1, \dots, t+i$$

$$+ \boldsymbol{\Phi}_{1}^{\mathrm{T}} \mathbf{r}_{t+i,n,j,3}^{U} - \boldsymbol{\Phi}_{1}^{\mathrm{T}} \mathbf{r}_{t+i,n,j,3}^{L} \qquad \forall i = 1, \dots, P$$

$$= -\mathbf{X}_{t+i,j(n)}^{\mathrm{T}}$$

$$\mathbf{p}_{t+i,n,j,3}^{U}, \mathbf{p}_{t+i,n,j,3}^{L}, \mathbf{r}_{t+i,n,j,3}^{U}, \mathbf{r}_{t+i,n,j,3}^{L} \geq \mathbf{0} \qquad \forall j = t, \dots, t+i \quad \forall i = 1, \dots, P$$

$$\mathrm{y}_{t+i,n,j,3}^{U}, \mathrm{y}_{t+i,n,j,3}^{U} \geq 0 \qquad \forall j = t+1, \dots, t+$$

$$\forall i = 1, \dots, P$$

For the upper bound of the equations (1e):

$$\begin{aligned}
&\sum_{j=t}^{t+i} \mathbf{ez}_{\mathrm{F}}^{\mathrm{T}} \mathbf{p}_{t+i,n,j,4}^{U} + \sum_{j=t}^{t+i} \mathbf{ez}_{\mathrm{F}}^{\mathrm{T}} \mathbf{p}_{t+i,n,j,4}^{L} + \sum_{j=t}^{t+i} \beta \mathrm{Fy}_{t+i,n,j,4}^{U} \\
&\quad + \sum_{j=t}^{t+i} \beta \mathrm{Fy}_{t+i,n,j,4}^{L} \\
&\quad + \left(\mathbf{x}^{U} - \mathbf{x}_{t}^{\mathrm{Nom}}\right) \mathbf{r}_{t+i,n,t,4}^{U} \\
&\quad + \left(\mathbf{x}_{t}^{\mathrm{Nom}} - \boldsymbol{x}^{L}\right) \mathbf{r}_{t+i,n,t,4}^{L} \\
&\quad + \sum_{j=t+1}^{t+i} \mathbf{e}^{U} \mathbf{r}_{t+i,n,j,4}^{U} + \sum_{j=t+1}^{t+i} \mathbf{e}^{L} \mathbf{r}_{t+i,n,j,4}^{L} \\
&\quad \leq -\boldsymbol{x}_{t+i(n)}^{0} + \mathbf{x}_{(n)}^{U}
\end{aligned} \qquad \forall i = 1, \dots, P$$

$$\begin{aligned}
&\mathbf{p}_{t+i,n,t,4}^{U} - \mathbf{p}_{t+i,n,t,4}^{L} + \mathrm{y}_{t+i,n,t,4}^{U} \mathbf{ez}_{\mathrm{F}} - \mathrm{y}_{t+i,n,t,4}^{L} \mathbf{ez}_{\mathrm{F}} \\
&\quad + \boldsymbol{\Phi}_{0}^{\mathrm{T}} \mathbf{r}_{t+i,n,t,4}^{U} - \boldsymbol{\Phi}_{0}^{\mathrm{T}} \mathbf{r}_{t+i,n,t,4}^{L} \\
&\quad = \mathbf{X}_{t+i,t(n)}^{\mathrm{T}}
\end{aligned} \qquad \forall i = 1, \dots, P \tag{A6}$$

$$\begin{aligned}
&\mathbf{p}_{t+i,n,j,4}^{U} - \mathbf{p}_{t+i,n,j,4}^{L} + \mathrm{y}_{t+i,n,j,4}^{U} \mathbf{ez}_{F} - \mathrm{y}_{t+i,n,j,4}^{L} \mathbf{ez}_{F} \\
&\quad + \boldsymbol{\Phi}_{1}^{\mathrm{T}} \mathbf{r}_{t+i,n,j,4}^{U} - \boldsymbol{\Phi}_{1}^{\mathrm{T}} \mathbf{r}_{t+i,n,j,4}^{L} \\
&\quad = \mathbf{X}_{t+i,j(n)}^{\mathrm{T}}
\end{aligned} \qquad \begin{aligned} &\forall j = t+1, \dots, t+i \\ &\forall i = 1, \dots, P \end{aligned}$$

$$\mathbf{p}_{t+i,n,j,4}^{U}, \mathbf{p}_{t+i,n,j,4}^{L}, \mathbf{r}_{t+i,n,j,4}^{U}, \mathbf{r}_{t+i,n,j,4}^{L} \geq \mathbf{0} \qquad \forall j = t, \dots, t+i \quad \forall i = 1, \dots, P$$

$$\mathrm{y}_{t+i,n,j,4}^{U}, \mathrm{y}_{t+i,n,j,4}^{U} \geq 0 \qquad \begin{aligned} &\forall j = t+1, \dots, t+i \\ &\forall i = 1, \dots, P \end{aligned}$$

For the equations (1f):

$$\begin{aligned}
\boldsymbol{v}_{t+i}^{0} &= \boldsymbol{v}_{t+M-1}^{0} && \forall i = M, \dots, P-1 \\
\mathbf{U}_{t+i,j} &= \mathbf{U}_{t+M-1,j} && \forall i = M, \dots, P-1 \\
& && \forall j = t, \dots, t+M-1 \\
\mathbf{U}_{t+i,j} &= \mathbf{0} && \forall i = M, \dots, P-1 \\
& && \forall j = t+M, \dots, t+P-1
\end{aligned} \tag{A7}$$

Bibliography

(1) Seborg, D. E. *Process Dynamics and Control*, 3rd ed.; John Wiley & Sons, Inc: Hoboken, N.J, 2011.

(2) Sakizlis, V.; Kakalis, N. M. P.; Dua, V.; Perkins, J. D.; Pistikopoulos, E. N. Design of Robust Model-Based Controllers via Parametric Programming. *Automatica* **2004**, *40* (2), 189–201.

(3) Alessio, A.; Bemporad, A. A Survey on Explicit Model Predictive Control. In *Nonlinear Model Predictive Control*; Magni, L., Raimondo, D. M., Allgöwer, F., Eds.; Morari, M., Thoma, M., Series Eds.; Springer Berlin Heidelberg: Berlin, Heidelberg, 2009; Vol. 384, pp 345–369.

(4) Mayne, D. Q.; Rawlings, J. B.; Rao, C. V.; Scokaert, P. O. M. Constrained Model Predictive Control: Stability and Optimality. *Automatica* **2000**, *36*, 789–814.

(5) Mayne, D. Q. Model Predictive Control: Recent Developments and Future Promise. *Automatica* **2014**, *50* (12), 2967–2986.

(6) Bemporad, A.; Morari, M.; Dua, V.; Pistikopoulos, E. N. The Explicit Linear Quadratic Regulator for Constrained Systems. *Automatica* **2002**, *38*, 3–20.

(7) Bemporad, A.; Borrelli, F.; Morari, M. Min-Max Control of Constrained Uncertain Discrete-Time Linear Systems. *IEEE Transactions on Automatic Control* **2003**, *48* (9), 1600–1606.

(8) Gosiewski, K. Dynamic Modelling of Industrial SO2 Oxidation Reactors Part I. Model of "hot" and "Cold" Start-Ups of the Plant. *Chemical Engineering and Processing* **1993**, *32*, 111–129.

(9) Doering, F. J.; Gaddy, J. L. Optimization of the Sulfuric Acid Process with a Flowsheet Simulator. *Computers and Chemical Engineering* **1980**, *4* (1), 113–122.

(10) Panos, C.; Kouramas, K. I.; Georgiadis, M. C.; Pistikopoulos, E. N. Modelling and Explicit Model Predictive Control for PEM Fuel Cell Systems. *Chemical Engineering Science* **2012**, *67* (1), 15–25.

(11) Tejeda-Iglesias, M.; Szuba, J.; Koniuch, R.; Ricardez-Sandoval, L. Optimization and Modeling of an Industrial-Scale Sulfuric Acid Plant under Uncertainty. *Industrial & Engineering Chemistry Research* **2018**, *57* (24), 8253–8266.

(12) Lee, J. H. Model Predictive Control: Review of the Three Decades of Development. *International Journal of Control, Automation and Systems* **2011**, *9* (3), 415–424.

(13) Kouramas, K. I.; Panos, C.; Faísca, N. P.; Pistikopoulos, E. N. An Algorithm for Robust Explicit/Multi-Parametric Model Predictive Control. *Automatica* **2013**, *49* (2), 381–389.

(14) Kerrigan, E. C.; Maciejowski, J. M. Feedback Min-Max Model Predictive Control Using a Single Linear Program: Robust Stability and the Explicit Solution. *International Journal of Robust and Nonlinear Control* **2004**, *14* (4), 395–413.

(15) Pistikopoulos, E. N.; Faısca, N. P.; Kouramas, K. I.; Panos, C. Explicit Robust Model Predictive Control ⋆. *Proceedings of the International Symposium on Advanced Control of Chemical Process* **2009**, 249–254.

(16) Kouramas, K.; Panos, C.; Pistikopoulos, E. N. Algorithm for Robust Explicit/Multi-Parametric MPC in Embedded Control Systems. *IFAC Proceedings Volumes* **2011**, *44* (1), 1344–1349.

(17) Wang, K.; Shao, Z.; Biegler, L. T.; Lang, Y.; Qian, J. Robust Extensions for Reduced-Space Barrier NLP Algorithms. *Computers & Chemical Engineering* **2011**, *35* (10), 1994–2004.
(18) Chaffart, D.; Ricardez-Sandoval, L. A. Robust Dynamic Optimization in Heterogeneous Multiscale Catalytic Flow Reactors Using Polynomial Chaos Expansion. *Journal of Process Control* **2017**, *60*, 128–140.
(19) Chaffart, D.; Rasoulian, S.; Ricardez-Sandoval, L. A. Distributional Uncertainty Analysis and Robust Optimization in Spatially Heterogeneous Multiscale Process Systems. *AIChE Journal* **2016**, *62* (7), 2374–2390.
(20) Rasoulian, S.; Ricardez-Sandoval, L. A. Stochastic Nonlinear Model Predictive Control Applied to a Thin Film Deposition Process under Uncertainty. *Chemical Engineering Science* **2016**, *140*, 90–103.
(21) Koller, R. W.; Ricardez-Sandoval, L. A.; Biegler, L. T. Stochastic Back-off Algorithm for Simultaneous Design, Control, and Scheduling of Multiproduct Systems under Uncertainty. *AIChE Journal* **2018**, *64* (7), 2379–2389.
(22) Rafiei, M.; Ricardez-Sandoval, L. A. Stochastic Back-Off Approach for Integration of Design and Control Under Uncertainty. *Industrial & Engineering Chemistry Research* **2018**, *57* (12), 4351–4365.
(23) Lao, L.; Ellis, M.; Durand, H.; Christofides, P. D. Real-Time Preventive Sensor Maintenance Using Robust Moving Horizon Estimation and Economic Model Predictive Control. *AIChE Journal* **2015**, *61* (10), 3374–3389.
(24) Ellis, M.; Zhang, J.; Liu, J.; Christofides, P. D. Robust Moving Horizon Estimation Based Output Feedback Economic Model Predictive Control. *Systems & Control Letters* **2014**, *68*, 101–109.
(25) Steimel, J.; Engell, S. Optimization-Based Support for Process Design under Uncertainty: A Case Study. *AIChE Journal* **2016**, *62* (9), 3404–3419. https://doi.org/10.1002/aic.15400.
(26) Ben-Tal, A.; El Ghaoui, L.; Nemirovski, A. S. *Robust Optimization*; Princeton series in applied mathematics; Princeton University Press: Princeton, 2009.
(27) Mesbah, A. Stochastic Model Predictive Control: An Overview and Perspectives for Future Research. *IEEE Control Systems* **2016**, *36* (6), 30–44.
(28) Nascu, I.; Lambert, R. S. C.; Krieger, A.; Pistikopoulos, E. N. Simultaneous Multi-Parametric Model Predictive Control and State Estimation with Application to Distillation Column and Intravenous Anaesthesia. *Computer Aided Chemical Engineering* **2014**, *33*, 541–546.
(29) Papathanasiou, M. M.; Avraamidou, S.; Oberdieck, R.; Mantalaris, A.; Steinebach, F.; Morbidelli, M.; Mueller-Spaeth, T.; Pistikopoulos, E. N. Advanced Control Strategies for the Multicolumn Countercurrent Solvent Gradient Purification Process. *AIChE Journal* **2016**, *62* (7), 2341–2357.
(30) Khajuria, H.; Pistikopoulos, E. N. Dynamic Modeling and Explicit/Multi-Parametric MPC Control of Pressure Swing Adsorption Systems. *Journal of Process Control* **2011**, *21* (1), 151–163.
(31) Johansen, T. A. Approximate Explicit Receding Horizon Control of Constrained Nonlinear Systems. *Automatica* **2004**, *40* (2), 293–300.
(32) Grancharova, A.; Johansen, T. A. Computation, Approximation and Stability of Explicit Feedback Min–Max Nonlinear Model Predictive Control. *Automatica* **2009**, *45* (5), 1134–1143.

(33) Domínguez, L. F.; Pistikopoulos, E. N. Recent Advances in Explicit Multiparametric Nonlinear Model Predictive Control. *Industrial & Engineering Chemistry Research* **2011**, *50* (2), 609–619.
(34) Bemporad, A.; Filippi, C. Suboptimal Explicit Receding Horizon Control via Approximate Multiparametric Quadratic Programming. *Journal of Optimization Theory and Applications* **2003**, *117* (1), 9–38.
(35) Jones, C. N.; Barić, M.; Morari, M. Multiparametric Linear Programming with Applications to Control. *European Journal of Control* **2007**, *13* (2–3), 152–170.
(36) Bemporad, A.; Filippi, C. An Algorithm for Approximate Multiparametric Convex Programming. *Computational Optimization and Applications* **2006**, *35* (1), 87–108.
(37) Johansen, T. A.; Grancharova, A. Approximate Explicit Constrained Linear Model Predictive Control via Orthogonal Search Tree. *IEEE Transactions on Automatic Control* **2003**, *48* (5), 810–815.
(38) Summers, S.; Jones, C. N.; Lygeros, J.; Morari, M. A Multiresolution Approximation Method for Fast Explicit Model Predictive Control. *IEEE Transactions on Automatic Control* **2011**, *56* (11), 2530–2541.
(39) Canale, M.; Fagiano, L.; Milanese, M. Set Membership Approximation Theory for Fast Implementation of Model Predictive Control Laws. *Automatica* **2009**, *45* (1), 45–54.
(40) Jones, C. N.; Morari, M. Polytopic Approximation of Explicit Model Predictive Controllers. *IEEE Transactions on Automatic Control* **2010**, *55* (11), 2542–2553.
(41) Chakrabarty, A.; Dinh, V.; Corless, M. J.; Rundell, A. E.; Zak, S. H.; Buzzard, G. T. Support Vector Machine Informed Explicit Nonlinear Model Predictive Control Using Low-Discrepancy Sequences. *IEEE Transactions on Automatic Control* **2017**, *62* (1), 135–148.
(42) Pin, G.; Filippo, M.; Pellegrino, F. A.; Fenu, G.; Parisini, T. Approximate Model Predictive Control Laws for Constrained Nonlinear Discrete-Time Systems: Analysis and Offline Design. *International Journal of Control* **2013**, *86* (5), 804–820.
(43) Bertsimas, D.; Brown, D. B.; Caramanis, C. Theory and Applications of Robust Optimization. *SIAM Review* **2011**, *53* (3), 464–501.
(44) Shi, H.; You, F. A Computational Framework and Solution Algorithms for Two-Stage Adaptive Robust Scheduling of Batch Manufacturing Processes under Uncertainty. *AIChE Journal* **2016**, *62* (3), 687–703.
(45) Thiele, A.; Terry, T.; Epelman, M. Robust Linear Optimization With Recourse. *Rapport technique* **2009**, 4–37.
(46) Zeng, B.; Zhao, L. Solving Two-Stage Robust Optimization Problems Using a Column-and-Constraint Generation Method. *Operations Research Letters* **2013**, *41* (5), 457–461.
(47) Lappas, N. H.; Gounaris, C. E. Multi-Stage Adjustable Robust Optimization for Process Scheduling under Uncertainty. *AIChE Journal* **2016**, *62* (5), 1646–1667.
(48) Goulart, P. J.; Kerrigan, E. C.; Maciejowski, J. M. Optimization over State Feedback Policies for Robust Control with Constraints. *Automatica* **2006**, *42* (4), 523–533.
(49) Chemsystems. *Sulfuric Acid, Chemsystems Process Evaluation Research Planning Report PERP07/08S8*; White Plains, New York, USA, 2009.
(50) King, M. J.; Davenport, W. G.; Moats, M. S. *Sulfuric Acid Manufacture - Analysis, Control, and Optimization*, 2nd ed.; Elsevier Ltd, 2013.
(51) Apodaca, L. E. *Sulfur Mineral Commodity Summary*; Washington, D.C., 2012.

(52) Ashar, N. G.; Golwalkar, K. R. *A Practical Guide to the Manufacture of Sulfuric Acid, Oleums, and Sulfonating Agents*; Springer, 2013.
(53) Friedman, L. J.; Friedman, S. J. The Single Absorption – Scrubbing Sulfuric Acid Process.
(54) Lloyd, L. *Handbook of Industrial Catalysts*, 1st ed.; Springer US, 2011.
(55) Louie, D. Design Considerations for Sulphuric Acid Plants [PowerPoint Slides]. Hamburg 2010.
(56) DKL Engineering. Acid Plant Database http://www.sulphuric-acid.com/sulphuric-acid-on-the-web/acid plants/Acid_Plant_Index.htm (accessed Dec 2, 2017).
(57) Gosiewski, K. Unsteady States in Metallurgical Sulphuric Acid Plants after SO2 Concentration Drop in the Feed Gas. *The Canadian Journal of Chemical Engineering* **1996**, *74*, 621–625.
(58) Ravindra, P. V; Rao, D. P.; Rao, M. S. A Model for the Oxidation of Sulfur Dioxide in a Trickle-Bed Reactor. *Industrial & Engineering Chemistry Research* **1997**, *36* (12), 5125–5132.
(59) Huixiong, W.; Shuzeng, Z.; Chengyue, L. Study of Unsteady-State Catalytic Oxidation of Sulfur Dioxide by Periodic Flow Reversal. *The Canadian Journal of Chemical Engineering* **1996**, *74*, 766–771.
(60) Hong, R.; Li, X.; Li, H.; Yuan, W. Modeling and Simulation of SO_2 Oxidation in a Fixed-Bed Reactor with Periodic Flow Reversal. *Catalysis Today* **1997**, *38*, 47–58.
(61) Snyder, J. D.; Subramaniam, B. Numerical Simulation of a Periodic Flow Reversal Reactor for Sulfur Dioxide Oxidation. *Chemical Engineering Science* **1993**, *48* (24), 4051–4064.
(62) de Koeijer, G.; Johannessen, E.; Kjelstrup, S. The Second Law Optimal Path of a Four-Bed SO2 Converter with Five Heat Exchangers. *Energy* **2004**, *29* (4), 525–546.
(63) Nodehi, A.; Mousavian, M. A. Simulation and Optimization of an Adiabatic Multi-Bed Catalytic Reactor for the Oxidation of SO2. *Chemical Engineering and Technology* **2006**, *29* (1), 84–90.
(64) Jia, M.; Chen, C.; Kou, W.; Niu, D.; Wang, F. Real-Time Optimization of Converter Inlet Temperature in Acid Production with Flue Gas. *Chemical Engineering Research and Design* **2017**, *122*, 226–232.
(65) Kiss, A. A.; Bildea, C. S.; Grievink, J. Dynamic Modeling and Process Optimization of an Industrial Sulfuric Acid Plant. *Chemical Engineering Journal* **2010**, *158* (2), 241–249.
(66) Kothare, M. V.; Balakrishnan, V.; Morari, M. Robust Constrained Model Predictive Control Using Linear Matrix Inequalities. *Automatica* **1996**, *32* (10), 1361–1379.
(67) Camacho, E. F.; Alba, C. B. *Model Predictive Control*, 2nd ed.; Springer-Verlag London, 2007.
(68) Gorissen, B. L.; Yanıkoğlu, I.; Hertog, D. den. A Practical Guide to Robust Optimization. *Omega* **2015**, *53*, 124–137.
(69) Chen, X.; Zhang, Y. Uncertain Linear Programs: Extended Affinely Adjustable Robust Counterparts. *Operations Research* **2009**, *57* (6), 1469–1482.
(70) Kuhn, D.; Wiesemann, W.; Georghiou, A. Primal and Dual Linear Decision Rules in Stochastic and Robust Optimization. *Mathematical Programming* **2011**, *130* (1), 177–209.
(71) Bertsimas, D.; Georghiou, A. Design of Near Optimal Decision Rules in Multistage Adaptive Mixed-Integer Optimization. *Operations Research* **2015**, *63* (3).

(72) Ricardez Sandoval, L. A.; Budman, H. M.; Douglas, P. L. Simultaneous Design and Control of Processes under Uncertainty: A Robust Modelling Approach. *Journal of Process Control* **2008**, *18* (7–8), 735–752.
(73) Miles, F. D.; Niblock, H.; Smith, D. The Heat Of Formation Of Oleum. *Transactions of the Faraday Society* **1944**, *40*, 281–295.
(74) Bhat, C.; Pinjala, V. Sulphuric Acid Plant Modelling. *Sulphur* **2010**, No. 330, 1–5.
(75) Taylor, R.; Krishna, R. *Multicomponent Mass Transfer*; John Wiley & Sons, Inc., 1954.
(76) American Society of Heating Refrigerating and Air Conditioning Engineergs Inc. *ASHRAE Handbook - Fundaments (I-P Edition)*; 2009.
(77) Wang, G. Q.; Yuan, X. G.; Yu, K. T. Review of Mass-Transfer Correlations for Packed Columns. *Industrial and Engineering Chemistry Research* **2005**, *44* (23), 8715–8729.
(78) Hikita, H.; Asai, S.; Tsuji, T. Absorption of Sulfur Dioxide into Aqueous Sodium Hydroxide and Sodium Sulfite Solutions. *AIChE Journal* **1977**, *23* (4), 538–544.
(79) Queiroz, J. A.; Rodrigues, V. M. S.; Matos, H. A.; Martins, F. G. Modeling of Existing Cooling Towers in ASPEN PLUS Using an Equilibrium Stage Method. *Energy Conversion and Management* **2012**, *64* (February 2017), 473–481.
(80) Gmitro, J. I.; Vermeulen, T. Vapor-Liquid Equilibria for Aqueous Sulfuric Acid. *AIChE Journal* **1964**, *10* (5), 740–746.
(81) Bolsaitis, P.; Elliott, J. F. Thermodynamic Activities and Equilibrium Partial Pressures for Aqueous Sulfuric-Acid-Solutions. *Journal of Chemical Engineering Data* **1990**, No. 35, 69–85.
(82) Que, H.; Song, Y.; Chen, C.-C. Thermodynamic Modeling of the Sulfuric Acid-Water-Sulfur Trioxide System with the Symmetric Electrolyte NRTL Model. *Industrial & Engineering Chemistry Research* **2011**, *56*, 963–977.
(83) Aspen Plus V8.8. Aspen Technology, Inc. 2015.
(84) Torczon, V. On The Convergence of Pattern Search Algorithms. *SIAM Journal on Optimization* **1997**, *7* (1), 1–25.
(85) Ricardez-Sandoval, L. A. Optimal Design and Control of Dynamic Systems under Uncertainty: A Probabilistic Approach. *Computers & Chemical Engineering* **2012**, *43* (10), 91–107.
(86) de Ruiter, F. J. C. T.; Zhen, J.; den Hertog, D. Dual Approach for Two-Stage Robust Nonlinear Optimization, 2018.